ISTANBUL TECHNICAL UNIVERSITY ★ GRADUATE SCHOOL

THE FRACTIONAL DERIVATIVE APPROACH TO THE SOLUTION OF DIFFRACTION PROBLEM FOR THE STRIP

Ph.D. THESIS

Kamil KARAÇUHA

Department of Applied Informatics

Information and Communication Engineering Programme

FEBRUARY 2021

ISTANBUL TECHNICAL UNIVERSITY ★ GRADUATE SCHOOL

THE FRACTIONAL DERIVATIVE APPROACH TO THE SOLUTION OF DIFFRACTION PROBLEM FOR THE STRIP

Ph.D. THESIS

Kamil KARAÇUHA
(708172001)

Department of Applied Informatics

Information and Communication Engineering Programme

Thesis Advisor: Prof. Dr. Eldar VELIYEV
Co-Advisor: Assoc. Prof. Dr. Vasil TABATADZE

FEBRUARY 2021

İSTANBUL TEKNİK ÜNİVERSİTESİ ★ LİSANSÜSTÜ EĞİTİM ENSTİTÜSÜ

KESİRLİ TÜREV YAKLAŞIMIYLA ŞERİTTEN SAÇILMA PROBLEMİNİN ÇÖZÜMÜ

DOKTORA TEZİ

Kamil KARAÇUHA
(708172001)

Bilişim Uygulamaları Anabilim Dalı

Bilgi ve Haberleşme Mühendisliği Programı

Tez Danışmanı: Prof. Dr. Eldar VELIYEV
Eş Danışman: Doç. Dr. Vasil TABATADZE

ŞUBAT 2021

Kamil KARAÇUHA, a Ph.D. student of ITU Graduate School student ID 708172001 successfully defended the thesis entitled "THE FRACTIONAL DERIVATIVE APPROACH TO THE SOLUTION OF DIFFRACTION PROBLEM FOR THE STRIP", which he prepared after fulfilling the requirements specified in the associated legislations, before the jury whose signatures are below.

Thesis Advisor :	**Prof. Dr. Eldar VELIYEV** Istanbul Technical University	....
Co-advisor :	**Assoc. Prof. Dr. Vasil TABATADZE** Istanbul Technical University	....
Jury Members :	**Prof. Dr. İbrahim AKDUMAN** Istanbul Technical University	....
	Prof. Dr. Hülya ŞAHİNTÜRK Yıldız Technical University	....
	Prof. Dr. Orhan İÇELLİ Yıldız Technical University	....
	Dr. Sebahattin EKER Istanbul Technical University	....
	Prof. Dr. Şehabeddin Taha İMECİ International University of Sarajevo	....

Date of Submission : 17 January 2021
Date of Defense : 16 February 2021

To my father,

FOREWORD

First of all, I would like to express my deep gratitude to my supervisor Prof. Dr. Eldar VELIYEV. His assistance and entire support in all the stages of the thesis and research help me to conclude this thesis. Besides, I would like to thank my co-advisor Assoc. Prof. Dr. Vasil TABATADZE for his unlimited help and affords. He spent his valuable time on my thesis as it was his own thesis. Not only he guided me on my research but also, he has shown me how to look at the problems and deduce applicable and reasonable comments or answer to them. Therefore, I present my appreciation to him.

During undergraduate and graduate education, I have met wonderful academicians in the area of mathematical physics and electrical engineering. I would like to thank Damla ALPTEKİN, Prof. Dr. Özlem AYDIN ÇİVİ, and Prof. Dr. Sibel BAŞKAL from Middle East Technical University that I am very lucky that I met you in Ankara. Also, I need to mention that Assoc. Prof. Dr. Fatih DİKMEN, Prof. Dr. Ali ALKUMRU, and Prof. Dr. Oleg A. TRETYAKOV from Gebze Technical University enlarged my horizon in the electromagnetic theory and amazed me with their deep and specified backgrounds. I would like to express my gratitude to Dr. Sebahattin EKER and Prof. Dr. Ali YAPAR from Istanbul Technical University for their support. They always motivated me in research and the future.

I also acknowledge the members of my thesis jury for accepting this work for examination and thank them for their valuable comments and suggestions. They are: Prof. Dr. İbrahim AKDUMAN, Prof. Dr. Hülya ŞAHİNTÜRK, Prof. Dr. Orhan İÇELLİ, Prof. Dr. Şehabeddin Taha İMECİ and Dr. Sebahattin EKER.

I would like to thank my beloved friends. Without them, I am sure that I will not be able to finish this thesis. Especially for his valuable critics and comments, I would like to thank Feza Turgay ÇELİK for his motivated and passionate approach to electromagnetics. I also would like to Ömer PEPEOĞLU and Gülfem Ceren YAVUZ. They are always with me and they know every hard step I have encountered throughout the thesis and they helped me a lot. Besides, I am very grateful and feel lucky that I am a friend of Yasemin ÖZDEMİR, Selin YAMAN, Utku ÇELEBİ, Kubilay YILMAZ, Beril KADIOĞLU, Şefika AKTAŞ, Yiğit PİLAVCI, Hakan AYDIN, Süleyman ALAN, Atınç AKGÜN, Doğukan BAŞ, Haluk AKÇAY, Servet ERBAŞ, Cengiz TOKSAVUL, Deniz GENÇ, Halil İbrahim ÜÇKOL, Nisa TUĞRUL and Gulcin Delal NOZHATZADEH. You are very valuable to me. Moreover, I should not forget to thank my colleagues and especially roommates at my office. My life in ITU is more joyful and fruitful with you. Also, I am very happy that I am a member of the Informatics Institute. I would like to thank the administrative and academic staff of the Informatics Institute for their help with different topics and cases. Finally, I need to give my best wishes to my violin teacher, Dr. Ali Seçim PAK from Marmara University. He is always curious about my thesis and supports me. Thank you all.

Finally, I would like to thank my family from my heart. The words cannot express my gratitude to them. I am very honored and happy that I am the son of Sibel and Ertuğrul

Karaçuha family. This thesis cannot be completed without the motivation and guidance of my father Ertuğrul KARAÇUHA and my mother Sibel KARAÇUHA. I would like to express my best wishes to my sister, Bahar KARAÇUHA. Her everlasting love and encouragement are precious.
I need to highlight the support of the National Center for High-Performance Computing (UHEM).

I want to thank the Scientific and Technological Research Council of Turkey (TÜBITAK) for the financial support they provided through 2211-A National Scholarship Programme for Ph.D. Students.

February 2021 Kamil KARAÇUHA

TABLE OF CONTENT

Page

ABBREVIATIONS

FBC : Fractional Boundary Condition
FDTD : Finite Difference Time Domain Method
FEM : Finite Element Method
FMM : Fast Multipole Method
FO : Fractional Order
IE : Integral Equation
MAS : Method of Auxiliary Sources
MLFMA : Multi-Level Fast Multipole Algorithm
MoM : Method of Moments
PEC : Perfect Electric Conductor
PMC : Perfect Magnetic Conductor
PO : Physical Optics
PWTD : Plane Wave Time-Domain
RP : Radiation Pattern
SLAE : System of Linear Algebraic Equations
TRCS : Total Radar Cross Section

LIST OF FIGURES

Page

THE FRACTIONAL DERIVATIVE APPROACH TO THE SOLUTION OF DIFFRACTION PROBLEM FOR THE STRIP

SUMMARY

In the thesis, it is aimed to solve the problem of diffraction by two-dimensional thin strip and double strips with a new method. The actual problem has already a solution. The purpose of the research is to develop a new approach to the problems. In previous studies, perfect electrical or magnetic conducting strips and impedance strips under specified conditions were performed. The fractional derivative method, as stated in its name, allows researchers to generalize boundary conditions and solve the existing problem in the most general way by using the fractional derivative approach. In this thesis, a new approach will be introduced that is simpler, faster to calculate, and can solve for different materials compared to existing methods in the literature where the fractional approach has been used in electromagnetics for 30 years. The method, which is generally used for metamaterial and materials with memory, is employed by many scientists in the area of electromagnetics. The first studies on the implementation of the fractional approach to the electromagnetic theory in the 1990s were done by Nader Engheta. He presented the idea of "fractionalization in electromagnetic" in the 90s, stating that there are continuous intermediate stages between the two canonical states of the electromagnetic field. Since then, several studies have been carried out on scattering problems. In the thesis, using the features of the fractional derivative approach, the intermediate stages of the boundary conditions between the two canonical states will be explained by the means of electric field distribution, radiation pattern, radar cross-sections, and current distribution. However, there are many different geometries in the literature that have not been studied yet by the proposed method. The fractional boundary condition (or integral boundary condition) that corresponds to an intermediate boundary condition between Dirichlet and Neumann boundary conditions is used to describe the scattering properties of different geometries. By determining the fractional-order, scattering properties of different materials are examined in the thesis. The new proposed boundary conditions describe a new material property (between Perfect Electric Conductor (PEC) and Perfect Magnetic Conductor (PMC)). The fractional boundary condition is the generalization of the Dirichlet and Neumann boundary conditions. In this case, the fractional derivative of the tangential component of the total electric field in the direction of the surface normal is zero on the surface of the scatterer. When the fractional-order becomes zero, this corresponds to Dirichlet Boundary Condition whereas, while the fractional-order is equal to one, this means the boundary condition is equal to Neumann Boundary Condition. In the middle, the boundary condition corresponds to different materials between perfectly electric conducting (PEC) and perfectly magnetic conducting (PMC) surfaces. The method for the solution of the diffraction problem satisfying the fractional boundary condition in this thesis is one of the hybrid methods which is employed and developed as presented in Veliev's previous studies. The reason why a hybrid method is preferred is that both analytical and numerical methods have some drawbacks. They have some limitations. Especially, the desired accuracy

and the electrical dimension of the scatterer puts a limit on the applicability of the numerical solution for a specific problem because higher frequency source and electrically large objects require a greater number of discretizing. This yields to demand computation power. On the other hand, analytical methods, in general, are applicable to some finite numbers of geometry. Therefore, hybrid methods are developed to combine the advantageous sides of both analytical and numerical approaches. In analytical methods, some closed expressions can only be obtained for the high-frequency regime whereas Hybrid methods can calculate the field expressions by wider frequency regimes. This property leads to investigating resonances for double strip problems with Hybrid methods. In this thesis, the orthogonal polynomials method is employed to solve the diffraction problems. The main approach to solving the diffraction problem as follows. First, the scattered field is defined as an integral. To obtain this integral, Green's Theorem and Fourier analysis are employed. Then, the total field is forced to satisfy the fractional boundary condition. Then, the integral equation is obtained. For the fractional-order 0.5 case, the problem is solved analytically with some approximation. For the general solution, to solve the integral equation or coupled integral equations (double strip case), the current density on the strips is expressed as the summation of the special orthogonal functions regarding the geometry and edge condition. The current distribution is expanded as the summation of Gegenbauer polynomials with unknown constant coefficients regarding geometry. This manipulation allows one to convert the integral equation into a system of linear algebraic equations with unknown constant coefficients. These coefficients are obtained by employing the orthogonality and other important properties of corresponding orthogonal functions such as Gegenbauer or Laguerre polynomials. After that, numerical experiments and verification are done. To verify these findings, a comparison with another method and previous outcomes are investigated.

KESİRLİ TÜREV YAKLAŞIMIYLA ŞERİTTEN SAÇILMA PROBLEMİNİN ÇÖZÜMÜ

ÖZET

Tezde iki boyutlu ince şerit ve çift şeritlerde kırınım probleminin yeni bir yöntemle çözülmesi amaçlanmıştır. Bu problemlerin mükemmel iletken ve magnetik iletken için çözümleri literatürde vardır. Araştırmanın amacı, problemlere yeni bir yaklaşım geliştirmektir ve genelleştirmektir. Literatürdeki önceki çalışmalarda, belirtilen koşullar altında mükemmel elektriksel veya manyetik iletken şeritlerden veya empedans şeritlerinden saçılma problemleri üzerine çalışmalar mevcuttur. Kesirli türev yöntemi, isminde de belirtildiği gibi, sınır koşullarını genelleştirmemize ve kesirli türev yaklaşımını kullanarak mevcut problemi en genel şekilde çözmemize olanak tanır. Bu araştırma ile literatürdeki mevcut yöntemlere göre daha basit, hesaplaması daha hızlı ve farklı malzemeler için çözülebilen yeni bir yaklaşım tanıtılacaktır. Kesirsel yaklaşım elektromanyetikte 30 yıldır kullanılmaktadır. Genellikle metamalzeme ve hafızalı malzemeler için kullanılan yöntem elektromanyetik alanında birçok bilim insanı tarafından kullanılmaktadır. Elektromanyetik teoriye kesirli yaklaşımın uygulanmasına ilişkin ilk çalışmalar, 1990'larda Nader Engheta tarafından yapılmıştır. Engheta, elektromanyetik alanın iki kanonik durumu arasında sürekli ara aşamalar olduğunu belirterek 90'larda "elektromanyetikte fraksiyonelleşme" fikrini sundu. O zamandan beri saçılma problemleri üzerine çeşitli çalışmalar yapılmıştır.

Tezde, kesirli türev yaklaşımının özellikleri kullanılarak, iki kanonik durum arasındaki sınır koşullarının ara aşamaları; elektrik alan dağılımı, ışıma örüntüsü, radar kesitleri ve akım dağılımı ile açıklanacaktır. Bununla birlikte, literatürde önerilen yöntemle henüz çalışılmamış birçok farklı geometri vardır. Dirichlet ve Neumann sınır koşulları arasındaki bir ara sınır koşuluna karşılık gelen kesirli sınır koşulu (veya integral sınır koşulu), farklı geometrilerdeki yüzeylerin saçılma özelliklerini tanımlamak için kullanılır. Kesir mertebesi belirlenerek, farklı malzemelerin saçılma özellikleri tezde incelenmiştir. Yeni önerilen sınır koşulları, yeni bir malzeme özelliğini (Mükemmel elektrik iletken (PEC), mükemmel manyetik iletken (PMC) veya bunlar arasında) tanımlar. Kesirli sınır koşulu, Dirichlet ve Neumann sınır koşullarının genelleştirilmesidir. Bu durumda, kesirli sınır koşulu kısaca şu şekilde özetlenebilir: toplam elektrik alanın teğetsel bileşeninin yüzey normal yönündeki kesirli türevi, saçıcının yüzeyinde sıfırdır. Kesirli mertebe sıfır olduğunda, bu Dirichlet Sınır Koşuluna karşılık gelirken, kesirli mertebe bire eşitken, sınır koşulunun Neumann Sınır Koşuluna eşit olduğu anlamına gelir. Ortada, sınır koşulu, mükemmel elektrik ileten ve mükemmel manyetik iletken yüzeyler arasındaki farklı malzemelere karşılık gelir.

Çalışmamızda, Veliev'in önceki çalışmalarında sunulduğu gibi melez yöntem kullanılacaktır. Melez yöntem kullanılmasının birtakım sebepleri vardır. Hem analitik hem de sayısal yöntemlerin bazı dezavantajları ve bazı sınırlamaları vardır. Arzu edilen doğruluk ve saçıcının elektriksel boyutu, belirli bir problem için sayısal çözümün uygulanabilirliğine bir sınır getirir çünkü daha yüksek frekans kaynağı ve elektriksel olarak büyük nesneler daha fazla sayıda ayrıklaştırma gerektirir. Bu, hesaplama gücü talebini doğurur. Öte yandan, analitik yöntemler genel olarak bazı sonlu sayıdaki geometriler için uygulanabilir. Bu nedenle, hem analitik hem de sayısal yaklaşımların avantajlı yönlerini birleştirmek için melez yöntemler geliştirilmiştir. Analitik yöntemlerde, bazı kapalı ifadeler yalnızca yüksek frekans rejimi için elde edilebilirken, melez yöntemler, alan ifadelerini daha geniş frekans rejimlerinde hesaplayabilir. Bu özellik, melez yöntemlerle çift şerit problemleri için rezonansların araştırılmasına imkan tanır. Bu tezde, kırınım problemlerini çözmek için ortogonal polinomlar yöntemi kullanılmıştır. Kırınım problemini çözmek için ana yaklaşımı kısaca şöyle ifade edebiliriz. İlk olarak, saçılan alan bir integral olarak tanımlanır. Bu integrali elde etmek için Green Teoremi ve Fourier analizi kullanılır. Ardından, toplam alan, kesirli sınır koşulunu sağlamaya zorlanır. Ardından integral denklem elde edilir. Kesirli mertebeden 0.5 durumu için, problem analitik olarak bazı yaklaşımlarla çözülür. Genel çözüm için, integral denklemi veya kuple integral denklemleri (çift şerit durumu) çözmek için, şeritlerin üzerindeki akım yoğunluğu, geometri ve ayrıt koşulu dikkate alınarak özel ortogonal fonksiyonların toplamı olarak ifade edilir. Buradaki problemlerde, akım dağılımı, geometri ile ilgili bilinmeyen sabit katsayılara sahip Gegenbauer polinomlarının toplamı olarak genişletilir. Bu manipülasyon, integral denklemini, diklik bağıntıları kullanılarak, bilinmeyen sabit katsayılara sahip bir doğrusal cebirsel denklem sistemine dönüştürmeyi sağlar. Katsayıların bulunması, elde edilen lineer denklem sisteminin tersinin alınması ile gerçeklenir.

Çalışmanın tek şerit için ana odağı, şerit üzerindeki akım dağılımını incelemek olup, yapılan çalışmada kesirli derecenin 0.5 olması durumu detaylı olarak incelenmiştir. Bu kesirli türevde akımın yüzey üzerinde diğer derecelere gere daha homojen dağıldığı gözlenmiş olup, dağılıma etki eden en önemli parametrenin, gelen dalganın açısı olduğu gözlenmiştir. Tek şeritten saçılmada, belli yaklaşıklılarla analitik ifadeler elde edilmiş ve önceki yapılmış çalışmalarla kıyaslamalar gerçeklenmiştir. Çizgisel kaynağın, uzak alana yerleştirilmesi ve saçılan alanın uzak alanda incelenmesi için yapılan yaklaşıklıklarla, 0.5 kesirli derece için, analitik ifadeler elde edilmiştir. Aynı zamanda, mükemmel elektriksel iletken tek şerit için, çizgisel kaynaktan saçılan alanın oluşturduğu yüzey akımlarını, Fiziksel Optik ve Momentler Yöntemi ile de modelleyip, bu tezde öne sürülen yöntemle kıyaslaması yapılmıştır. Bulgular, Momentler Yöntemin ve Tezde kullanılan yöntemin, Fiziksel Optiğe göre daha iyi sonuç verdiğini ortaya koymuştur. Önceden belirtildiği gibi, tezde aynı zamanda birbirine paralel, genişlikleri değişebilen çift şeritten saçılma da incelenmiştir. Burada ise ana amaç, oluşan rezonansları gözlemlemek ve analitik sonuçlarla kıyaslamak olmuştur. Bunun için radar kesit alanı incelemeleri yapılmıştır ve saçılan alanda belli dalgaboyları için yüksek artışlar ve doruk noktaları gözlenmiştir. Buradaki dalgaboylarında incelemeler yapıldığında, saçılan alanın değerinde diğer dalgaboylarına göre artış dikkat çekmiştir. Bu dalgaboylarındaki araştırmalarda, kaynaklar şeritlerin arasında olmamasına rağmen, toplam alan şeritler arasında diğer bölgelere kıyasla yüksek değerler almıştır. Bu tür rezonanslar, farklı sınır koşullarına sahip şeritler için önem teşkil etmektedir. Bu çalışmada, kesirli derecenin 0 ile 1 arasındaki değişimine göre, rezonansların genlik değerlerindeki değişimleri ve rezonansların şeritler arasındaki dağılımı detaylı bir şekilde incelenmiştir. Belli şartlar altında, kesirli derecenin 0.5 olduğu durumda, rezonans değerleri diğer kesirli derecelere göre daha yüksek çıktığı gözlenmiştir. Bu kuramsal yüzey, ileride rezonatör, anten veya elektromanyetik dalgaların yönlendirilmesinde kullanılan aletlerin tasarımında kullanılmak için uygun olabileceği düşünülmektedir. Bu tür bir yapı, anten sentezinde, dalga kılavuzlarında ve rezonatör probleminde kullanılabilir. Çalışmanın bir diğer önemli çıktısı ise, kesirli derecenin sıfıra yakın olduğu durumda (0-0.5 arasında), yüzeyin; mükemmel elektrik iletken yüzeye yakın bir karakteristiğe sahip olduğu, kesirli derecenin bire yakın olduğu durumlarda (0.5-1) ise mükemmel manyetik iletken yüzeye yakın bir karakteristiğe sahip olduğu gözlenmiştir.

1. INTRODUCTION

This study contains the investigation of electromagnetic wave diffraction by a single strip and the two-dimensional double-strip. For the double-strip case, some important resonance characteristics and mode analysis are also considered. The surplus-value of the thesis is to solve the two-dimensional diffraction problems for generalized boundary conditions. In the thesis, double strips with different lengths and the same boundary conditions and both different length and boundary conditions are investigated mainly. Also, for the single strip, important outcomes are highlighted for specific cases. Since the diffraction problems are one of the essential and important research areas in the electromagnetic theory and its applications, the solution of the problems are employed in antenna theory, antenna design, guided wave structures, resonators, artificial surface design, and validation of the computation tools specified for electromagnetic waves and its application In the section, the Purpose of the Thesis, Literature Review, and Original Contribution of the Thesis are presented, respectively.

1.1 Purpose of the Thesis

The thesis aims to obtain the mathematical expression and distribution of the electromagnetic field mainly in the vicinity of two-dimensional double strips for different scenarios such as different sizes of strip widths, the variable distance between the strips, the angle of incidence, wavenumber, and the boundary conditions. For the double-strip investigation, the resonances occur for a specific wavenumber. The study for the resonances and validation of the resonance frequencies with different methods are valuable and important scientific research topics because the field distribution at the resonance frequency is critical for different guiding structures (double-strip). In other words, since the different surfaces mean different boundary conditions, a wide range of frequency investigation is required for different boundary conditions. In the thesis, it is aimed to solve the problem of diffraction by two-dimensional thin strip and double strips, with a new method. The actual problems have already solutions for the Dirichlet, Neumann, and Impedance boundary conditions [1]. The purpose of the research is to develop a new approach to the problems and generalize the boundary conditions. In previous studies, perfect electrical or magnetic conducting strips and impedance strips under specified conditions were performed. This method, as stated in its name, allows us to generalize boundary conditions and solve the existing problem in the most general way by using the fractional derivative approach where the fractional-order determines the surface properties. With this research, a new approach will be introduced that is simpler, faster to calculate, and can solve for different materials compared to existing methods in the literature.

The fractional approach has been used in electromagnetics for 30 years [2-4]. The method, which is generally used for metamaterial and materials with memory, is employed by many scientists in the area of electromagnetics. The first study on the implementation of the fractional approach to the electromagnetic theory was done in the 1990s by Engheta. Engheta presented the idea of " fractionalization in electromagnetic " in the 90s, stating that there are continuous intermediate stages between the two canonical states of the electromagnetic field. Since then, several studies have been carried out on scattering problems. In the thesis, using the features of the fractional derivative approach, the intermediate stages of the fields or sources between the two canonical states will be explained [5,6]. However, there are many different geometries in the literature that have not been studied yet by the proposed method. The fractional boundary condition (or integral boundary condition) corresponds to an intermediate boundary condition between Dirichlet and Neumann boundary conditions which is used to describe the scattering properties of different surfaces. By determining the fractional-order, scattering properties of different materials will be examined in the thesis. The new proposed boundary conditions describe a new material property (Perfect Electric Conductor (PEC), Perfect Magnetic Conductor (PMC), or between them) [7,8]. In the thesis, theoretical and numerical results for one strip, two strips will be obtained. In the thesis, the electromagnetic plane wave diffraction of double strips with different widths satisfying the fractional boundary condition is analyzed in detail. Various situations such as different operating frequencies, strip lengths, and fractional order will be studied both theoretically and numerically. Then, solutions obtained by the hybrid method presented in this thesis are compared with other methods (Moments Method and Physical Optics).

1.2 Literature Review

Like all the branches of science such as physics and engineering, electromagnetic theory is built upon mathematical modeling. The models in electromagnetics in general have the unknowns as electric and magnetic fields which are satisfying specific partial differential equations such as the Laplace, Poisson, Helmholtz, and wave equations in general. The main aim is to solve these differential equations and find the unknowns by including radiation, edge, and boundary conditions [9,10]. In other words, the main interest in electromagnetic scattering can be summarized as the following. Under predefined conditions, the problem itself is modeled with mathematics and its tools. Here, the modeling is done by the partial differential equations, integral equations in general. Then, the solution is required. For this, throughout many years, the solution to partial differential equations and the integral equations have been studied by many researchers. The approaches can be categorized by methodology as the following. The solution can be obtained by analytical, numerical-analytical, and numerical methods [9,10]. In the analytical methods, the exact solution of the problem can be obtained whereas the number of the problem which can be solved by analytical methods is very limited since the analytical approach can be applied for only canonical geometries. For the analytical approaches, the following methods can be listed. The separation of variables, series expansion, conformal mapping, and perturbation methods [9]. During the 1960s and 1970s, asymptotic techniques are intensively studied. For the higher frequency regime, the approximate field expressions can be achieved by analytical tools. Well-known examples of these techniques are the Geometrical and Physical Optics, mainly [9,10]. Improved versions of these techniques are namely the Geometrical, Physical, and Uniform Theories of Diffraction. After the 1970s, the fast and enormous developments in computational tools, the numerical methods are developed in a very concrete manner. The main advantage of numerical techniques is to have the ability to employ in any arbitrary shape with the desired accuracy. On the other hand, for the electrically large objects, still, the computation power is challenging nowadays for specific problems and, approximate analytical techniques are employed in such cases in order to overcome challenges. In the numerical, first differential or integral equations are discretized, then, in the time domain or frequency domain, the equation is tried to be solved to find the field distribution over the required region with the given conditions. For this, well-known techniques can be listed as the Method of

Moments (MoM), Finite Element Method (FEM), Finite Difference Time Domain Method (FDTD), and Method of Auxiliary Sources (MAS). Since these techniques require tremendous computation power, the researchers develop a new approach to reduce computation costs. These techniques are the fast multipole method (FMM) (frequency domain), the multi-level fast multipole algorithm (MLFMA) (frequency domain), the plane wave time-domain (PWTD) method (time-domain) [9-11].

Even though the solution approach for different techniques is quite distinct, the purpose always the same. The aim in general is to obtain the scattered field and the induced current due to obstacles. The curiosity and interest due to the existence of the obstacles which are finite or having the edges like in the real-life lead researchers to have studied on the subject, especially in 20^{th} century due to the need for radar technologies, aviation, remote control, and sensing [9].

Due to the progress in microwave communication systems and circuits, electromagnetic waves with high frequency have become the interest of scientists since the 20th century. Note that, for the electromagnetic diffraction, the high frequency is a relative term and corresponds to the incidence wavelength is smaller than the obstacle itself in the region of interest. The questions related to the total field in the vicinity of the obstacles and the distribution of the fields in the region of interest have arisen. Here, the electrically small obstacles, edges, and discontinuities cannot be ignored. The investigation of the total field in the region of interest becomes hard to evaluate. Therefore, a general approach is to divide the problem fundamental parts and to approach them separately. Then, the real problem can be thought of as a combination of canonical problems. This yields to formulate the problem without losing the physical structure of the obstacle and space by solving the diffracted waves in the high-frequency regime asymptotically in general. In other words, the problem reduced to the combination of the canonical problems is in general, a boundary value problem for the Helmholtz equation with mixed boundary conditions [9, 10]. By having the boundary, edge, and radiation condition, the field distribution can be found by employing different techniques such as Wiener Hopf, Orthogonal Polynomials, The geometrical theory of the diffraction, the physical theory of the diffraction and Maliuzhinets, etc. [12-19].

In the 1950s, the analytical solutions for electromagnetic diffraction by some canonical objects such as half-plane, wedge, strips, and cylinders are studied intensively. During the first half of the previous century, all studies done in the electromagnetic diffraction problem consist of perfectly conducting structures such as half-plane, wedge, and cylinder [12-14]. However, in 1952, the first study by Senior is done for the diffraction of an E-polarized plane wave by the metallic half-plane with finite conductance [13,14]. In these studies, the impedance condition, which is the combination of Dirichlet and Neumann boundary conditions, is used. The approach for the solution of the diffraction problem in these studies is to express the scattered field by the re-radiation of the induced current on the surface of the objects which comes from the boundary conditions. For the edges of the object, special treatment is required. The current behavior changes depending on the polarization and the boundary conditions to have a unique solution to the Helmholtz equation. For this, the edge condition is introduced by Senior and Meixner for the asymptotic behavior of the current and also field expression at the edges [14,15,17]. As an example, assume that there is an edge at $x = 0$ for the half-plane located at $y = 0$ and $x \in [0, \infty)$. The electric and magnetic current densities behave as $O(x^{-\frac{1}{2}})$ and $O(x^{\frac{1}{2}})$, respectively for $x \to 0$. By taking account of these facts, the solution for the scattered field and then, the total field can be found uniquely.

After having the solution of the half-plane, wedge, and cylinder structures with different polarization and finite conductance, the researchers seek more complex structures such as aperture, slits, or gratings. To solve these geometries, some approximations and modifications in the solution of the half-plane are employed. They are mainly ignoring the edge-to-edge interaction in the diffraction. Later, the many geometries, such as strip, slit, half-plane, wedge, truncated waveguide, stepped strips with different boundary conditions such as Dirichlet, Neumann Impedance, and Mixed Boundary Conditions are obtained by different types of modified Wiener-Hopf techniques [20-22].

After fast and huge developments in computational technology, many problems in electromagnetic diffraction including non-conical problems, arbitrary shapes, and moving materials are investigated [20-22]. As it is mentioned above, discretizing is the key point of the numerical tools. After that, solving the governing differential or integral equations by applying the required conditions is followed. To solve the equations, in general, a system of linear algebraic equations is solved which required computational power. For example, in the Method of Moments, the surface currents induced on the object are expanded as the summation of the base function and corresponding integral equation obtained by applying the boundary condition. The integral equation includes the unknown coefficients for the current densities. To solve the integral equation, the integral equation is converted into the system of linear algebraic equations. After inversion, the coefficients corresponding to the current density on the surface are obtained. Then, post-processing for the field distributions and other physical characteristics can be achieved [10].

Both analytical and numerical methods have some drawbacks. They have some limitations. Especially, the desired accuracy and the electrical dimension of the scatterer puts a limit on the applicability of the numerical solution for a specific problem because higher frequency source and electrically large objects require a greater number of discretizing. This yields to demand computation power. On the other hand, analytical methods, in general, are applicable to some finite numbers of geometry. Therefore, hybrid methods are developed to combine the advantageous sides of both analytical and numerical approaches. In analytical methods, some closed expressions can only be obtained for the high-frequency regime whereas Hybrid methods can calculate the field expressions by wider frequency regimes. Hybrid methods may have the expression for electrical small, resonance, and electrical large regions by utilizing tools of the analytical and numerical methods under some circumstances [23-26]. For instance, apart from the Method of Moments, the integral equation with an unknown induced current on the finite object can be expanded as the summation of the Chebyshev polynomials including the edge condition. In this way, the convergence of the Chebyshev polynomials will be faster and the requirement of the computation power will be less for the solution with the desired accuracy. After expanding, the orthogonality of the polynomials and Fourier transform properties are employed to find the unknown weighting constant coefficient in the current expansion. Then, the required current density is obtained with the desired accuracy by tuning the truncation in the summation [23-28]. First, Butler and then, Veliev suggest the idea of stating the induced current on the scatterer as the summation of the orthogonal polynomials, which are chosen depending on the geometry of the problem. For instance, for the strip problems, Chebyshev or Gegenbauer polynomials are preferred because the polynomials are defined in a finite region, whereas, in half-plane or wedge problems, Laguerre Polynomial are preferred due to being defined between $[0, \infty)$ [27-29].

In this thesis, the hybrid method will be employed as presented in Veliev's previous studies [26-28,30,31]. The current distribution is expanded as the summation of Gegenbauer polynomials with unknown constant coefficients regarding geometry. Besides, the boundary condition is different from the well-known boundary conditions. Here, the boundary condition is called the fractional boundary condition [30-39]. The fractional boundary condition is the generalization of the Dirichlet and Neumann boundary conditions. In this case, the fractional derivative of the tangential component of the total electric field in the direction of the surface normal is zero on the surface of the scatterer. When the fractional-order becomes zero, this corresponds to Dirichlet Boundary Condition whereas, the fractional-order is one means that the boundary condition is equal to Neumann Boundary Condition. In the middle, the boundary condition corresponds to different materials between perfectly electric conducting and perfectly magnetic conducting surfaces.

The history of the fractional calculus is considerably aged. The differential and integration are assumed to be the same operator for the fractional-order operator. In other words, one unified notation corresponds to both differentiation and integration of arbitrary real order is defined. First, it is argued between famous mathematicians Guillaume de L'Hôpital and Gottfried Wilhelm Leibniz in 1695. However, employing the fractional calculus in fundamental sciences and engineering problems is not as early as the first discussion [39-43]. The huge steps are taken in fractional calculus are in the second half of the 20^{th} century. In the last decades, it is getting widely used in chemical processes, signal processing, finance, economics, electromagnetics, bioengineering, mathematical modeling, and control [39-45]. The main advantage of fractional calculus is to have the ability to explain the hereditary phenomena with memory because the fractional derivative has a non-locality property contrary to the conventional derivative operator. Therefore, such topics related to memory are intensively studied with the fractional calculus. Besides, the cases between two known canonical states are related to the fractional calculus since the intermediate cases between two known states can be analyzed and clarified [41,44,45]. First studies employing the fractional calculus in the electromagnetic theory and its applications were achieved by Nader Engheta [2-4]. In these studies, it has been shown that there are infinite continuous states between two canonical states of the electromagnetic fields. Using the properties and tools of the fractional calculus, the intermediate stages of fields, sources, and operators such as Curl, the divergence between two known states can be depicted [2-4,32]. Furthermore, related to this thesis, the generalization of the boundary condition (Dirichlet and Neumann) for the electromagnetic wave was studied [33-38]. The generalization is achieved by changing the fractional order in the derivative operator from 0 to 1. When the fractional-order (FO) becomes 0, the derivative operator takes the derivative of the total tangential electric field on the surface in the order of zero (i.e. not taking the derivative). This corresponds to the Dirichlet boundary condition. On the other hand, the Neumann boundary condition is obtained when the fractional order is equal to 1. For the fractional-order between 0 and 1, the material is assumed to be between the perfect electric and magnetic conducting surfaces. In [46], the first time, the Wiener-Hopf Technique is used including the fractional boundary condition in the solution of diffraction by the strip. By changing the fractional-order (FO), the investigation of scattering properties of the strip can be obtained.

1.3 The Original Contribution of the Thesis

The thesis focuses on the electromagnetic plane wave diffraction by the parallel-located double strips and single strip. Previously, the electromagnetic plane and cylindrical wave diffraction by single strip, the electromagnetic plane wave by double-strip with the same width and boundary conditions are considered mathematically. In this thesis, for the first time, double strips with variable boundary conditions and widths are taken into account, and one strip with a detailed explanation of the radar cross-section and current distributions. The comparison with the previous findings is included in the study and for future studies, a road map will be given. The comparison with the previous finding and the method moment solution will be presented in the thesis to show the accuracy of the study. For the fractional-order 0.5 case, the field expressions are obtained analytically under the high-frequency regime assumption. Therefore, cylindrical wave diffraction by a single strip in the case of 0.5 fractional order is also included in the thesis because the cylindrical wave diffraction can be validated with previous studies. Also, in the literature, it is the first study of the cylindrical wave diffraction by the strip with the fractional boundary condition.

2. FORMULATION OF THE PROBLEMS

2.1 Fractional Calculus

Before starting the problem statement, it is better to investigate the definition of the fractional derivative and the fractional derivative of the exponential function. The main reason is to focus on the derivative of the exponential function because there is an ability to express the incidence wave and the scattered electromagnetic waves in terms of exponential. Then, the fractional boundary condition on the surface of the scatterer can be satisfied easily if the fractional derivative of the exponential functions is known. In (2.1), the Riemann-Liouville definition of the fractional derivative is given [44,45].

$$D_x^{\alpha} f(x) \stackrel{\text{def}}{=} \frac{1}{\Gamma(1-\alpha)} \frac{d}{dx} \int_{-\infty}^{x} \frac{f(t)}{(x-t)^{\alpha}} dt \tag{2.1}$$

Here, $\Gamma(1-\alpha)$ is the Gamma function, and D_x^{α} is the fractional derivative operator which states that the derivative is taken with respect to x in the order of α which is between $(0,1)$ including the edges.

To solve the diffraction problem, the boundary value problem needs to be solved where the boundary condition is the fraction boundary condition [7,8]. The fractional boundary condition, which requires the fractional derivative of the total tangential field component with respect to the direction of the surface normal, is the generalization of the Dirichlet and Neumann boundary conditions. Then, it is important to obtain the fractional derivative of the exponential function e^{-ikx} where i is equal to $\sqrt{-1}$ (imaginary unit) and k is a real number. It is time to find the expression when $f(x) = e^{-ikx}$.

First, it is required to apply the change of variable as $x - t = u$. Note that, in the integrand of (2.1), t is a dummy variable.

$$D_x^{\alpha} f(x) = \frac{d^{\alpha} f(x)}{dx^{\alpha}} = \frac{1}{\Gamma(1-\alpha)} \frac{d}{dx} \int_{0}^{\infty} \frac{f(x-u)}{u^{\alpha}} du \tag{2.2}$$

After having (2.2), put $f(x) = e^{-ikx}$ in the same equation.

$$\frac{d^\alpha e^{-ikx}}{dx^\alpha} = \frac{1}{\Gamma(1-\alpha)}\frac{d}{dx}\int_0^\infty \frac{e^{-ik(x-u)}}{u^\alpha}du$$

$$= \frac{1}{\Gamma(1-\alpha)}\frac{d}{dx}e^{-ikx}\int_0^\infty \frac{e^{iku}}{u^\alpha}du$$

$$= \frac{1}{\Gamma(1-\alpha)}(-ik)e^{-ikx}\int_0^\infty \frac{e^{iku}}{u^\alpha}du \tag{2.3}$$

For simplicity, call $I = \int_0^\infty \frac{e^{iku}}{u^\alpha}du$.

After defining I, the change of variable $\left(u = \frac{iy}{k}\right)$ is required to make a resemblance between function I and Gamma function.

Then, I becomes as

$$I = \left(\frac{1}{-ik}\right)^{-\alpha+1}\int_0^{-i\infty} e^{-y}y^{-\alpha}dy \tag{2.4}$$

For further manipulation, it is better to express the definition of Gamma Function (Γ) which is given in (2.5).

$$\Gamma(x) = \int_0^\infty y^{x-1}e^{-y}dy \tag{2.5}$$

Then, $\Gamma(1-\alpha) = \int_0^\infty e^{-y}y^{-\alpha}dy$.

Note that, the integral part of I in (2.4) and $\Gamma(1-\alpha)$ have the same integrand. Here, we have the same integral but with different boundaries. As we know from Complex Integral, We can choose a closed-loop and if there is no singularity inside, the closed-loop integral is zero from Cauchy's Principle on the complex plane [47,48]. Due to having $0 < \alpha < 1$, there is a singularity at zero. In Figure 2.1, we can see the integration path. Here, path 2 stands for the path of Gamma function by definition with the argument $(1-\alpha)$. Note that, the reverse direction of path 1 is needed for our purpose (the integral I).

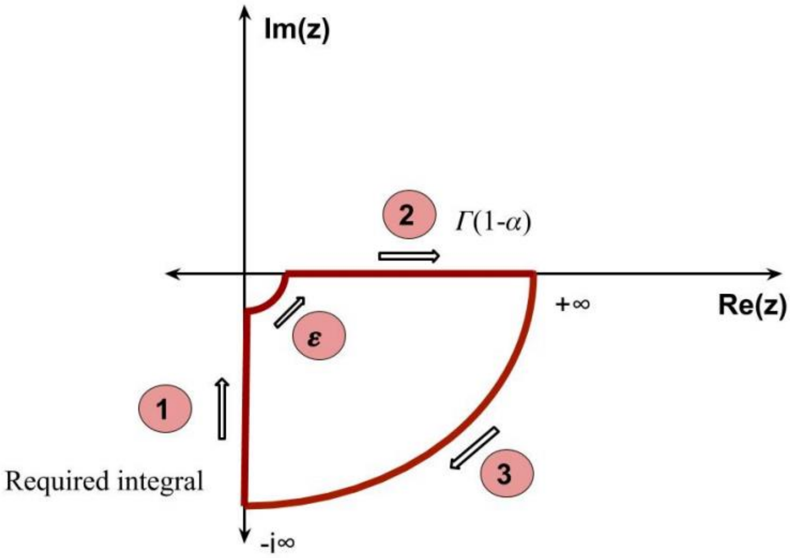

Figure 2.1 : Integration Path.

From Cauchy's Principle [47,48],

$$\oint e^{-z} z^{-\alpha} dz = \int_1 e^{-z} z^{-\alpha} dz + \int_2 e^{-z} z^{-\alpha} dz + \int_3 e^{-z} z^{-\alpha} dz + \int_\epsilon e^{-z} z^{-\alpha} dz = 0 \tag{2.6}$$

From Jordan Theorems [47,48]:

$$\lim_{z \to 0} z f(z) = 0\,, \quad then \quad \int_\epsilon f(z) dz = 0$$

$$\lim_{z \to \infty} z f(z) = 0\,, \quad then \quad \int_3 f(z) dz = 0$$

By Jordan Theorems, $\int_\epsilon e^{-z} z^{-\alpha} dz$ and $\int_3 e^{-z} z^{-\alpha} dz$ go to zero. Then,

$$\int_1 e^{-z} z^{-\alpha} dz = -\int_2 e^{-z} z^{-\alpha} dz \tag{2.7}$$

Note that $\int_2 e^{-z} z^{-\alpha} dz = \Gamma(1-\alpha)$ and $\int_1 e^{-z} z^{-\alpha} dz = -I$

This yields that

$$\frac{d^\alpha e^{-ikx}}{dx^\alpha} = \frac{1}{\Gamma(1-\alpha)} (-ik) e^{-ikx} \left(\frac{1}{-ik}\right)^{-\alpha+1} \int_0^{-i\infty} e^{-y} y^{-\alpha} dy$$

$$= \frac{1}{\Gamma(1-\alpha)} (-ik)^\alpha e^{-ikx} \Gamma(1-\alpha) \tag{2.8}$$

$$= (-ik)^{\alpha} e^{-ikx}$$

As it is seen in (2.8), the fractional derivative of the exponential function is obtained. With this property, one can obtain the fractional derivative of an exponential function without going through the formal definition given in (2.1).

2.2 Double-strips with the Same Boundary Conditions

In this section, the plane wave diffraction by double-strips satisfying the same boundary condition is investigated. Here, there exist two strips located parallel with respect to the x-axis with different widths. They are two-dimensional structures. In other words, the strips have infinite lengths on the z-axis and infinitesimal height on the y-axis. The width of the strips are $2a_1$ and $2a_2$ respectively. In Figure 2.2, the geometry of the problem is given. Due to having the infinite extension in the z-axis, the problem has no dependency on the z-axis. Therefore, the field distributions are the function of (x, y).

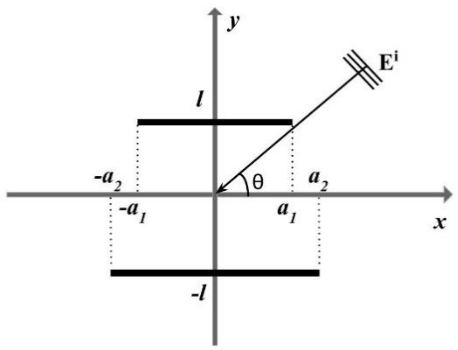

Figure 2.2 : The geometry of the problem.

The excitation is done by $E_z^i = e^{-ik(x\cos\theta + y\sin\theta)}$ which is called the incidence electric field. Here, k is the wavenumber and θ is the angle of incidence. Note that, the incidence electric field has only z-directed field component. In other words, the incidence wave is said to be E-polarized. The total electric field can be written as the summation of the incidence and the components of the scattered fields as $E_z = E_z^i + E_z^s$ where E_z is the total electric field and E_z^s stands for the scattered field. Note that, it should be highlighted that, the scattering field has two components resulting from the upper and lower strips in the space, respectively. These corresponding fields result from the induced currents on each strip. In other words, $E_z^s(x, y) = E_z^{s1}(x, y) + E_z^{s2}(x, y)$ where $E_z^{s1}(x, y)$ stands for the scattered field from the upper strip and

$E_z^{s2}(x,y)$ corresponds to the scattered field from the lower strip [5,35,37]. Before going through mathematical manipulations, it is better to highlight that throughout the formulation, the time dependency is $e^{-i\omega t}$ where ω is the angular frequency (rad/sec). Due to having a sinusoidal excitation, throughout the solution, time dependency is omitted. After defining the notation and the mathematical expression for the incidence wave, the boundary condition needed to be mentioned. In the fractional boundary condition, the fractional derivative of the total tangential electric field component with respect to the dimensionless parameter of ky should be zero on the scatterer surface. Here y-direction is the normal direction of the strips as given in (2.9) [5,35,37]. The fractional boundary condition (FBC) is the generalization of the Dirichlet and Neumann boundary conditions. For different values of fractional order α, the boundary condition is changing which leads to having surfaces with different features.

$$D_{ky}^{\alpha} E_z(x,y) = 0, y \to \pm l, x \in (-a_i, a_i), i = 1,2 \tag{2.9}$$

where α is a fractional-order (FO). Here, fractional derivative in (2.9) D_{ky}^{α} is the fractional derivative operator and the derivative is taken with respect to ky in the order of α. It is better to express again the fractional derivative operator, here for the sake of completeness. The formal expression of the fractional derivative for the Riemann-Liouville definition is given in (2.10) [34-38].

$$D_y^{\alpha} f(y) = \frac{1}{\Gamma(1-\alpha)} \frac{d}{dy} \int_{-\infty}^{y} \frac{f(t)}{(y-t)^{\alpha}} dt \tag{2.10}$$

where, $\Gamma(1-\alpha)$ is Gamma Function and, $\alpha \epsilon (0,1)$.

When $\alpha = 0$, the surface stands for the perfect electric conductor (PEC). On PEC, the total tangential electric field vanishes. When $\alpha = 1$, it corresponds to the Perfect Magnetic Conductor (PMC). The total tangential magnetic field becomes zero in that case or the normal derivative of the electric field vanishes. For FO between $0 < \alpha < 1$, FBC coincides with the intermediate case between the PEC and PMC [34-38].

Previous studies indicate that when fractional order is between 0 and 1, the strip has an imaginary impedance which we can call fractional impedance [30,31], and the relation between the fractional-order and approximate fractional impedance can be found with the following formula $\eta_\alpha = -\frac{i}{\sin\theta} tan\left(\frac{\pi}{2}\alpha\right)$ for any incidence angle. Also, it is easily found that the relation between the fractional-order and the fractional impedance can be deduced from the previous formula as $\alpha = \frac{1}{i\pi}\ln\left(\frac{1-\eta_\alpha sin\theta}{1+\eta_\alpha sin\theta}\right)$ [34-38]. Note that, there η_α corresponds to the relative impedance of the one strip. It should be highlighted that the formula for expressing the relation between the relative impedance and the fractional-order is an approximate formula and obtained for the electrically large strips [30,31].

To go further, the scattered electric field for each strip can be written as the convolution of the current density with Green's function as given in (2.11). Note that here, $G^\alpha(x-x', y_j)$ is the fractional green function and $f_j^{1-\alpha}(x')$ is the fractional current density which has only non-zero values on the strips [30,31]. Physically, (2.11) states that all the induced current on the strip is summed to find the overall effect of the corresponding scatterer in the space.

$$E_z^{sj}(x,y) = \int_{-\infty}^{\infty} f_j^{1-\alpha}(x') G^\alpha(x-x', y_j) dx', \quad j = 1,2, \; y_1 = y - l, \; y_2 = y + l, \tag{2.11}$$

where,

$$G^\alpha(x-x', y) = i\frac{1}{4\pi} D_{ky}^\alpha \int_{-\infty}^{\infty} e^{ik\left[q(x-x')+|y|\sqrt{1-q^2}\right]} (1-q^2)^{\frac{\alpha-1}{2}} dq.$$

Here, $j = 1,2$ corresponds to upper or lower strip, respectively and $G^\alpha(x-x', y) = -\frac{i}{4} D_{ky}^\alpha H_0^{(1)}\left(k\sqrt{(x-x')^2+y^2}\right)$ [5, 8]. Note that, $H_0^{(1)}(z)$ is the Hankel function of the first kind and zero-order. The reason why the plane wave expansion of the Hankel function is employed is to have the ability to take the fractional derivative of the exponential functions easily as mentioned in the previous section. If the fractional Green's function expression is put into (2.11) and represent $f_j^{1-\alpha}(x')$ with its corresponding Fourier transform $F_j^{1-\alpha}(q)$ as it is accomplished in the works [8-10], (2.12) is obtained.

$$E_z^{sj}(x,y) = -i\frac{e^{\pm i\frac{\pi}{2}\alpha}}{4\pi}\int_{-\infty}^{\infty} F_j^{1-\alpha}(q)e^{ik\left(xq+|y_j|\sqrt{1-q^2}\right)}(1-q^2)^{\frac{\alpha-1}{2}}dq, \tag{2.12}$$

where, $y_1 = y - l,\ \ y_2 = y + l, j = 1,2$ and

$$F_j^{1-\alpha}(q) = \int_{-1}^{1} \widetilde{f_J}^{1-\alpha}(\xi)e^{-i\varepsilon q\xi}d\xi,$$

$$\widetilde{f_J}^{1-\alpha}(\xi) = \frac{\varepsilon_j}{2\pi}\int_{-\infty}^{\infty} F_j^{1-\alpha}(q)e^{i\varepsilon_j q\xi}dq,$$

$\widetilde{f_J}^{1-\alpha}(\xi) = af_j^{1-\alpha}(\xi),\ \ \epsilon_j = ka_j,\ \xi = \frac{x}{a_j}$.

Note that, (2.11) and (2.12) satisfy the Helmholtz equation and Sommerfeld radiation condition at the infinity [30,31]. After expressing the incidence and the scattered electric fields in a mathematical form, the FBC is applied for each strip. First, the FBC is applied on the upper strip for each field component as

$$D_{ky}^{\alpha}E_z^{i}(x,y)|_{y_1=0} = D_{ky}^{\alpha}e^{-ik(xcos\theta+(y_1+l)sin\theta)}|_{y_1=0}$$
$$= (-i)^{\alpha}e^{-ik(xcos\theta+lsin\theta)}\sin^{\alpha}\theta$$

$$D_{ky}^{\alpha}E_z^{s1}(x,y)|_{y_1=0} = -i\frac{e^{-i\frac{\pi}{2}\alpha}(-i)^{\alpha}}{4\pi}\int_{-\infty}^{\infty} F_1^{1-\alpha}(q)e^{ikxq}(1-q^2)^{\alpha-1/2}dq$$

$$D_{ky}^{\alpha}E_z^{s2}(x,y)|_{y_1=0} = -i\frac{e^{+i\frac{\pi}{2}\alpha}(i)^{\alpha}}{4\pi}\int_{-\infty}^{\infty} F_2^{1-\alpha}(q)e^{ik\left(xq+2l\sqrt{1-q^2}\right)}(1-q^2)^{\alpha-\frac{1}{2}}dq$$

(2.13)

Then, (2.14) is obtained by employing (2.9).

$$\int_{-\infty}^{\infty} F_1^{1-\alpha}(q)e^{ikxq}(1-q^2)^{\alpha-\frac{1}{2}}dq$$
$$= -i4\pi e^{+i\frac{\pi}{2}\alpha}e^{-ik(xcos\theta+lsin\theta)}\sin^{\alpha}\theta$$
$$-e^{+2\pi i\alpha}\int_{-\infty}^{\infty} F_2^{1-\alpha}(q)e^{ik\left(xq+2l\sqrt{1-q^2}\right)}(1-q^2)^{\alpha-\frac{1}{2}}dq \tag{2.14}$$

The same procedure is applied for the lower strip as

$$D_{ky}^{\alpha}E_z^{i}(x,y)|_{y_2=0} = D_{ky}^{\alpha}e^{-ik(xcos\theta+(y_2-l)sin\theta)}|_{y_2=0}$$

$$= (-i)^{\alpha}e^{-ik(xcos\theta-lsin\theta)}\sin^{\alpha}\theta$$

$$D_{ky}^{\alpha}E_z^{s2}(x,y)|_{y_2=0} = -i\frac{e^{+i\frac{\pi}{2}\alpha}(i)^{\alpha}}{4\pi}\int_{-\infty}^{\infty}F_2^{1-\alpha}(q)e^{ikxq}(1-q^2)^{\alpha-1/2}dq$$

$$D_{ky}^{\alpha}E_z^{s1}(x,y)|_{y_2=0} = -i\frac{e^{-i\frac{\pi}{2}\alpha}(-i)^{\alpha}}{4\pi}\int_{-\infty}^{\infty}F_1^{1-\alpha}(q)e^{ik\left(xq+2l\sqrt{1-q^2}\right)}(1-q^2)^{\alpha-\frac{1}{2}}dq \tag{2.15}$$

Then, (2.16) is obtained by employing (2.9).

$$\int_{-\infty}^{\infty}F_2^{1-\alpha}(q)e^{ikxq}(1-q^2)^{\alpha-\frac{1}{2}}dq = -i4\pi e^{-i\frac{3\pi}{2}\alpha}e^{-ik(xcos\theta-lsin\theta)}\sin^{\alpha}\theta$$
$$-e^{-2\pi i\alpha}\int_{-\infty}^{\infty}F_1^{1-\alpha}(q)e^{ik\left(xq+2l\sqrt{1-q^2}\right)}(1-q^2)^{\alpha-\frac{1}{2}}dq \tag{2.16}$$

After applying the FBC to the total field and multiplying both sides of the integral equation with $\int_{-a_i}^{a_i}e^{-ikx\tau}\,dx$ for each corresponding strip, the integral equation system becomes as (2.17) where for $i=1$, upper sign, and for $i=2$, the lower sign should be taken into account. Different signs in the exponentials ($e^{\mp iklsin\theta}$) stand for the upper and lower strip, respectively. However, for $(\pm i)$ which is resulting from the fractional boundary condition, (+) sign is taken for the upper part of each strip and the (–) sign stands for the lower part of each strip due to the absolute value operator in the integrand. For each strip, there exists one integral equation. When (2.17) is investigated, the left-hand side of the integral equation stands for the scattered field due to the corresponding strip whereas, the last term at the right-hand side of the integral equation stands for the interaction term corresponding to the effect of the scattering field due to the other strip. Finally, the first term at the right-hand side of (2.17) is for incidence wave.

$$\int_{-\infty}^{\infty} F_i^{1-\alpha}(q)\frac{\sin\left(ka_i(q-\tau)\right)}{(q-\tau)}(1-q^2)^{\alpha-\frac{1}{2}}dq$$

$$= -i4\pi(\pm i)^{\alpha}e^{\mp iklsin\theta}\sin^{\alpha}\theta\frac{\sin(ka_i(\tau+cos\theta))}{(\tau+cos\theta)} -$$

$$-\int_{-\infty}^{\infty} F_j^{1-\alpha}(q)\frac{\sin\left(ka_\iota(q-\tau)\right)}{(q-\tau)}e^{ik2l\sqrt{1-q^2}}(1-q^2)^{\alpha-\frac{1}{2}}dq \qquad (2.17)$$

Here, $i,j = 1,2,\ i \neq j$

After having (2.17), it is required to solve the integral equations for each strip. To solve the set of integral equations (IE) in (2.17), the fractional current density should be expressed as the summation of special orthogonal polynomials by taking into account the edge conditions. IE can be reduced to the system of linear algebraic equation (SLAE) by expanding the fractional current density as the summation of Gegenbauer polynomials C_n^{α} with the unknown constant coefficients $\zeta_{n_i}^{\alpha}$ as given in (2.18) [17,34-38,49]. The reason why Gegenbauer polynomials are employed is that they are defined in a finite interval which is suitable for the strip geometry. For different geometries, optimum and suitable polynomials can vary. To have better convergence and edge condition satisfaction, weightings can be included for the expression of the current density function. Note that, the weighting function $(1-\xi_i^2)^{\alpha-\frac{1}{2}}$ in the equation is not only for satisfying the edge condition and also for increasing the convergence [34]. The details of the edge condition are expressed in Appendix A [17,34-38,49].

$$\tilde{f}_i^{1-\alpha}(\xi_i) = (1-\xi_i^2)^{\alpha-\frac{1}{2}}\sum_{n=0}^{\infty}\zeta_{n_i}^{\alpha}\frac{C_n^{\alpha}(\xi_i)}{\alpha} \qquad (2.18)$$

Note that $\zeta_{n_i}^{\alpha}$ is the unknown constant coefficients. Keep in mind that $\lim_{\alpha\to 0}\frac{C_n^{\alpha}(\xi_i)}{\alpha} = \begin{Bmatrix}\frac{2}{n}T_n(\xi_i), n\neq 0\\ 1,\ n=0\end{Bmatrix}$ [31,32]. Here, T_n is the Chebyshev polynomials. The corresponding Fourier transform [50]. Also, the derivation can be found in Appendix B:

$$F_i^{1-\alpha}(q) = \frac{2\pi}{\Gamma(\alpha+1)}\sum_{n=0}^{\infty}(-i)^n\zeta_{n_i}^{\alpha}\beta_n^{\alpha}\frac{J_{n+\alpha}(\epsilon_i q)}{(2\epsilon_i q)^{\alpha}}\ , \qquad (2.19)$$

where,

$$\epsilon_i = ka_i\ ,\ \ \beta_n^\alpha = \frac{\Gamma(n+2\alpha)}{\Gamma(n+1)}\ , \qquad i = 1,2.$$

Note that, $J_{n+\alpha}(x)$ is the Bessel function. Then, (2.19) is inserted in (2.17) for each integral equation corresponding to the upper and lower strips.

$$\frac{2\pi}{\Gamma(\alpha+1)}\sum_{n=0}^{\infty}(-i)^n\zeta_{n_i}^\alpha\beta_n^\alpha \int_{-\infty}^{\infty}\frac{J_{n+\alpha}(\epsilon_i q)}{(2\epsilon_i q)^\alpha}\,\frac{\sin\big(ka_i(q-\tau)\big)}{(q-\tau)}\,(1-q^2)^{\alpha-\frac{1}{2}}dq$$

$$= -i4\pi e^{+i\frac{\pi}{2}\alpha}e^{\mp iklsin\theta}\sin^\alpha\theta\,\frac{\sin(ka_i(\tau+cos\theta))}{(\tau+cos\theta)}$$

$$-\frac{2\pi}{\Gamma(\alpha+1)}\sum_{n=0}^{\infty}(-i)^n\zeta_{n_j}^\alpha\beta_n^\alpha \int_{-\infty}^{\infty}\frac{J_{n+\alpha}\big(\epsilon_j q\big)}{\big(2\epsilon_j q\big)^\alpha}\,\frac{\sin\Big(ka_j(q-\tau)\Big)}{(q-\tau)}\,e^{ik2l\sqrt{1-q^2}}(1 - q^2)^{\alpha-\frac{1}{2}}dq \qquad (2.20)$$

where $i,j = 1,2$, and $i \neq j$.

After multiplying (2.20) by $\frac{J_{k+\alpha}(\epsilon_1\tau)}{\tau^\alpha}$ and $\frac{J_{k+\alpha}(\epsilon_2\tau)}{\tau^\alpha}$ for each strip, respectively and then, (2.20) is integrated with parameter τ between $(-\infty,\infty)$, overall results for the upper and lower strips become as

$$\sum_{n=0}^{\infty}(-i)^n\zeta_{n_i}^\alpha\beta_n^\alpha C_{kn}^{\alpha\ (i,i)} + \left(\frac{\epsilon_i}{\epsilon_j}\right)^\alpha\sum_{n=0}^{\infty}(-i)^n\zeta_{n_j}^\alpha\beta_n^\alpha C_{kn}^{\alpha\ (i,j)} = \gamma_k^{i,\alpha} \qquad (2.21)$$

Here, $i,j = 1,2\ \ i \neq j$, and

$$C_{kn}^{\alpha\ (i,i)} = \int_{-\infty}^{\infty} J_{n+\alpha}(\epsilon_i q)J_{k+\alpha}(\epsilon_i q)\,\frac{(1-q^2)^{\alpha-\frac{1}{2}}}{q^{2\alpha}}dq,$$

$$C_{kn}^{\alpha\ (i,j)} = \int_{-\infty}^{\infty} J_{n+\alpha}\big(\epsilon_j q\big)J_{k+\alpha}(\epsilon_i q)\,e^{ik2l\sqrt{1-q^2}}\frac{(1-q^2)^{\alpha-\frac{1}{2}}}{q^{2\alpha}}dq\,, i \neq j,$$

$$\gamma_k^{i,\alpha} = -i2(\pm i)^\alpha(2\epsilon_i)^\alpha\Gamma(\alpha+1)e^{\mp iklsin\theta}\,tan^\alpha\theta\,(-1)^k J_{k+\alpha}(\epsilon_i cos\theta).$$

Note that, during integration, the following property is utilized [31,50].

$$\frac{1}{\pi}\int_{-\infty}^{\infty}\frac{J_{n+\alpha}(\epsilon q)}{q^\alpha}\frac{\sin\epsilon(q\mp\beta)}{q\mp\beta}dq = (\pm 1)^n\frac{J_{n+\alpha}(\epsilon\beta)}{\beta^\alpha}$$

After having (2.21), the unknowns $\zeta_{n_i}^{\alpha}$ and $\zeta_{n_j}^{\alpha}$ can be found by the inversion of SLAE. Then, by utilizing (2.18) and (2.19), the current density on the strips and the scattered electric field distribution can be obtained. Note that, for the fractional-order $\alpha = 0.5$ case, the approximate analytical solution can be found for $ka_i \gg 1$ [34-38]. In (2.16), the term $(1-q^2)^{\alpha-\frac{1}{2}}$ is dropped for $\alpha = \frac{1}{2}$ and the term $\frac{\sin(ka_i(q-\tau))}{(q-\tau)}$ behaves like a Dirac delta function for $ka_i \gg 1$. This leads to having the Fourier Transform of the current density directly with an approximation. In (2.17), the analytical expression of the Fourier transform of the current density for $ka_i \gg 1$ is given.

$$F_i^{0.5}(\tau) = \Delta\left(\frac{\left(\frac{\sin(ka_i(\tau+cos\theta))}{(\tau+cos\theta)}e^{\mp iklsin\theta}\right)}{\left[1-e^{ik4l\sqrt{1-\tau^2}}\right]} - \frac{\left(\frac{\sin(ka_j(\tau+cos\theta))}{(\tau+cos\theta)}e^{\pm iklsin\theta}e^{ik2l\sqrt{1-\tau^2}}\right)}{\left[1-e^{ik4l\sqrt{1-\tau^2}}\right]}\right) \quad (2.22)$$

Here, $\Delta = -i4e^{\frac{i\pi}{4}}\sqrt{sin\theta}$, $i,j = 1,2,$ and $i \neq j.$

Having the expressions for $F_i^{1-\alpha}$ in (2.15), the radiation pattern of the total scattered field in the far zone can be found by using (2.23) by the steepest descent method [51,52]. The formulation can be found in Appendix C. Note that, $\rho = \sqrt{x^2+y^2}$ and φ is the angle between the $\hat{e}_\rho$ unit vector along in ρ and $\hat{e}_x$.

Using the steepest descent method for $ka \to \infty$, the scattered electric field gets the following form (detail can be found in Appendix C):

$$E_z^s(x,y) = A(kr)\,\Phi^\alpha(\varphi) \quad (2.23)$$

Here,

$$A(kr) = \sqrt{\frac{2}{\pi kr}}e^{ikr-\frac{i\pi}{4}}, \text{ and } \Phi^\alpha = \Phi_1^\alpha(\varphi) + \Phi_2^\alpha(\varphi),$$

where

$$\Phi_1^\alpha(\varphi) = -\frac{i}{4}e^{\pm\frac{i\pi\alpha}{2}}F_1^{1-\alpha}(cos\varphi)(\sin^\alpha\varphi)e^{-iklsin\varphi},$$

$$\Phi_2^\alpha(\varphi) = -\frac{i}{4} e^{\pm\frac{i\pi\alpha}{2}} F_2^{1-\alpha}(cos\varphi)(\sin^\alpha\varphi) e^{+iklsin\varphi}.$$

In (2.23), ϕ is the observation angle in the space in the cylindrical coordinates. The upper sign stands for $\varphi \in [0,\pi]$, and the lower sign is for $\varphi \in [\pi, 2\pi]$. Here, $A(kr)$ and $\Phi^\alpha(\varphi)$ is the radial and the angular parts of the scattered electric field at the far zone, respectively. For the angular variation at the far zone, the expression of radiation pattern (RP) $\Phi^\alpha(\varphi)$ is used. To analyze the resonance characteristics of the scattered field, (2.24) will be used for total radar cross-section estimation. Total Radar Cross Section (σ_t) can be obtained as [53]

$$\sigma_t = \frac{1}{4\epsilon_1} \int_0^{2\pi} |\Phi^\alpha|^2 d\varphi \tag{2.24}$$

Here, for the normalization, the upper strip is chosen $\left(\frac{1}{4\epsilon_1}\right)$.

To investigate the power flow in the vicinity of the scatterer, the Poynting vector $\vec{S}$ is found. As the electric field has only the z component, $\vec{S}$ has x and y components S_x and S_y, respectively and can be found as (2.25) [51,52].

$$S = \frac{1}{2} Re[\vec{E} \times \vec{H}^*],\ S_x = -\frac{1}{2} Re\left[E_z H_y^*\right],\quad S_y = \frac{1}{2} Re[E_z H_x^*]. \tag{2.25}$$

Here, ($\times$) is a cross product, (*) denotes complex conjugate and $\vec{H}$ is the magnetic field.

2.3 Double-strips with Different Boundary Conditions

This section is the continuation of the previous section. Here, also fractional order of each strip is variable. In other words, the boundary condition for each strip can differ. As it was in the previous section, the strips have infinite lengths on the z-axis, infinitesimal height on the y-axis, and the distance between the strips is $2l$. In Figure 2.3, the geometry of the problem is presented. The upper and the lower strip has a width of $2a_1$ and $2a_2$ and located at $y = l$, and $y = -l$, respectively. This is a more general solution of electromagnetic plane wave diffraction by double strips with variable widths and boundary conditions.

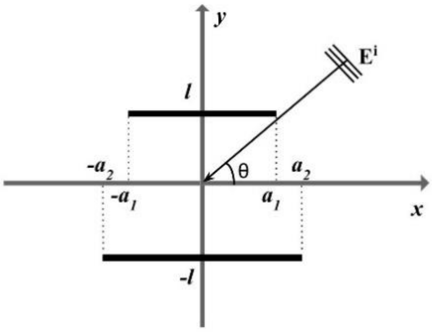

Figure 2.3 : The geometry of the problem.

After expressing the geometry of the problem, again, the definition of the fractional boundary condition which is the generalization of Dirichlet and Neumann Boundary Conditions is done more formally. The fractional boundary condition (FBC) is defined by the fractional derivatives of the tangential electric field components $U(x, y)$ on an infinitely thin surface S located in the plane $y = \pm l$ in the direction of normal of the surface. FBC, mathematically, defined as [34-38]

$$D_y^{\alpha} U(x, y)\Big|_{y \epsilon S} = 0, \quad y \to \pm l \tag{2.26}$$

In this section, as the incidence wave, the uniform plane wave is investigated. The mathematical expression for the incidence wave can be represented as $e^{-ik(xcos\theta + ysin\theta)}\hat{e}_z$ where k is the wavenumber in the free space $\left(k = \frac{2\pi}{\lambda}\right)$, θ is the angle of incidence, $\hat{e}_z$ is the unit vector directed through the z-axis and λ is the wavelength. $E_z\hat{e}_z$ is the total electric field in the space and the total tangential field satisfies the fractional boundary condition on the surface. In our problem, the total electric field is already tangential to the strips [34-38]. For our problem, the boundary condition is a fractional boundary condition and the total field on the surface is required to satisfy the boundary condition. The fractional-order for the boundary condition is defined in the range of $0 \leq \alpha_i \leq 1$ as

$$D_{ky}^{\alpha_i} E_z(x, y_j) = 0 \tag{2.27}$$

For: $y_j \to 0, x \in [-a_i, a_i]$

Here, i takes the value of 1 and 2 correspondence with the upper strip and the lower strips, respectively. Each strip has its own different boundary conditions regarding α_i. For example, one strip may be the perfectly electric conducting surface whereas the other one could be the perfectly magnetic conducting surface or vice versa. Another important point here is that the derivative is taken with respect to ky which is a dimensionless parameter where y is the normal direction of the surface. Due to having two strips leading to two corresponding scattering fields, the total field has three components as the following.

$$E_z(x,\mathrm{y}) = E_z^{\mathrm{i}}(x,\mathrm{y}) + E_z^{s1}(x,\mathrm{y}) + E_z^{s2}(x,\mathrm{y}) \tag{2.28}$$

In (2.28), $E_z^{s1}(x,y)$ and $E_z^{s2}(x,y)$ correspond to the scattered fields for the upper and the lower strips, respectively. The total scattered electric field is denoted as $E_z^{s}(x,y)$ and is the sum of two parts, as mentioned above. Before going into details, time dependency should be highlighted again to proceed easily. Here, the incidence wave is a sinusoidal signal and, the dependency on time throughout the study is determined as $e^{-i\omega t}$. We can express the scattered field as the convolution of the current density on the strip with the fractional Green's function. This yields to find the scattered electric field of the corresponding strips. The mathematical expression is given in (2.29) [5-7].

$$E_z^{sj}(x,y) = \int_{-\infty}^{\infty} f_j^{1-\alpha_j}(x')G^{\alpha_j}\left(x-x',y_j\right)dx', \;\; j=1,2, y_1 = y-l, y_2 = y+l, \tag{2.29}$$

where, $G^{\alpha_j}(x-x',y) = -\frac{i}{4}D_{ky}^{\alpha_j}H_0^{(1)}\left(k\sqrt{(x-x')^2+y^2}\right)$.

Here, $f^{1-\alpha_j}(x')$ is the fractional surface current density on the strip. In (2.29), $j=1,2$ stands for the upper or lower strip, respectively. Note that, $G^{\alpha_j}(x-x',y)$ is the fractional Green's function which is, in the two-dimensional case (for this problem); $H_0^{(1)}(z)$ is the Hankel function of the first kind and zero-order. Due to the requirement of taking derivative, it is better to express the functions in terms of the exponential function because its fractional derivative is easier. Therefore, the plane wave expansion of the Hankel function is employed as given in (2.30).

$$G^{\alpha}(x-x',y) = -i\frac{1}{4\pi}D_{ky}^{\alpha}\int_{-\infty}^{\infty} e^{ik\left[q(x-x')+|y|\sqrt{1-q^2}\right]}(1-q^2)^{\frac{\alpha-1}{2}}dq. \tag{2.30}$$

$$= -i\frac{\pm i}{4\pi}\int_{-\infty}^{\infty} e^{ik\left[q(x-x')+|y|\sqrt{1-q^2}\right]}(1-q^2)^{\alpha-\frac{1}{2}}dq.$$

where, + (-) for y >0 ($y < 0$).

Then, (2.30) is put into (2.31) and Fourier transforms properties are used to obtain the final form of the scattered electric field expression for each strip [34-38].

$$E_z^{sj}(x,y) = -\frac{e^{\pm\frac{i\pi}{2}\alpha_j}}{4\pi} i \int_{-\infty}^{\infty}\int_{-\infty}^{\infty} f_j^{1-\alpha_j}(x')e^{ik\left[q(x-x')+|y|\sqrt{1-q^2}\right]}(1-q^2)^{\alpha_j-\frac{1}{2}}dq\ dx' \tag{2.31}$$

where $j = 1,2,\ y_1 = y - l, y_2 = y + l,$

$$F_j^{1-\alpha_j}(q) = \int_{-1}^{1} \tilde{f}_j^{1-\alpha_j}(\xi)e^{-i\varepsilon_j q\xi}d\xi,\ \tilde{f}_j^{1-\alpha_j}(\xi) = \frac{\varepsilon_j}{2\pi}\int_{-\infty}^{\infty} F_j^{1-\alpha_j}(q)e^{i\varepsilon_j q\xi}dq,$$

$$\tilde{f}_j^{1-\alpha_j}(\xi) = a_j f_j^{1-\alpha_j}(\xi),\quad \epsilon_j = ka_j,\ \xi = \frac{x}{a_j}$$

Here, $F_j^{1-\alpha_j}$ is the Fourier transform of the normalized fractional current density $\tilde{f}_j^{1-\alpha_j}$. By changing the integration order in (2.31), the scattering electric field is obtained as:

$$E_z^{sj}(x,y) = -i\frac{e^{\pm\frac{i\pi}{2}\alpha_j}}{4\pi}\int_{-\infty}^{+\infty} F_j^{1-\alpha_j}(q)e^{ik\left(xq+|y_j|\sqrt{1-q^2}\right)}(1-q^2)^{\frac{\alpha_j-1}{2}}dq \tag{2.32}$$

After (2.32), the total field has complete mathematical expression. This yields to apply the fractional boundary condition easily because all the components of the field expressions are obtained in terms of exponentials. Note that, each strip has a different fractional-order boundary condition as α_1 and α_2. Then, the boundary condition should be taken for each surface. First, take the derivative on the upper surface in the order of α_1 for each field component [33-38].

$$D_{ky_1}^{\alpha_1}E_z^i(x,y)|_{y_1=0} = (-i)^{\alpha_1}e^{-ik(xcos\theta+lsin\theta)}(sin\theta)^{\alpha_1}$$

$$D_{ky_1}^{\alpha_1}E_z^{s1}(x,y)|_{y_1=0} = -i\frac{e^{\pm\frac{i\pi}{2}\alpha_1}}{4\pi}(i)^{\alpha_1}\int_{-\infty}^{+\infty} F_1^{1-\alpha_1}(q)e^{ik(xq)}(1-q^2)^{\alpha_1-\frac{1}{2}}dq$$

$$D_{ky_1}^{\alpha_1}E_z^{s2}(x,y)|_{y_1=0}$$

$$= -i\frac{e^{\pm\frac{i\pi}{2}\alpha_2}}{4\pi}(i)^{\alpha_1}\int_{-\infty}^{+\infty} F_2^{1-\alpha_2}(q)e^{ik\left(xq+2l\sqrt{1-q^2}\right)}(1-q^2)^{\frac{\alpha_1+\alpha_2-1}{2}}dq$$

Apply Boundary condition on the upper strip as (2.33)

$$(-i)^{\alpha_1}e^{-ik(xcos\theta+lsin\theta)}(sin\theta)^{\alpha_1}$$
$$= i\frac{(i)^{\alpha_1}}{4\pi}e^{\frac{i\pi}{2}\alpha_1}\left[\int_{-\infty}^{+\infty}F_1^{1-\alpha_1}(q)e^{ik(xq)}(1-q^2)^{\alpha_1-\frac{1}{2}}dq\right.$$
$$\left.+e^{\frac{i\pi}{2}(\alpha_2-\alpha_1)}\int_{-\infty}^{+\infty}F_2^{1-\alpha_2}(q)e^{ik\left(xq+2l\sqrt{1-q^2}\right)}(1-q^2)^{\frac{\alpha_1+\alpha_2-1}{2}}dq\right] \tag{2.33}$$

Second, take the derivative on the lower surface in the order of α_2 for each field component.

$$D_{ky_2}^{\alpha_2}E_z^i(x,y)|_{y_2=0} = (-i)^{\alpha_2}e^{-ik(xcos\theta-lsin\theta)}(sin\theta)^{\alpha_2}$$

$$D_{ky_2}^{\alpha_2}E_z^{s1}(x,y)|_{y_2=0}$$
$$= -i\frac{e^{\pm\frac{i\pi}{2}\alpha_1}}{4\pi}(i)^{\alpha_2}\int_{-\infty}^{+\infty}F_1^{1-\alpha_1}(q)e^{ik\left(xq+2l\sqrt{1-q^2}\right)}(1-q^2)^{\frac{\alpha_1+\alpha_2-1}{2}}dq$$

$$D_{ky_1}^{\alpha_1}E_z^{s2}(x,y)|_{y_1=0} = -i\frac{e^{\pm\frac{i\pi}{2}\alpha_2}}{4\pi}(i)^{\alpha_2}\int_{-\infty}^{+\infty}F_2^{1-\alpha_2}(q)e^{ik(xq)}(1-q^2)^{\alpha_2-\frac{1}{2}}dq$$

Apply Boundary condition on the lower strip as (2.34)

$$(-i)^{\alpha_2}e^{-ik(xcos\theta-lsin\theta)}(sin\theta)^{\alpha_2}$$
$$= i\frac{e^{\frac{i\pi}{2}\alpha_2}}{4\pi}(i)^{\alpha_2}\left[\int_{-\infty}^{+\infty}F_2^{1-\alpha_2}(q)e^{ik(xq)}(1-q^2)^{\alpha_2-\frac{1}{2}}dq\right.$$
$$\left.+e^{-\frac{i\pi}{2}(\alpha_2+\alpha_1)}\int_{-\infty}^{+\infty}F_1^{1-\alpha_1}(q)e^{ik\left(xq+2l\sqrt{1-q^2}\right)}(1-q^2)^{\frac{\alpha_1+\alpha_2-1}{2}}dq\right] \tag{2.34}$$

After having the integral equation for the upper strip, (2.33) is multiplied by $e^{-ik\tau x}$ and take the integral from $-a_1$ to a_1 as [22-24]

$$\int_{-a_1}^{a_1} e^{-ik\tau x}dx\,(-i)^{\alpha_1}e^{-ik(xcos\theta+lsin\theta)}(sin\theta)^{\alpha_1}$$

$$= \int_{-a_1}^{a_1} e^{-ik\tau x}dx\, i\frac{(i)^{\alpha_1}}{4\pi}e^{\frac{i\pi}{2}\alpha_1}\left[\int_{-\infty}^{+\infty} F_1^{1-\alpha_1}(q)e^{ik(xq)}(1-q^2)^{\alpha_1-\frac{1}{2}}dq\right.$$
$$\left. + e^{\frac{i\pi}{2}(\alpha_2-\alpha_1)}\int_{-\infty}^{+\infty} F_2^{1-\alpha_2}(q)e^{ik\left(xq+2l\sqrt{1-q^2}\right)}(1-q^2)^{\frac{\alpha_1+\alpha_2-1}{2}}dq\right] \tag{2.35}$$

After having the integral equation for the lower strip, (2.36) is multiplied by $e^{-ik\tau x}$ and take the integral from $-a_2$ to a_2 as

$$\int_{-a_2}^{a_2} e^{-ik\tau x}dx\,(-i)^{\alpha_2}e^{-ik(xcos\theta-lsin\theta)}(sin\theta)^{\alpha_2}$$

$$= \int_{-a_2}^{a_2} e^{-ik\tau x}dx\, i\frac{e^{\frac{i\pi}{2}\alpha_2}}{4\pi}(i)^{\alpha_2}\left[\int_{-\infty}^{+\infty} F_2^{1-\alpha_2}(q)e^{ik(xq)}(1-q^2)^{\alpha_2-\frac{1}{2}}dq\right.$$
$$\left. + e^{-\frac{i\pi}{2}(\alpha_2+\alpha_1)}\int_{-\infty}^{+\infty} F_1^{1-\alpha_1}(q)e^{ik\left(xq+2l\sqrt{1-q^2}\right)}(1-q^2)^{\frac{\alpha_1+\alpha_2-1}{2}}dq\right] \tag{2.36}$$

Then, (2.35) and (2.36) become (2.37) and (2.38), respectively.

$$\int_{-\infty}^{\infty} F_1^{1-\alpha_1}\frac{\sin\left(ka_1(q-\tau)\right)}{q-\tau}\,(1-q^2)^{\alpha_1-\frac{1}{2}}dq$$
$$= -4i\pi e^{i\frac{\pi}{2}\alpha_1}e^{-iklsin\theta}(sin\theta)^{\alpha_1}\frac{\sin\left(ka_1(cos\theta+\tau)\right)}{cos\theta+\tau}$$
$$- e^{\frac{i\pi}{2}(\alpha_2-\alpha_1)}\int_{-\infty}^{+\infty} F_2^{1-\alpha_2}(q)e^{ik\left(2l\sqrt{1-q^2}\right)}\frac{\sin\left(ka_1(q-\tau)\right)}{q-\tau}(1$$
$$-q^2)^{\frac{\alpha_1+\alpha_2-1}{2}}dq \tag{2.37}$$

$$\int_{-\infty}^{\infty} F_2^{1-\alpha_2} \frac{\sin\left(ka_2(q-\tau)\right)}{q-\tau} \left(1-q^2\right)^{\alpha_2-\frac{1}{2}} dq$$

$$= -4i\pi e^{i\frac{\pi}{2}\alpha_2} e^{+iklsin\theta} (sin\theta)^{\alpha_2} \frac{\sin\left(ka_2(cos\theta+\tau)\right)}{cos\theta+\tau}$$

$$- e^{-\frac{i\pi}{2}(\alpha_2-\alpha_1)} \int_{-\infty}^{+\infty} F_1^{1-\alpha_1}(q) e^{ik\left(2l\sqrt{1-q^2}\right)} \frac{\sin\left(ka_2(q-\tau)\right)}{q-\tau} (1$$

$$- q^2)^{\frac{\alpha_1+\alpha_2-1}{2}} dq \qquad (2.38)$$

To solve the set of integral equations given in (2.37) and (2.38), the fractional current density is expressed as given in (2.39) (see Appendix A) [17,34-38,49,54].

$$\tilde{f}_j^{1-\alpha_j}(\xi_j) = \left(1-\xi_j^2\right)^{\alpha_j-\frac{1}{2}} \sum_{n=0}^{\infty} f_{n_j}^{\alpha_j} \frac{C_n^{\alpha_j}(\xi_j)}{\alpha_j}, j = 1,2 \qquad (2.39)$$

Here, $C_n^{\alpha_j}(\xi_j)$ is the Gegenbauer polynomials. The corresponding Fourier transform of the fractional current density is given as follows (2.40). By introducing an unknown coefficient $f_{\mathrm{n}}^{\alpha_j}$ for the fractional current density and substituting (2.40) into IE (2.37) and (2.38), the IE is converted into the system of linear algebraic equations SLAE (see Appendix B) [17,34-38,49,50].

$$F_j^{1-\alpha_j}(q) = \frac{2\pi}{\Gamma(\alpha_j+1)} \sum_{n=0}^{\infty} (-i)^n f_n^{\alpha_j} \beta_n^{\alpha_j} \frac{J_{n+\alpha_j}(\epsilon_j q)}{\left(2\epsilon_j q\right)^{\alpha_j}}, j = 1,2 \qquad (2.40)$$

Here, $J_{n+\alpha_j}(\epsilon_j q)$ is the Bessel function. After inserting (2.40) into IE (2.37) and (2.38), the following equations are obtained, respectively.

$$\frac{2\pi}{2^{\alpha_1}\Gamma(\alpha_1+1)}\sum_{n=0}^{\infty}(-i)^n f_n^{\alpha_1}\beta_n^{\alpha_1}\int_{-\infty}^{\infty}\frac{J_{n+\alpha_1}(\epsilon_1 q)}{(\epsilon_1 q)^{\alpha_1}}\frac{\sin\left(\epsilon_1(q-\tau)\right)}{q-\tau}(1-q^2)^{\alpha_1-\frac{1}{2}}dq$$
$$= -4i\pi e^{i\frac{\pi}{2}\alpha_1}e^{-iklsin\theta}(sin\theta)^{\alpha_1}\frac{\sin\left(\epsilon_1(cos\theta+\tau)\right)}{cos\theta+\tau} - \Omega_1\sum_{n=0}^{\infty}(-i)^n f_n^{\alpha_2}\beta_n^{\alpha_2}\int_{-\infty}^{+\infty}\frac{J_{n+\alpha_2}(\epsilon_2 q)}{(\epsilon_2 q)^{\alpha_2}}e^{ik\left(2l\sqrt{1-q^2}\right)}\frac{\sin\left(\epsilon_1(q-\tau)\right)}{q-\tau}(1-q^2)^{\frac{\alpha_1+\alpha_2-1}{2}}dq \qquad (2.41)$$

Here, $\Omega_1 = e^{\frac{i\pi}{2}(\alpha_2-\alpha_1)}\ \frac{2\pi}{2^{\alpha_2}\Gamma(\alpha_2+1)}$

$$\frac{2\pi}{\Gamma(\alpha_2+1)}\sum_{n=0}^{\infty}(-i)^n f_n^{\alpha_2}\beta_n^{\alpha_2}\int_{-\infty}^{\infty}\frac{J_{n+\alpha_2}(\epsilon_2 q)}{(2\epsilon_2 q)^{\alpha_2}}\frac{\sin\left(\epsilon_2(q-\tau)\right)}{q-\tau}(1-q^2)^{\alpha_2-\frac{1}{2}}dq$$
$$= -4i\pi e^{i\frac{\pi}{2}\alpha_2}e^{+iklsin\theta}(sin\theta)^{\alpha_2}\frac{\sin\left(\epsilon_2(cos\theta+\tau)\right)}{cos\theta+\tau} - \Omega_2\sum_{n=0}^{\infty}(-i)^n f_n^{\alpha_1}\beta_n^{\alpha_1}\int_{-\infty}^{+\infty}\frac{J_{n+\alpha_1}(\epsilon_1 q)}{(2\epsilon_1 q)^{\alpha_1}}e^{ik\left(2l\sqrt{1-q^2}\right)}\frac{\sin\left(\epsilon_2(q-\tau)\right)}{q-\tau}(1-q^2)^{\frac{\alpha_1+\alpha_2-1}{2}}dq \qquad (2.42)$$

Here, $\Omega_2 = e^{-\frac{i\pi}{2}(\alpha_2-\alpha_1)}\ \frac{2\pi}{2^{\alpha_1}\Gamma(\alpha_1+1)}$

Then, The following property is used [21-24]. To use, equations (2.41) and (2.42) are multiplied by $\frac{J_{n+\alpha_1}(\epsilon_1\tau)}{\tau^{\alpha_1}}$ and $\frac{J_{n+\alpha_2}(\epsilon_2\tau)}{\tau^{\alpha_2}}$, respectively and integrate from $-\infty$ to ∞ with respect to τ [17,34-38,49, 54].

$$\frac{1}{\pi}\int_{-\infty}^{\infty}\frac{J_{n+\alpha}(\epsilon q)}{q^{\alpha}}\frac{\sin\epsilon(q\mp\beta)}{q\mp\beta}dq = \frac{J_{n+\alpha}(\epsilon\beta)}{\beta^{\alpha}}(\pm 1)^n$$

The procedure is given as follows.

$$\frac{2\pi}{2^{\alpha_1}\Gamma(\alpha_1+1)}\sum_{n=0}^{\infty}(-i)^n f_n^{\alpha_1}\beta_n^{\alpha_1}\frac{1}{\pi}\int_{-\infty}^{\infty}\frac{J_{n+\alpha_1}(\epsilon_1\tau)}{\tau^{\alpha_1}}\int_{-\infty}^{\infty}\frac{J_{n+\alpha_1}(\epsilon_1 q)}{(\epsilon_1 q)^{\alpha_1}}\frac{\sin\big(\epsilon_1(q-\tau)\big)}{q-\tau}(1-q^2)^{\alpha_1-\frac{1}{2}}dqd\tau$$

$$=-4i\pi e^{i\frac{\pi}{2}\alpha_1}e^{-iklsin\theta}(sin\theta)^{\alpha_1}\frac{1}{\pi}\int_{-\infty}^{\infty}\frac{J_{n+\alpha_1}(\epsilon_1\tau)}{\tau^{\alpha_1}}\frac{\sin\big(\epsilon_1(cos\theta+\tau)\big)}{cos\theta+\tau}d\tau$$

$$-\Omega_1\sum_{n=0}^{\infty}(-i)^n f_n^{\alpha_2}\beta_n^{\alpha_2}\frac{1}{\pi}\int_{-\infty}^{\infty}\frac{J_{n+\alpha_1}(\epsilon_1\tau)}{\tau^{\alpha_1}}\int_{-\infty}^{+\infty}\frac{J_{n+\alpha_2}(\epsilon_2 q)}{(\epsilon_2 q)^{\alpha_2}}e^{ik\left(2l\sqrt{1-q^2}\right)}\frac{\sin\big(\epsilon_1(q-\tau)\big)}{q-\tau}(1-q^2)^{\frac{\alpha_1+\alpha_2-1}{2}}dqd\tau$$

$$\frac{2\pi}{\Gamma(\alpha_2+1)}\sum_{n=0}^{\infty}(-i)^n f_n^{\alpha_2}\beta_n^{\alpha_2}\frac{1}{\pi}\int_{-\infty}^{\infty}\frac{J_{n+\alpha_2}(\epsilon_2\tau)}{\tau^{\alpha_2}}\int_{-\infty}^{\infty}\frac{J_{n+\alpha_2}(\epsilon_2 q)}{(2\epsilon_2 q)^{\alpha_2}}\frac{\sin\big(ka_2(q-\tau)\big)}{q-\tau}(1-q^2)^{\alpha_2-\frac{1}{2}}dqd\tau$$

$$=-4i\pi e^{i\frac{\pi}{2}\alpha_2}e^{+iklsin\theta}(sin\theta)^{\alpha_2}\frac{1}{\pi}\int_{-\infty}^{\infty}\frac{J_{n+\alpha_2}(\epsilon_2\tau)}{\tau^{\alpha_2}}\frac{\sin\big(ka_2(cos\theta+\tau)\big)}{cos\theta+\tau}d\tau$$

$$-\Omega_2\sum_{n=0}^{\infty}(-i)^n f_n^{\alpha_1}\beta_n^{\alpha_1}\frac{1}{\pi}\int_{-\infty}^{\infty}\frac{J_{n+\alpha_2}(\epsilon_2\tau)}{\tau^{\alpha_2}}\int_{-\infty}^{+\infty}\frac{J_{n+\alpha_1}(\epsilon_1 q)}{(2\epsilon_1 q)^{\alpha_1}}(q)e^{ik\left(2l\sqrt{1-q^2}\right)}\frac{\sin\big(ka_2(q-\tau)\big)}{q-\tau}(1-q^2)^{\frac{\alpha_1+\alpha_2-1}{2}}dqd\tau$$

After all, the final expression for the coupled system of linear algebraic equations is given in (2.43) and (2.44), respectively.

$$\sum_{n=0}^{\infty}(-i)^n f_n^{\alpha_1}\beta_n^{\alpha_1}C_{kn}^{\alpha_1}+\frac{(2\epsilon_1)^{\alpha_1}}{(2\epsilon_2)^{\alpha_2}}\frac{\Gamma(\alpha_1+1)}{\Gamma(\alpha_2+1)}e^{-\frac{i\pi}{2}(\alpha_2-\alpha_1)}\sum_{n=0}^{\infty}(-i)^n f_n^{\alpha_2}\beta_n^{\alpha_2}C_{kn}^{\alpha_1\alpha_2}$$
$$=-2i(-1)^k(2\epsilon_1)^{\alpha_1}\Gamma(\alpha_1+1)e^{-iklsin\theta}(\tan\theta)^{\alpha_1}J_{k+\alpha_1}(\epsilon_1 cos\theta) \tag{2.43}$$

$$\sum_{n=0}^{\infty}(-i)^n f_n^{\alpha_2}\beta_n^{\alpha_2}C_{kn}^{\alpha_2}+\frac{(2\epsilon_2)^{\alpha_2}}{(2\epsilon_1)^{\alpha_1}}\frac{\Gamma(\alpha_2+1)}{\Gamma(\alpha_1+1)}e^{\frac{i\pi}{2}(\alpha_2-\alpha_1)}\sum_{n=0}^{\infty}(-i)^n f_n^{\alpha_1}\beta_n^{\alpha_1}C_{kn}^{\alpha_2\alpha_1}$$
$$=-2i(-1)^k(2\epsilon_2)^{\alpha_2}\Gamma(\alpha_2+1)e^{+iklsin\theta}(\tan\theta)^{\alpha_2}J_{k+\alpha_2}(\epsilon_2 cos\theta) \tag{2.44}$$

where,

$$C_{kn}^{\alpha_j\alpha_j} = \int_{-\infty}^{\infty} J_{n+\alpha_j}(\epsilon_j q) J_{k+\alpha_j}(\epsilon_j q) \frac{(1-q^2)^{\alpha_j-\frac{1}{2}}}{q^{2\alpha_j}} dq,$$

$$C_{kn}^{\alpha_j\alpha_i} = \int_{-\infty}^{\infty} J_{n+\alpha_i}(\epsilon_i q) J_{k+\alpha_j}(\epsilon_j q) e^{2ikl\sqrt{1-q^2}} \frac{(1-q^2)^{\frac{\alpha_j+\alpha_i-1}{2}}}{q^{\alpha_j+\alpha_i}} dq.$$

To get the physical characteristic of the geometry, the far-field pattern is required. After finding the expression for $F_j^{1-\alpha_j}$ in (2.40), the radiation pattern of the scattered field at the far zone can be calculated by using (2.45) in which the steepest descent method for $ka \to \infty$ is used [51,52] (see Appendix C).

$$E_z^s(x,y) = A(kr)\Phi^\alpha(\phi). \tag{2.45}$$

Here, $A(kr) = \sqrt{\frac{2}{\pi kr}} e^{ikr-\frac{i\pi}{4}}$, and $\Phi^\alpha(\phi) = \Phi_1^{\alpha_1}(\phi) + \Phi_2^{\alpha_2}(\phi)$,

where,

$$\Phi_1^{\alpha_1}(\phi) = -\frac{i}{4} e^{\pm\frac{i\pi\alpha_1}{2}} F_1^{1-\alpha_1}(cos\phi)(\sin^\alpha\phi) e^{-iklsin\phi},$$

$$\Phi_2^{\alpha_2}(\phi) = -\frac{i}{4} e^{\pm\frac{i\pi\alpha_2}{2}} F_2^{1-\alpha_2}(cos\phi)(\sin^{\alpha_2}\phi) e^{+iklsin\phi}.$$

In (2.45), the upper sign is chosen for $\phi \in [0,\pi]$, and the lower sign corresponds to $\phi \in [\pi, 2\pi]$ where ϕ is the observation angle. $A(kr)$ is the radial part and $\Phi^\alpha(\phi)$ is the angular part of the scattered electric field in the far zone [38,54]. The radiation Pattern (RP) which is expressed as $\Phi^\alpha(\phi)$ in (2.45) is also used for the Total Radar Cross Section which can be found as follows (2.46) [53].

$$\sigma_t = \frac{1}{4\epsilon_1} \int_0^{2\pi} |\Phi^\alpha|^2 d\phi. \tag{2.46}$$

2.4 Single-strip with Fractional Boundary Conditions

Final investigation in the thesis, the current distribution analysis for the one strip with a cylindrical wave excitation for the fractional-order 0.5 is done. Previously, the diffraction by a strip with the fractional boundary condition is studied [6,33,34,38]. The solution approach is the same. Therefore, a brief explanation is given in this section. Here, the current distribution, near electric field distribution, bi-static radar cross-section are investigated. Previously, the mathematical analysis and the numerical investigation of the diffraction of a line source by the strip with the fractional order 0.5 has not been investigated yet. In this section, the mathematical derivation and the definition of the radar cross-sections are given [6,33,34,38,54].

In Figure 2.4, the geometry of the problem is given. As it is seen at the point (x_o, y_o), there exists a line source $\vec{J}_e = \hat{e}_z J_e \delta(x - x_o)\delta(y - y_o)$ where δ is the Dirac distribution, $\hat{e}_z$ is the unit vector along the z-direction, and J_e is a constant amplitude for electric the current density. The problem is two-dimensional. The strip with 2a and is located on the plane $y = 0$. The strip has an infinite extension along the z-axis and infinitesimal height along the y-axis.

The problem is to investigate what is the current distribution on the surface of the strip, the near electric field, and the bi-static radar cross-section which has not been studied yet. A two-dimensional strip of width 2a on the plane y = 0 is located. The strip along the z-axis is infinite. The source of the cylindrical wave is located at the point (x_o, y_o) as shown in Figure 2.4. The time dependency is given as $e^{-i\omega t}$ and throughout the problem, it will be omitted. Apart from the previous problems, in this problem, the incidence wave is a cylindrical wave. Therefore, also the incidence wave should be expressed in terms of the exponential function to take the fractional derivative more easily for the further procedure [6,33,34,38].

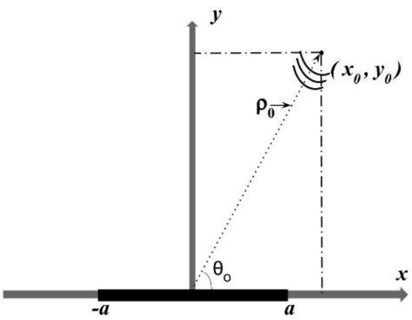

Figure 2.4 : The geometry of the problem.

The incidence electric field $\vec{E}_z^i$ mathematically can be represented as (2.47) under the condition of $e^{-i\omega t}$ time dependency [6,33,34,38,51].

$$\vec{E}_z^i(x, y) = -\vec{J}_e \frac{\eta_0 k}{4} H_0^{(1)}\left(k\sqrt{(x - x_o)^2 + (y - y_o)^2}\right) \tag{2.47}$$

Here, $H_0^{(1)}(k\mathrm{x})$ stands for the Hankel function of the first kind and zero-order, η_0 corresponds to the impedance of free space, and $k = \frac{2\pi}{\lambda}$ is the wavenumber. Then, the total electric field can be represented as a superposition of the incidence and the scattered electric fields as given in (2.48).

$$\vec{E}_z = \vec{E}_z^i + \vec{E}_z^s \tag{2.48}$$

After having (2), there are two main steps to be achieved. The first is to express the scattered field mathematically and then, to apply the fractional boundary condition to obtain an equation to solve with mathematical techniques. As shown previously, the scattered electric field can be expressed as the convolution of the required Green's function with the induced current density on the strip as (2.49) [6,33,34,38,54].

$$E_z^s(x,y) = \int_{-\infty}^{\infty} f^{1-\alpha}(x')G^{\alpha}(x-x',y)dx' \tag{2.49}$$

Here, $f^{1-\nu}(x')$ is called the fractional current density existing only on the strip and $G^{\nu}(x)$ is the fractional Green's function which has the following form [6,33,34,38]. As explained previously, the main motivation is to express everything in terms of exponential functions. Therefore, the spectral representation of the Hankel function will be employed to apply the fractional boundary condition easily.

$$G^{\alpha}(x-x',y) = -\frac{i}{4}\mathfrak{D}_{ky}^{\alpha}H_0^{(1)}\left(k\sqrt{(x-x')^2+y^2}\right) \tag{2.50}$$

where,

$$H_0^{(1)}\left(k\sqrt{(x-x')^2+y^2}\right) = \frac{1}{\pi}\int_{-\infty}^{\infty} e^{ik((x-x')q+|y|\sqrt{1-q^2})}\frac{dq}{\sqrt{1-q^2}}$$

Note that, $Im\{\sqrt{1-\alpha^2} > 0\}$ is assumed. Im is the imaginary operator which gives the imaginary part of the function of a function. By using (2.49) in (2.50) and taking into account the Fourier transform, the scattered field is obtained as follows.

$$E_z^s(x,y) = -i\frac{e^{i\frac{\pi}{2}\alpha}}{4\pi}\int_{-\infty}^{\infty} F^{1-\alpha}(\tau)e^{ik[\tau x+y\sqrt{1-\tau^2}]}(1-\tau^2)^{\frac{\alpha-1}{2}}d\tau \tag{2.51}$$

where,

$$F^{1-\alpha}(\tau) = \int_{-1}^{1} \tilde{f}^{1-\alpha}(\xi) e^{-i\varepsilon\tau\xi} d\xi, \tilde{f}^{1-\alpha}(\xi) = a f^{1-\alpha}(a\xi)$$

$$\varepsilon = ka,\ \ \xi = \frac{x}{a}, \quad \tilde{f}^{1-\alpha}(\xi) = \frac{\varepsilon}{2\pi}\int_{-\infty}^{\infty} F^{1-\alpha}(\tau) e^{i\varepsilon\tau\xi} d\tau$$

Here, $F^{1-\alpha}(\tau)$ is the Fourier transform of $\tilde{f}^{1-\alpha}(\xi)$ which is the normalized current density between $x \in [-1, 1]$ on the strip. As mentioned above, the second step is to apply the fractional boundary condition after having the mathematical expression for each component of the total electric fields. In (2.52), the fractional boundary condition is given [6,33,34,38].

$$\mathfrak{D}_{ky}^{\alpha} E_z(x, y)\big|_{y=\pm 0} = 0 \tag{2.52}$$

where, $x,\ \ -a < x < a, ky$ is a dimensionless parameter and α is a fractional-order (FO).

After applying FBC on the surface of the strip for the total tangential electric field, the following integral equation (IE) is obtained.

$$\begin{gathered} -i\frac{e^{i\pi\alpha}}{4\pi}\int_{-\infty}^{\infty} F^{1-\alpha}(\alpha) e^{ik\tau x}(1-\tau^2)^{\alpha-1/2} d\tau = \\ J_e \frac{\eta_0 k}{4\pi} e^{i\frac{\pi}{2}\alpha} \int_{-\infty}^{\infty} e^{ik\left((x-x_0)\tau - y_0\sqrt{1-\tau^2}\right)} (1-\tau^2)^{\frac{\alpha-1}{2}} d\tau \end{gathered} \tag{2.53}$$

To obtain a general solution for an arbitrary fractional order, both sides of (2.53) with $e^{-ikx\beta}$ needs to be multiplied and then, an integration from $-a$ to $+a$ with respect to x variable for this new expression is done. Then, (2.53) is converted into (2.54). Then, the current distribution is expressed as the summation of the Gegenbauer polynomials and the integral equation is converted into a system of linear algebraic equations to solve.

$$\begin{gathered} \int_{-\infty}^{\infty} F^{1-\alpha}(\tau) \frac{\sin \varepsilon(\tau-\beta)}{\tau-\beta}(1-\tau^2)^{\alpha-\frac{1}{2}} d\tau \ = \\ -4iB\pi e^{-i\frac{\pi}{2}\alpha} \int_{-\infty}^{\infty} e^{ik\left[-x_0\tau + y_0\sqrt{1-\tau^2}\right]} \frac{\sin \varepsilon(\tau-\beta)}{\tau-\beta}(1-\tau^2)^{\frac{\alpha-1}{2}} d\tau \end{gathered} \tag{2.54}$$

where $B = -J_e \frac{\eta_0 k}{4\pi}$.

The investigation for this thesis only focuses on the case where the fractional order is equal to 0.5. Apart from (2.54), for the fractional-order 0.5 case, the left-hand side of (2.53) becomes inverse Fourier Transform. Then, the fractional current density becomes as (2.55).

$$\tilde{f}^{0.5}(\xi) = -i2\varepsilon B e^{\mp i\frac{\pi}{4}} \int_{-\infty}^{\infty} e^{i\left[(\varepsilon\tau\xi - kx_0\tau) + ky_0\sqrt{1-\tau^2}\right]}(1-\tau^2)^{-\frac{1}{4}} d\tau \tag{2.55}$$

and, from (2.54), the Fourier Transform of the current density becomes (2.56) under the condition of $ka \gg 1$ because the term $\frac{\sin \varepsilon(\beta-\tau)}{(\beta-\tau)}$ behaves as a Dirac distribution for high values of ka.

$$F^{0.5}(\tau) \cong -i4Be^{\mp i\frac{\pi}{4}} \int_{-\infty}^{\infty} \frac{\sin \varepsilon(\beta-\tau)}{(\beta-\tau)} e^{i\left[(-kx_0\beta) + ky_0\sqrt{1-\beta^2}\right]}(1-\beta^2)^{-\frac{1}{4}} d\beta \tag{2.56}$$

Equations (2.55) are the special case where the normalized current density $\tilde{f}^{0.5}$ and the Fourier transform of the current density $F^{0.5}$ have been found analytically. Note that, by the steepest descent method [51], (2.56) can be evaluated for the large values of $k\rho_0$. To do this, the Cartesian coordinate system (x, y) is converted into a cylindrical coordinate system as $(\rho cos\varphi, \rho sin\varphi)$. Then, (2.57) is obtained for $k\rho_0 \to \infty$ (see Appendix C).

$$F^{0.5}(\alpha) = -i4Be^{\mp i\frac{\pi}{4}} \sqrt{\frac{2\pi}{k\rho_0}} \sqrt{sin\theta_0} \frac{\sin(\epsilon(cos\theta_0 + \alpha))}{(cos\theta_0 + \alpha)} e^{ik\rho_0 - \frac{i\pi}{4}} \tag{2.57}$$

In order to solve IE (2.56) for any fractional order, discretization is required. In this way, the integral equation is converted into SLAE. To do so, the fractional current density is expressed as (see Appendix A) [17,38,49,50]:

$$\tilde{f}^{1-\alpha}(\xi) = (1-\xi^2)^{\alpha-\frac{1}{2}} \sum_{n=0}^{\infty} f_n^{\alpha} \frac{C_n^{\alpha}(\xi)}{\alpha} \tag{2.58}$$

where, $C_n^{\alpha}(\xi)$ stands for Gegenbauer polynomials. At the edges, the edge condition needs to be satisfied. Therefore, the weighing $(1-\xi^2)^{\alpha-\frac{1}{2}}$ is inserted in (2.58). The behaviors of the current should act as [6,33,34,38]:

$$\tilde{f}^{1-\alpha}(\xi) = O\left((1-\xi^2)^{\alpha-\frac{1}{2}}\right), \xi \to \pm 1 \qquad (2.59)$$

The Fourier Transform of (2.58), $F^{1-\alpha}(\tau)$ can be obtained as (see Appendix B)[50,54].

$$F^{1-\alpha}(\tau) = \frac{2\pi}{\Gamma(\alpha+1)} \sum_{n=0}^{\infty} (-i)^n f_n^\alpha \beta_n^\alpha \frac{\mathcal{J}_{n+\alpha}(\varepsilon\tau)}{(2\varepsilon\tau)^\alpha} \qquad (2.60)$$

Here, β_n^α = Γ (n +2 α) / Γ (n + 1) and $\mathcal{J}_{n+\alpha}(\varepsilon\tau)$ stands for the Bessel functions. If (2.60) is put into IE (2.54), one can obtain a system of linear algebraic equations (SLAE). Then, by inversion, the unknown coefficients f_n^α can be obtained.

$$\sum_{n=0}^{\infty} (-i)^n f_n^\alpha \beta_n^\alpha C_{mn}^\alpha = \gamma_m^\alpha \qquad (2.61)$$

Here,

$$C_{mn}^\alpha = \int_{-\infty}^{\infty} \mathcal{J}_{n+\alpha}(\varepsilon\tau)\mathcal{J}_{m+\alpha}(\varepsilon\tau)(1-\tau^2)^{\alpha-\frac{1}{2}} \frac{d\tau}{\tau^{2\alpha}}$$

and

$$\gamma_m^\alpha = \Omega \int_{-\infty}^{\infty} \frac{\mathcal{J}_{m+\alpha}(\varepsilon\tau)}{\tau^\alpha} e^{i\left[-kx_0\tau + ky_0\sqrt{1-\tau^2}\right]} (1-\tau^2)^{\frac{\alpha-1}{2}} d\tau$$

where $\Omega = \frac{i}{2\pi}\Gamma(\alpha+1)e^{-i\frac{\pi}{2}\alpha}$

Then, the far-field expression of the scattered field can be obtained by assuming k$\rho \to \infty$. This time, the steepest descent method is utilized to derive the expression for the far-field $E_z^s(\rho, \varphi)$ as follows [6,33,34,38,51]. Note that, $\rho = \sqrt{x^2+y^2}$ and φ is the angle between the $\hat{e}_\rho$ unit vector along in ρ and $\hat{e}_x$.

$$E_z^s(\rho, \varphi) = A(k\rho)\Phi^\alpha(\varphi) \qquad (2.62)$$

where,

$$A(k\rho) = \sqrt{\frac{2}{\pi k\rho}} e^{ik\rho - i\pi/4}$$

$$\Phi^{0.5}(\varphi) = -\frac{i}{4}(\pm i)^{0.5} F^{0.5}(cos\varphi)\sqrt{sin\varphi}$$

Here, $A(k\rho)$ and $\Phi^{\alpha}(\varphi)$ stand for the radial and the angular parts of the scattered electric field at the far zone, respectively. Angular variation of the field is the main concern of the scattered field. Therefore, $\Phi^{\alpha}(\varphi)$ is called the scattered radiation pattern. For (2.62), (+) sign is for $0 < \varphi < \pi$,), and (-) sign is for $\pi < \varphi < 2\pi$ [38,54].

As given in [9, 10], the fractional-order is related to the impedance. Affiliation between the fractional-order α and the impedance η_{α} can be obtained for the normal incidence plane wave as shown in (2.63).

$$\alpha = \frac{1}{i\pi} ln \frac{1 - \eta_{\alpha}}{1 + \eta_{\alpha}}, \quad \eta_{\alpha} = \frac{1}{i} \tan\left(\frac{\pi\alpha}{2}\right) \tag{2.63}$$

Here, it should be highlighted that this result is derived for the plane wae as an incidence wave. On the other hand, for the large values of $k\rho_0$, it is a valid approximation to utilize the formula. Note that, for the values of the fractional-order $0 < \alpha < 1$, η_{α} is always pure imaginary. The value $\alpha = 0$ stands for the impedance $\eta_{\alpha} = 0$ (PEC) and $\nu = 1$ is equal to to $\eta_{\alpha} = -i\infty$ (PMC). For the fractional-order between (0,1), the impedance has pure imaginary values between 0 and $-i\infty$. For a special case, under the condition of $k\rho_0 \to \infty$ and $\alpha = 0.5$, the strip's impedance becomes $-i$ [6,33,34,38].

Finally, to understand scattering phenomena for a strip, radar cross-sections (RCS) are investigated. In this thesis, bi-static radar cross-section ($\sigma_{2\mathrm{d}}$) of a strip is numerically investigated. In order to calculate radar cross-sections, (2.64) is used for the bi-static and the monostatic radar cross-section, respectively [33,34].

$$\frac{\sigma_{2\mathrm{d}}}{\lambda}(\varphi) = \frac{2}{\pi} |\Phi(\varphi)|^2 \tag{2.64}$$

3. NUMERICAL RESULTS

3.1 Purpose of Analysis

In this chapter, the numerical results are presented. Here, depending on the problem, radar cross-sections, radiation patterns, electric field distributions, current distribution, power flow diagrams are given. First, the results of diffraction by double strips with the same boundary conditions, then, diffraction by double strips with different boundary conditions, and finally line source diffraction by single strip for the fractional-order 0.5 cases are given. For calculations, the MatLab simulation tool is employed whereas, for the illustrations, both LAE Service and MatLab Simulation Tools are utilized. Expressing the current density on the obstacles in terms of the Gegenbauer polynomials with the weighting factor $(1-\xi^2)^{\alpha-\frac{1}{2}}$ leads to having fastly converging series to the actual values of the current density found by analytical or numerical methods for the same problem because the edge condition is satisfied with that factor by default [1,5,17,49]. In this study, the summations are calculated up to $\epsilon+5$ values. For higher accuracy demand, this value can be increased. For more than 95% accuracy, the predefined value $\epsilon+5$ is enough. Note that ϵ is equal to ka which inherently, gives the information about the relative dimension of the scattered with respect to the wavelength of the incidence wave (i.e. electrical length) [8].

I the thesis, the hybrid method is employed for the diffraction problem. This method is called also, the numerical-analytical method which stems from the combination of the analytical and numerical methods. The first steps of the method start with analytical manipulations. The field components are expressed as analytical forms as summations or integrals regarding the geometry. Then, by the boundary conditions, the problem is reduced to a boundary value problem. After that, the initial operator equation is converted to an infinite system of a linear algebraic equation which is truncated for the numerical calculation as expected by introducing the orthogonal polynomials concerning the geometry. Here, the important point is that obtained SLAE utilizing analytical manipulations is much better than full numerical approaches for computing due to the requirement of less size of the inverted matrix and highly converting trends in the summations or integrals standing for the field components [7,24,34].

3.2 Double-strips with the Same Boundary Conditions

For the double strip problems, the resonance characteristics and radiation mechanism is investigated via total radar cross-section analysis. In Figure 3.1, the geometry of the problem is given.

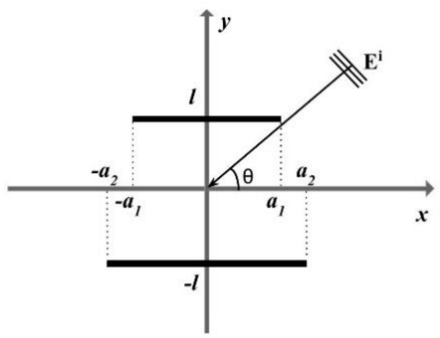

Figure 3.1 : The geometry of the problem.

To observe the resonances for the structure, the total radar cross-section is investigated. The peaks at the total radar cross-section calculation show the resonances where the total field is mainly captured between the strips. For different fractional-order, the values of the For Figure 3.2, the Total Radar Cross Section (σ_T) is obtained for the strips with the same lengths. The total radar cross-section is drawn with respect to $\epsilon_1 = ka_1$ for different Fractional orders ($\alpha = 0.5, 0.75, 1$) (normal incidence). As it is seen in Figure 3.2, the strips have resonance frequencies for all fractional-order values. For different values of the fractional-order combinations, the resonance values differ. Therefore, TRCS investigation is very crucial for resonator-like structures in order to observe resonance behavior for different boundary conditions. Note that, for the parallel plates, there exists an analytical expression to obtain the resonant frequencies. The resonant frequencies can be found for such quasi – resonators as $kl \approx \frac{n\pi}{2}$ (n=1, 2, 3, …) [5,35,37,48,51] Then, the first and second resonance wavenumbers are $\frac{\pi}{2}$ and π for the theoretical formulation. Note that, there exists a deviation between the numerical and theoretical results. The deviation from the analytical expression with the fractional approach is because the analytical expression is obtained when the width of the strip is much larger than the wavelength of the incidence wave $\left(a \gg \lambda = \frac{2\pi}{k}\right)$.

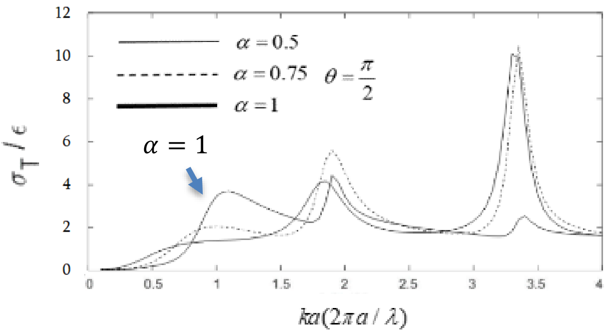

Figure 3.2 : σ_T when $a = a_1 = a_2 = 1, l = 1, \theta = \frac{\pi}{2}$ for $\alpha = 0.5,\ 0.75, 1$.

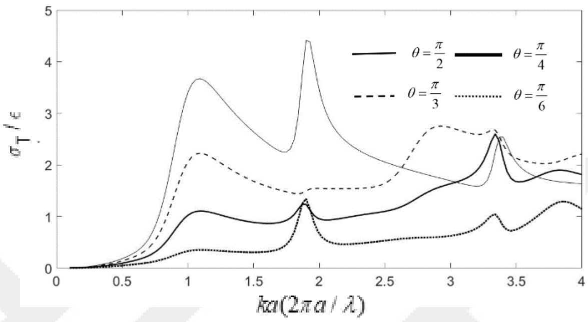

Figure 3.3 : σ_T when $a = a_1 = a_2 = 1, l = 1, \alpha = 1$ and $\theta = \frac{\pi}{6}, \frac{\pi}{4}, \frac{\pi}{3}, \frac{\pi}{2}$.

In Figure 3.3, for the different angles of incidence, the TRCS is calculated. Except for $\theta = \frac{\pi}{3}$, the resonances are at $ka \approx 1.9$ and $ka \approx 3.4$ as in Figure 3.2. Note that, the highest value in Figure 3.3 stands for $\theta = \frac{\pi}{2}$.

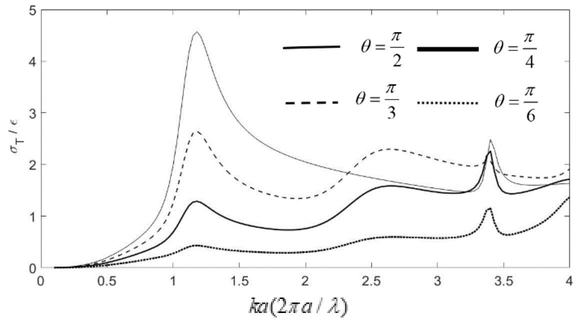

Figure 3.4 : σ_T when $a = a_1 = a_2 = 1, l = 0.5, \alpha = 1$ for $\theta = \frac{\pi}{6}, \frac{\pi}{4}, \frac{\pi}{3}, \frac{\pi}{2}$.

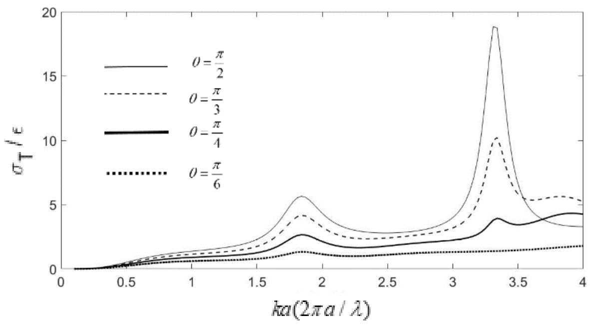

Figure 3.5 : σ_T when $a = a_1 = a_2 = 1, l = 1,\ \alpha = 0.5$ and $\theta = \frac{\pi}{6}, \frac{\pi}{4}, \frac{\pi}{3}, \frac{\pi}{2}$.

In Figure 3.4, the distance between the strips (l) is decreased in Figure 3.3. The resonance characteristic has changed. The resonance at $ka \approx 1.9$ is disappeared. In Figure 3.5, the fractional-order is equal to 0.5. This yields to have greater resonance values for the same parameters. As a common comment, the higher resonance characteristics can be obtained by normal incidence (90^0) regarding all figures above in this section. In the following figures, the electric field distributions are investigated for the resonant and non-resonant frequencies with different parameters [5,35,37].

Figure 3.6 stands for the total field E_z distribution. This field is obtained for the resonant value ($k = 3.4$) and as it is seen between the strips, there are high field values between the strips even though the source is not located between the strips. The high field values are inside the strip due to resonance. Inside the strips, there exist standing waves. Figure 3.7 is for the total field E_z distribution at the first resonance, $(k = 1.9)$. As it is seen, the field maximum in Figure 3.7 is higher than in Figure 3.6 (approximately 6 versus 4) as it was expected from Figure 3.3. When Figures 3.6 and 3.7 are compared, it can be easily noticed that different modes are excited between the strips. Figure 3.7 stands for the exciting first mode whereas Figure 3.6 corresponds to the second mode for this geometry. In these figures, it is easily noticed that the boundary conditions are satisfied. The total field's normal derivative with respect to the normal of the strip surface is zero [5,35,37].

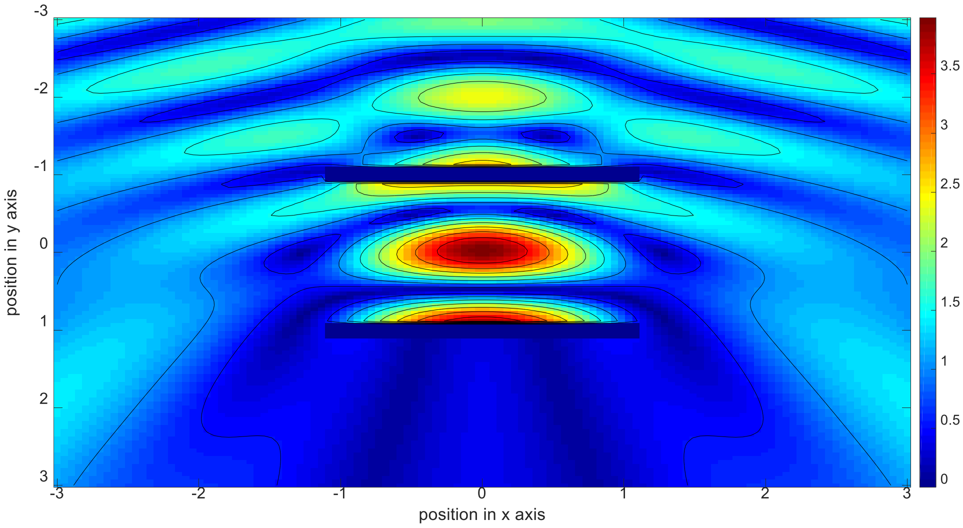

Figure 3.6 : Total Field $E_z, a_1 = a_2 = 1, l = 1, \ \alpha = 1, ka_1 = 3.4, \theta = \frac{\pi}{2}$.

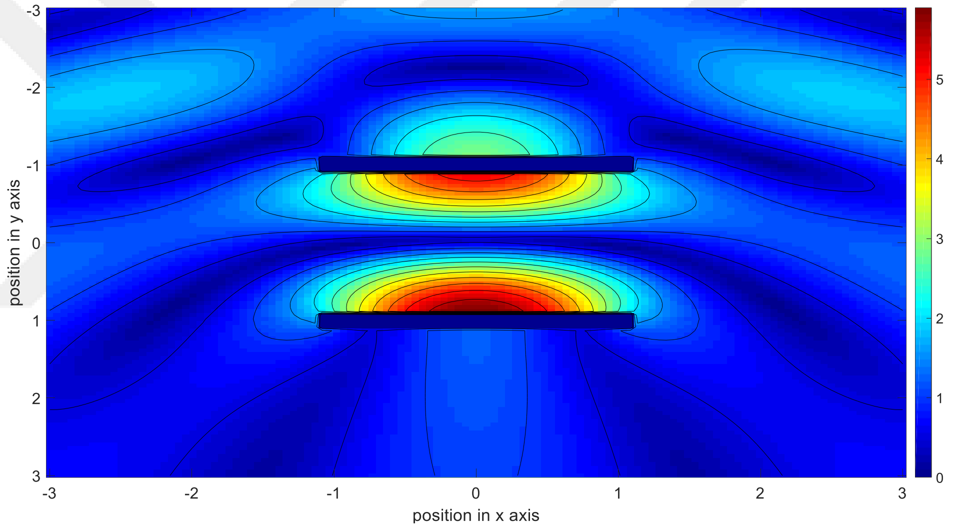

Figure 3.7 : Total Field $E_z, a_1 = a_2 = 1, l = 1, \alpha = 1, \ ka_1 = 1.9, \theta = \frac{\pi}{2}$.

Figure 3.8 represents the total field E_z distribution at a non-resonant frequency($k = 1.5$). As it is seen, the high field values are not observed inside the strips because the electric field is not accumulated between the strips.

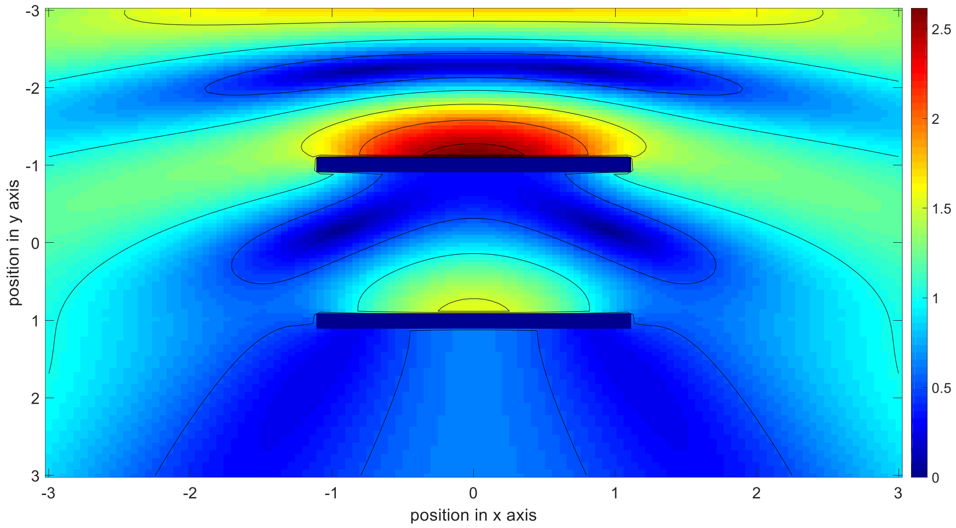

Figure 3.8 : Total Field $E_z,\ a_1 = a_2 = 1, l = 1, \alpha = 1,\ ka_1 = 1.5, \theta = \frac{\pi}{2}$.

In Figures 3.9 and 3.10, the total field E_z distribution for the intermediate fractional order is calculated at the resonance frequency. As it is noticed, the field maximum is 9 which is higher than Figure 3.6. In Figure 3.10, the field maximum reaches 10 for α=0.75.

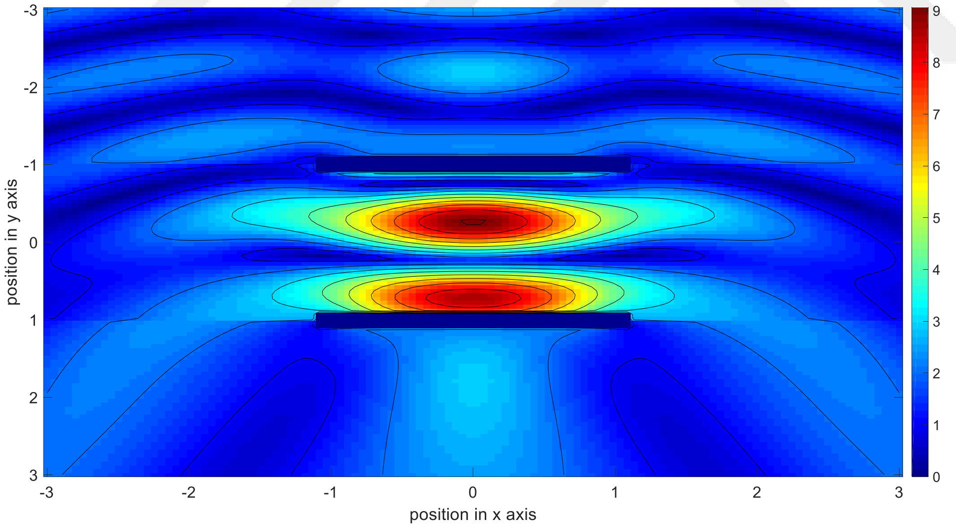

Figure 3.9 : Total Field $E_z, a_1 = a_2 = 1, l = 1, \alpha = 0.5, ka_1 = 3.4,\ \theta = \frac{\pi}{2}$.

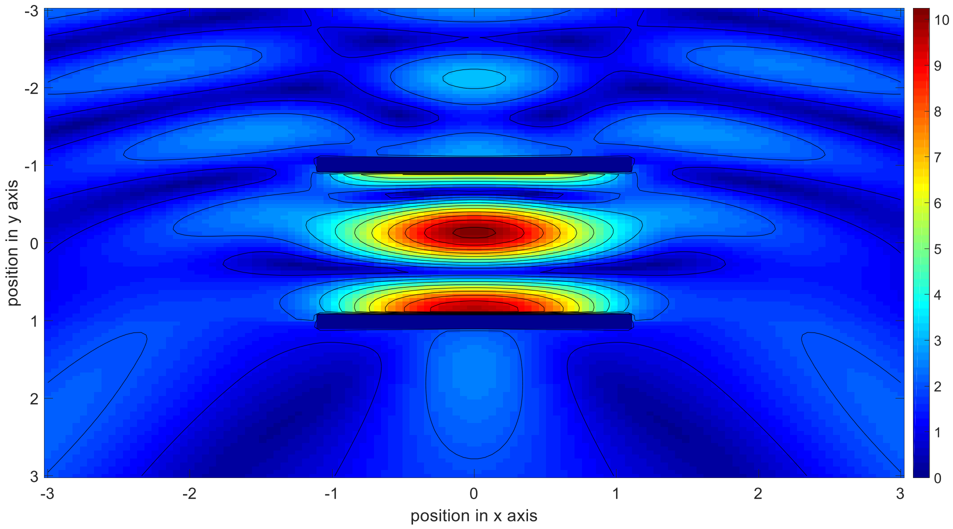

Figure 3.10 : Total Field $E_z, a_1 = a_2 = 1, l = 1, \alpha = 0.75, ka_1 = 3.4, \theta = \frac{\pi}{2}$.

For the incidence angle θ=π/3 instead of θ=π/2 (oblique incidence), the result is given in Figure 3.11. The resonant field inside the strip has a smaller amplitude with respect to the normal incidence case as given in Figure 3.10. If we change again the incident angle and take it as θ=π/4, the following result is obtained. The resonance disappears. Inside the strips, there are no high field values and standing waves between the strips. In Figure 3.12, the total electric field distribution is provided.

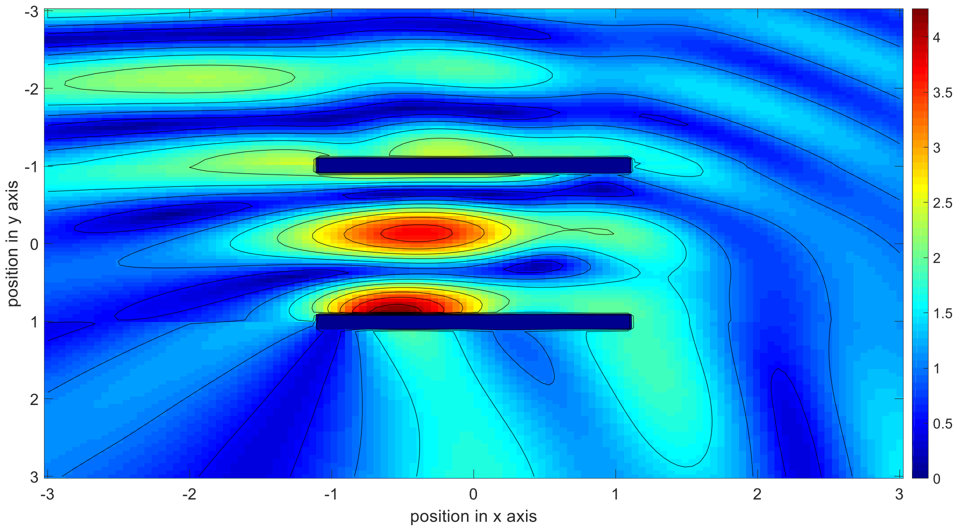

Figure 3.11 : Total Field $E_z, a_1 = a_2 = 1,\ l = 1, \alpha = 0.75, ka_1 = 3.4, \theta = \frac{\pi}{3}$.

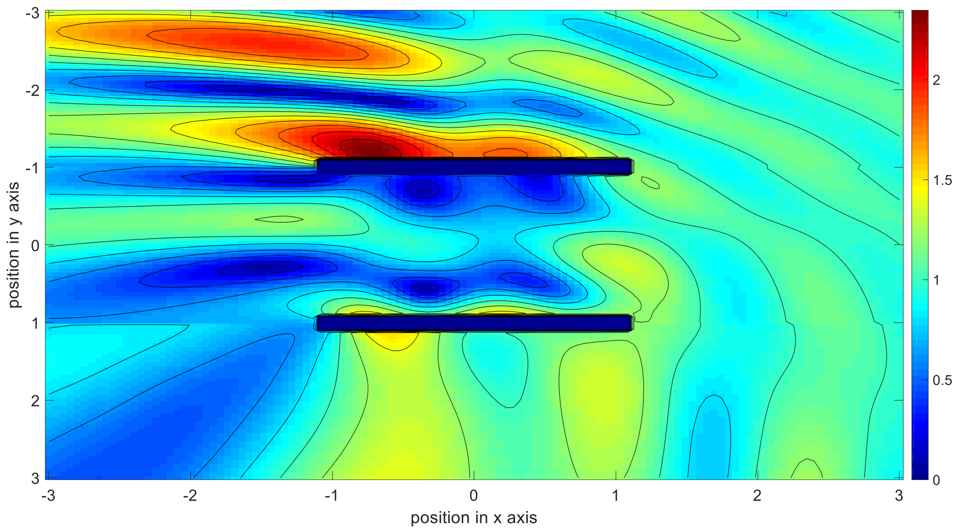

Figure 3.12 : Total Field $E_z, a_1 = a_2 = 1, l = 1, \alpha = 0.75, ka_1 = 3.4, \theta = \frac{\pi}{4}$.

After analyzing the equal length strips, it is better to analyze for $a_1 = 3; a_2 = 4$.

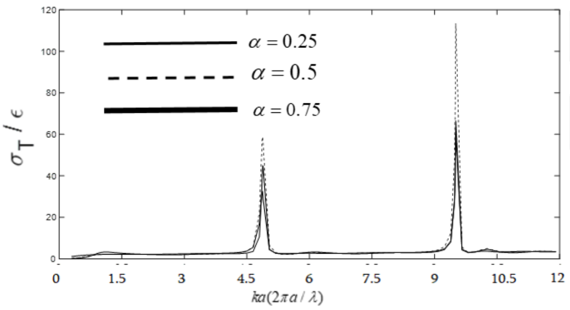

Figure 3.13 : σ_T for $a = a_1 = 3, a_2 = 4, l = 1, \theta = \frac{\pi}{2}$.

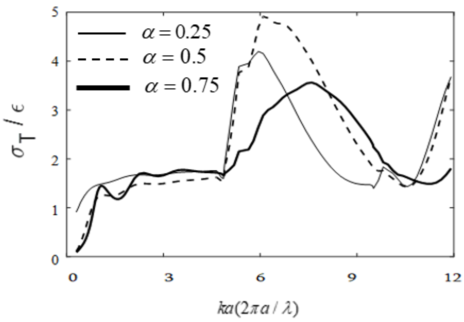

Figure 3.14 : σ_T for $a = a_1 = 3, a_2 = 4, l = 1, \theta = \frac{\pi}{4}$.

In Figure 3.14, the incidence angle is changed to $\theta = \frac{\pi}{4}$. In this case, the resonance behavior change and the resonance wavenumber are broadened.

After having the TRCS values, it is better to investigate the total field E_z distribution at the resonance frequencies. Figure 3.15 illustrates the total field distribution at the second resonance wavenumber. The field maximum is more than 70. The total field dominates inside the strips.

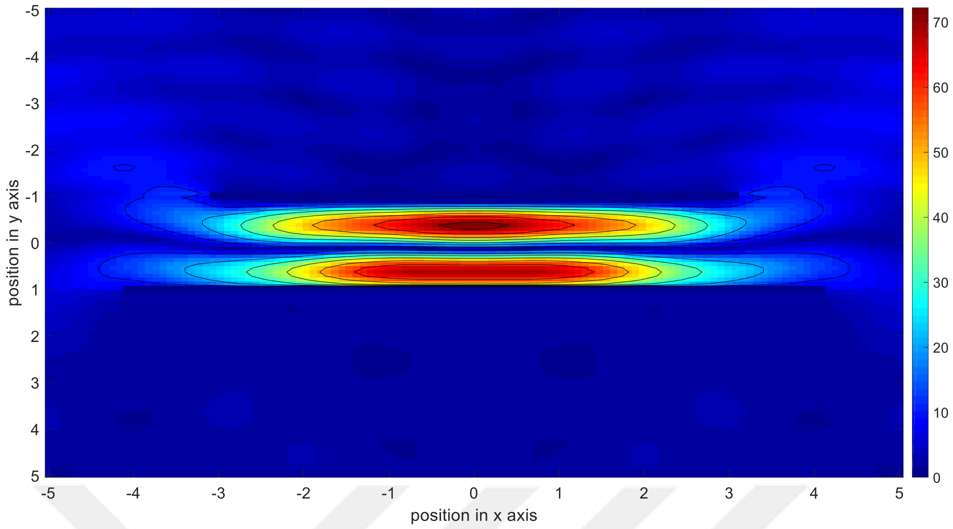

Figure 3.15 : Total Field E_z, $a_1 = 3, a_2 = 4,\ l = 1, \alpha = 0.25, ka_1 = 9.5$.

For the fractional-order $\alpha = 0.75$, the total field E_z distribution is given in Figure 3.16.

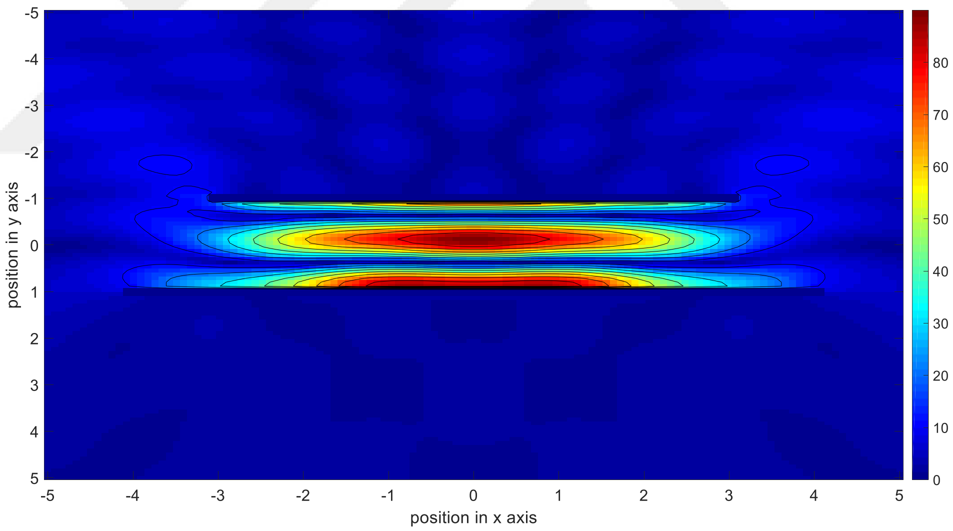

Figure 3.16 : Total Field E_z, $a_1 = 3, a_2 = 4,\ l = 1, \alpha = 0.75, ka_1 = 9.5$.

The fields characteristics of Figures 3.10 and 3.16 are the same. The only difference is the high field amplitudes in this case. If the incidence angle is changed and taken as $\theta = \frac{\pi}{3}$, the total field distribution gets the following form as Figure 3.17. Still, there is a resonance inside the strip with smaller field values.

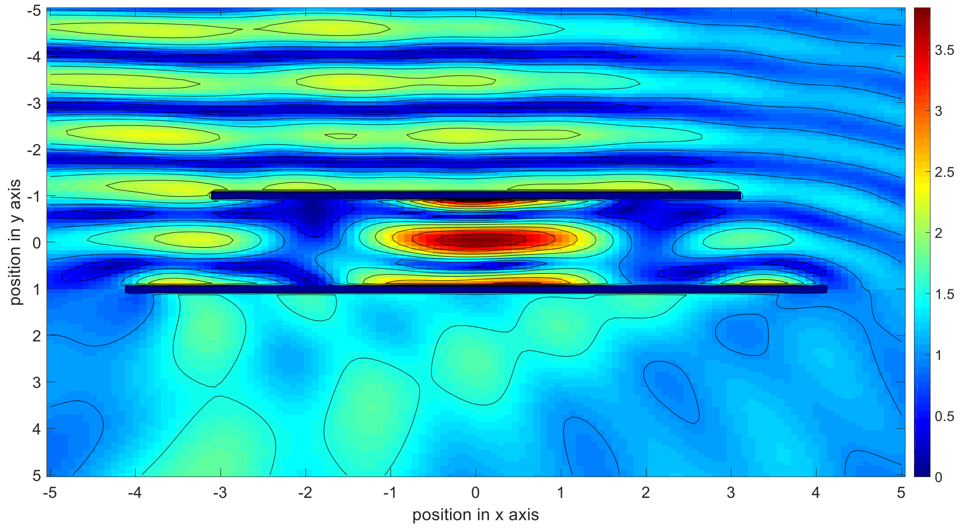

Figure 3.17 : Total Field $E_z, a_1 = 3, a_2 = 4, l = 1, \alpha = 0.75,\ ka_1 = 9, \theta = \frac{\pi}{3}$.

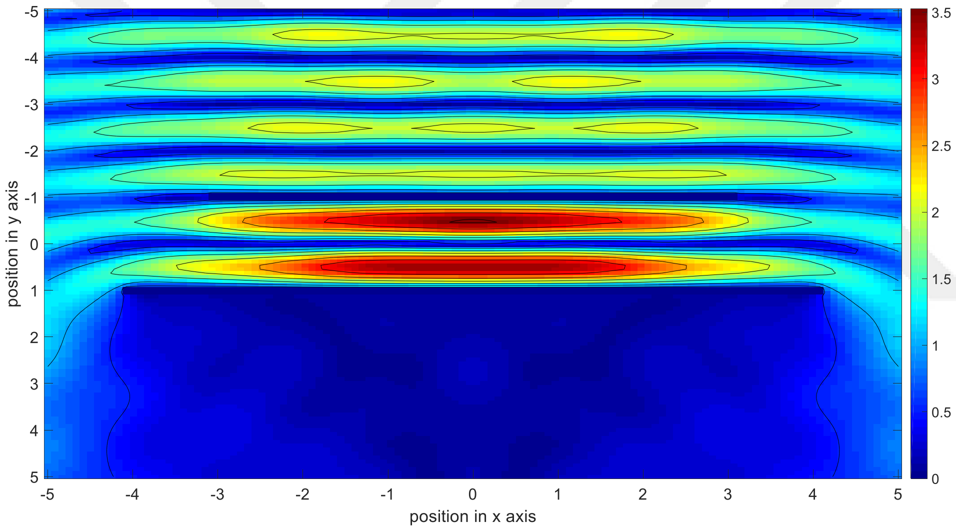

Figure 3.18 : Total Field $E_z, a_1 = 3, a_2 = 4, l = 1, \alpha = 0.01, ka_1 = 9.5, \theta = \frac{\pi}{2}$.

Figure 3.18 stands for the total field E_z distribution for the fractional-order $\alpha = 0.01$. This fractional-order is very close to the perfect electric conductor. The maximum field value is 3.5 which is smaller than $\alpha = 0.25$ and $\alpha = 0.75$ cases considered above. As it is seen, below the strips, there exists a shadow region and inside the strips, there is a resonance.

In Figures 3.19-3.22, the TRCS for different values of the fractional order and the distance between the strip are investigated. As expected, the resonance for the closer distance between the strips is at the higher values of ka. On the other hand, for this range of ka, more numbers of resonance values exist for the larger distance between the strips. As a general comment, the resonance has the highest value when the incidence wave is from the normal [5,35,37].

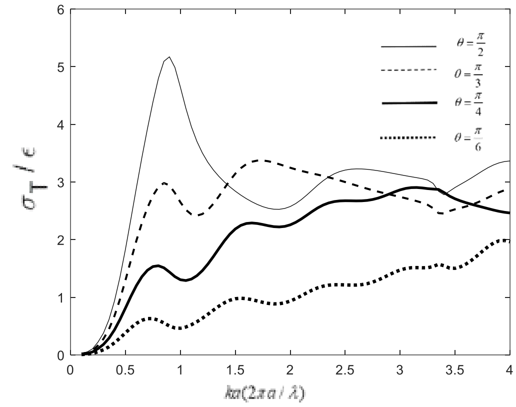

Figure 3.19 : σ_T for $a_1 = 1, a_2 = 2, l = 0.5, \alpha = 1.$

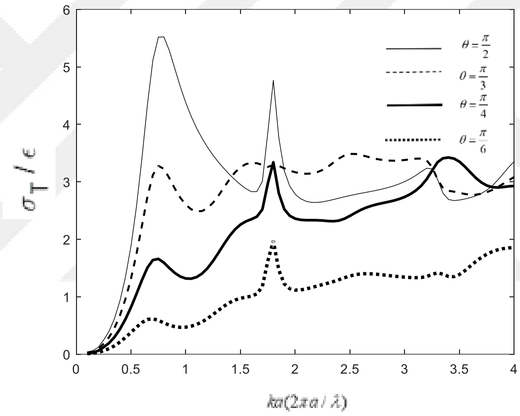

Figure 3.20 : σ_T for $a_1 = 1, a_2 = 2, l = 1, \alpha = 1.$

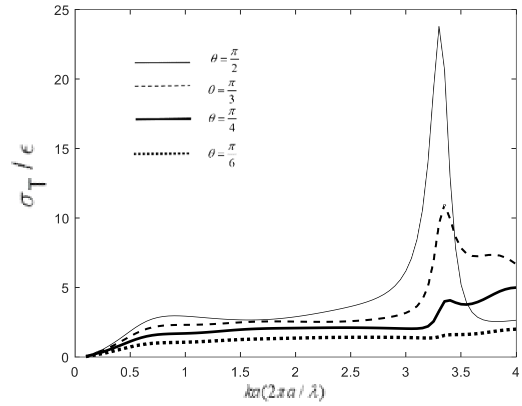

Figure 3.21 : σ_T for $a_1 = 1, a_2 = 1, l = 0.5, \alpha = 0.5.$

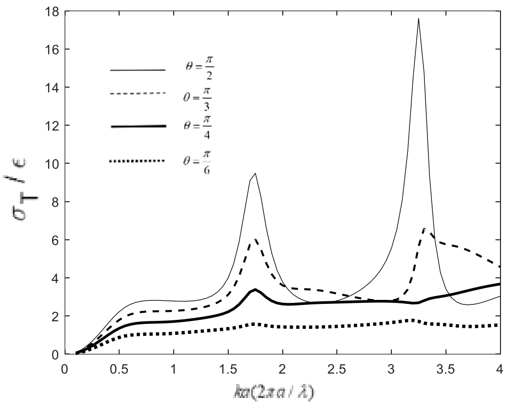

Figure 3.22 : σ_T for $a_1 = 1, a_2 = 1, l = 1, \alpha = 0.5$.

In Figures 3.23 and 3.24, the total electric field values are given. In Figure 3.23, a resonance is observed. The field values are greater between the strips compared to the outside. Notice that, the fractional-order is closer to the PMC case. The boundary condition is similar to the Neumann boundary condition because the fractional-order is much closer to 1 which stands for the Neumann boundary condition.

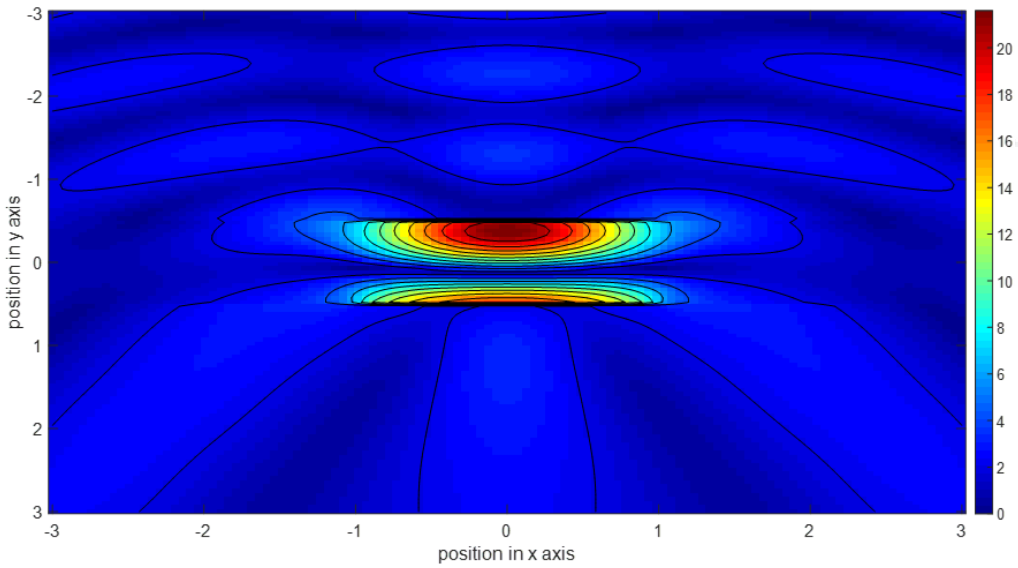

Figure 3.23 : Total Field E_z, $a_1, a_2 = 1, l = 0.5$, $\alpha = 0.75, k = 3.4$.

In Figure 3.24, a resonance is observed. The field values are greater between the strips compared to the outside. Notice that, the fractional-order corresponds to a PMC surface.

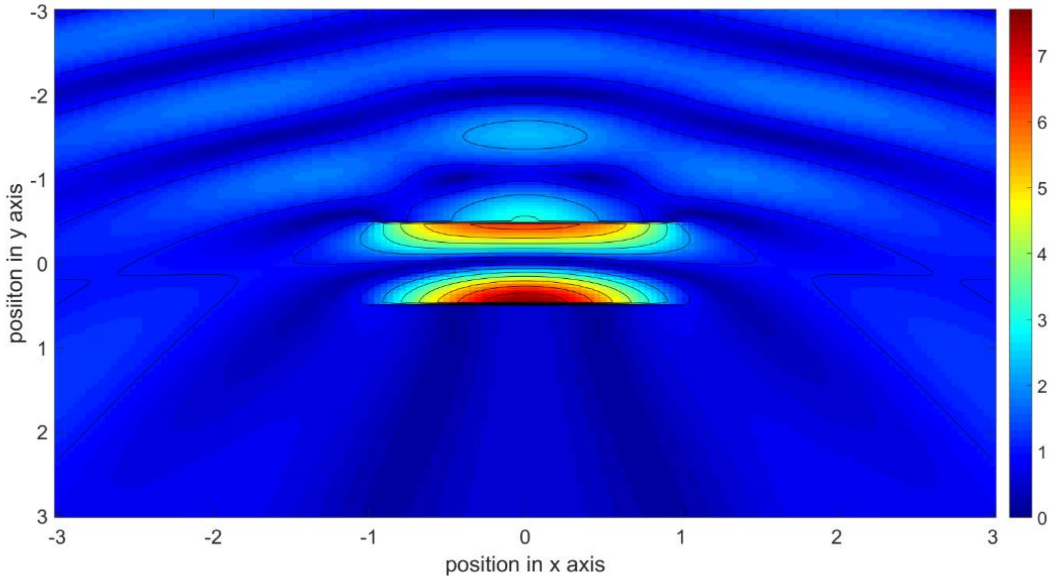

Figure 3.24 : Total Field E_z, $a_1, a_2 = 1, l = 0.5, \alpha = 1, k = 3.4$.

In Figures 3.25-3.27, normalized radiation patterns for different configurations are presented. In Figures 3.25 and 3.27, there is a normal incidence. For Figure 3.26, the incidence angle is 45^0.

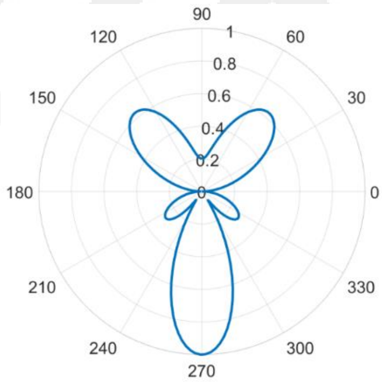

Figure 3.25 : RP for $a_1, a_2 = 1, l = 0.5,\ \alpha = 1\ k = 3$.

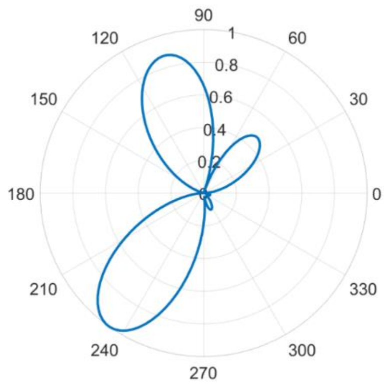

Figure 3.26 : RP for $a_1, a_2 = 1, l = 0.5,\ \alpha = 1\ k = 3$.

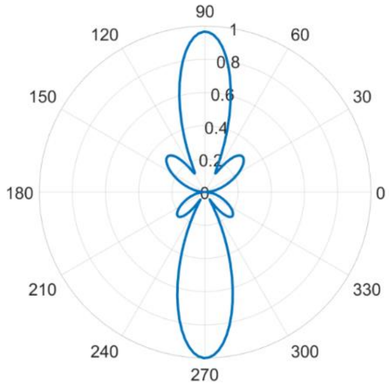

Figure 3.27 : RP for $a_1, a_2 = 2, l = 0.5,\ \alpha = 0.5, k = 3$.

Finally, in Figures 3.28 - 3.34, the distribution of the Poynting vectors in the vicinity of the strips for different scenarios is given by taking into account (13). Note that, the Poynting vectors are calculated by total fields. In Figure 3.28, the surfaces of the strips behave as PMC ($\alpha = 1$). In this case, energy flow penetrates through the strips whereas, in Figure 3.29, the energy goes around the strips since the boundary condition in the figure corresponds to the Dirichlet boundary condition. In Figure 3.29, the power behind the strips is low as expected because the strips create a shadow region behind when the strips behave as PEC [5,35,37]

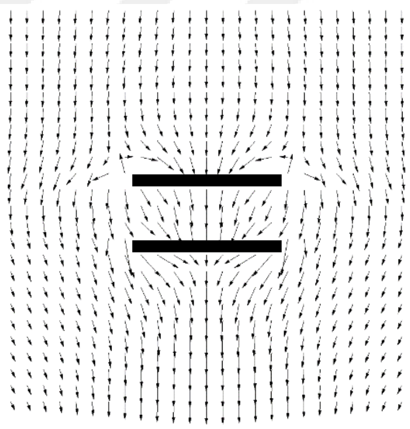

Figure 3.28 : Poynting Vector Distribution for $a_1 = 1,\ a_2 = 1, l = 0.5, \alpha = 1, ka_1 = 1, \theta = \frac{\pi}{2}$.

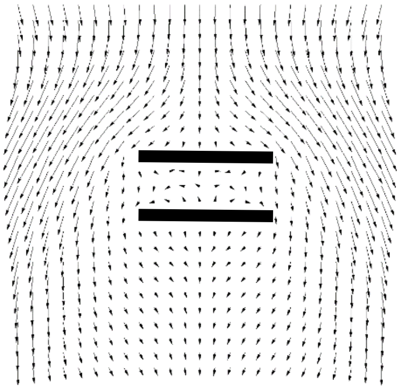

Figure 3.29 : Poynting Vector Distribution for $a_1 = 1,\ a_2 = 1, l = 0.5, \alpha = 0.01, ka_1 = 1, \theta = \frac{\pi}{2}$.

Figures 30 and 31 stand for the Poynting vector distribution in the cases of $\alpha = 0.5$ and $\alpha = 0.75$ respectively. In Figure 3.30, energy both goes around and penetrates through the strips from both sides. In the case of Figure 3.31, it is close to PMC due to having fractional-order $\alpha = 0.75$, so the flow of the energy resembles Figure 3.28.

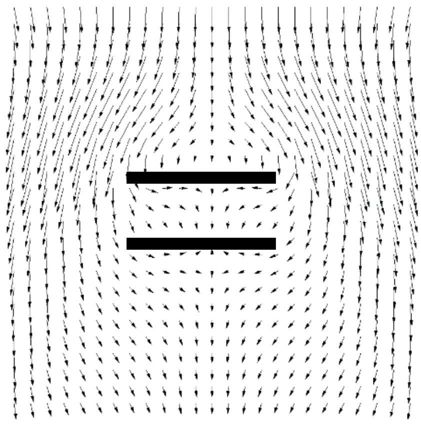

Figure 3.30 : Poynting Vector Distribution for $a_1 = 1, a_2 = 1,\ l = 0.5, \alpha = 0.5, ka_1 = 1, \theta = \frac{\pi}{2}$.

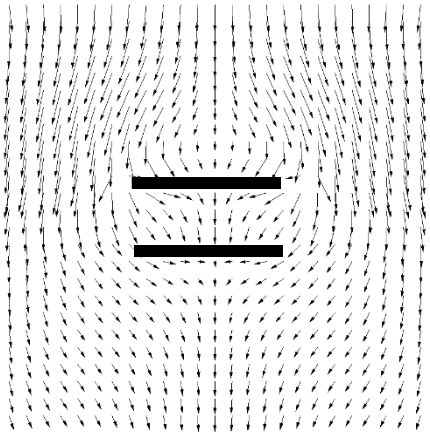

Figure 3.31 : Poynting Vector Distribution for $a_1 = 1, a_2 = 1,\ l = 0.5, \alpha = 0.75, ka_1 = 1, \theta = \frac{\pi}{2}$.

The Poynting vector distributions are also obtained while having different strip dimensions and distances between. Figures 3.32 and 3.33 illustrate the Poynting vector distribution when $a_1 = 3, a_2 = 4$ for $\alpha = 1$ and $\alpha = 0.01$, respectively. In Figures 3.32 and 3.33, the propagation cannot penetrate between the strips much [5,35,37].

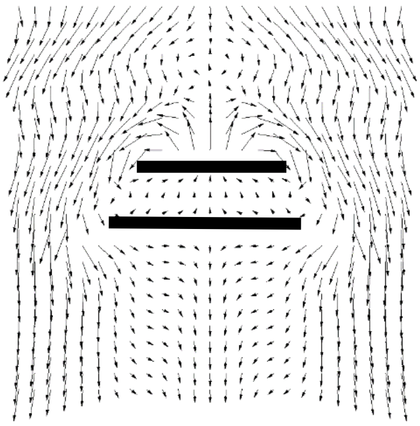

Figure 3.32 : Poynting Vector Distribution for $a_1 = 3,\ a_2 = 4, l = 1, \alpha = 1, ka_1, 3, \theta = \frac{\pi}{2}$.

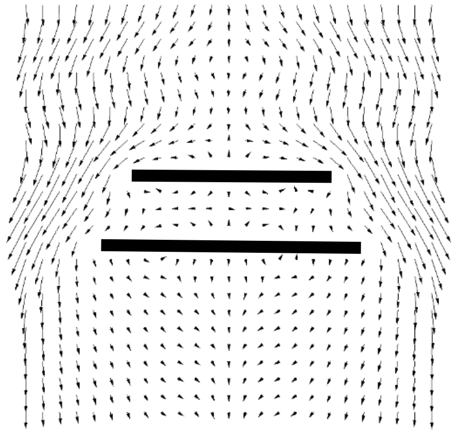

Figure 3.33 : Poynting Vector Distribution for $a_1 = 3,\ a_2 = 4, l = 1, \alpha = 0.01, ka_1 = 3, \theta = \frac{\pi}{2}$

The Poynting vector distribution when $a_1 = 3, a_2 = 4$ for $\alpha = 0.5$ is given in Figure 3.34. Here, vortexes on the upper part are observed.

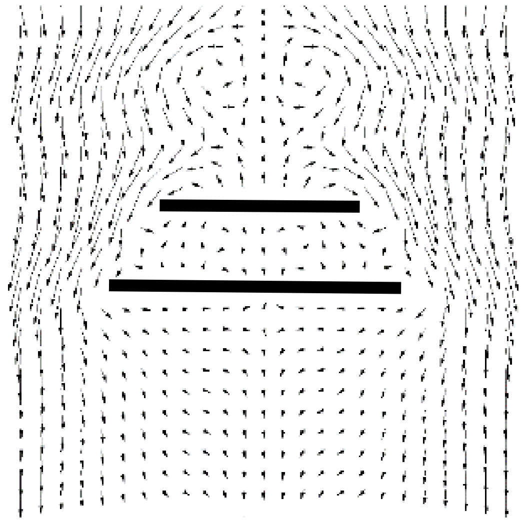

Figure 3.34 : Poynting Vector Distribution for $a_1 = 3, a_2 = 4, l = 1, \alpha = 0.5, ka_1 = 3, \theta = \frac{\pi}{2}$.

3.3 Double-strips with Different Boundary Conditions

In this section, the computational results of the diffraction by double strips with variable fractional boundary conditions are investigated. Here, the comparison with previous findings and Method of Moments is done for the total radar cross-section, field distributions, and radiation patterns. Apart from the previous section, here, the radiation patterns for different combinations of the parameters are presented. This problem is a more general version of the previous problem because, in this problem, the boundary condition for each strip can differ [35]. In Figure 3.35, the geometry of the problem is given

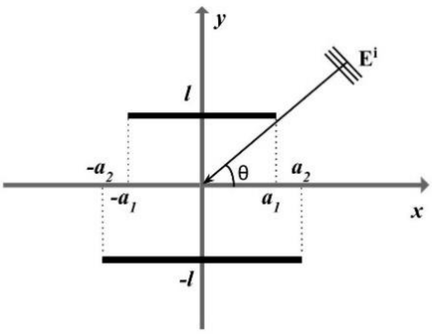

Figure 3.35 : The geometry of the problem.

For different parameters such as the fractional order, a_1, a_2, l and k, the investigations are done on the total near electric field, the far-field radiation pattern, and the total radar cross-section. For the total radar cross-section, the figures are drawn with respect to ka_1. In Figure 3.36, TRCS is obtained when the fractional orders are $\alpha_1 = 1, \alpha_2 = 0.01$. In this case, the upper strip satisfies the Neumann boundary condition for the electric field, which yields that the surface, behaves as the perfect magnetic conductor and the lower one behaves as the perfect electric conductor. Note that, in all figures, the normal incidence cases are studied.

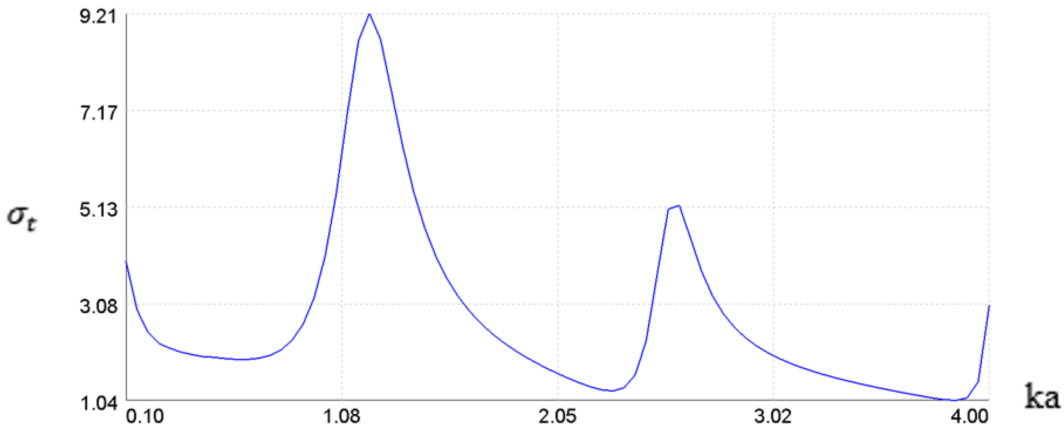

Figure 3.36 : Total radar cross section for $a_1 = 1, \mathrm{a}_2 = 1, \mathrm{l} = 1, \alpha_1 = 1, \alpha_2 = 0.01$.

From Figure 3.36, there are two resonance peaks in the given frequency range. In the following figure, the near and the far-field distributions for the first resonant peaks are given. As it can be seen from Figure 3.37, the boundary conditions for the electric field are satisfied. For the upper strips, the Neumann boundary condition is satisfied and the field's derivative becomes zero while approaching the strip whereas, for the lower strip, the Dirichlet boundary condition is satisfied and the field itself becomes zero while approaching the strip. Due to the resonance, the high amplitude electric field values occur around the upper strip. The reason why field distribution is not symmetrical is due to having two strips with different fraction orders. Note that, below the lower strip, there is a shadow region as expected because the lower strip corresponds to PEC material [35].

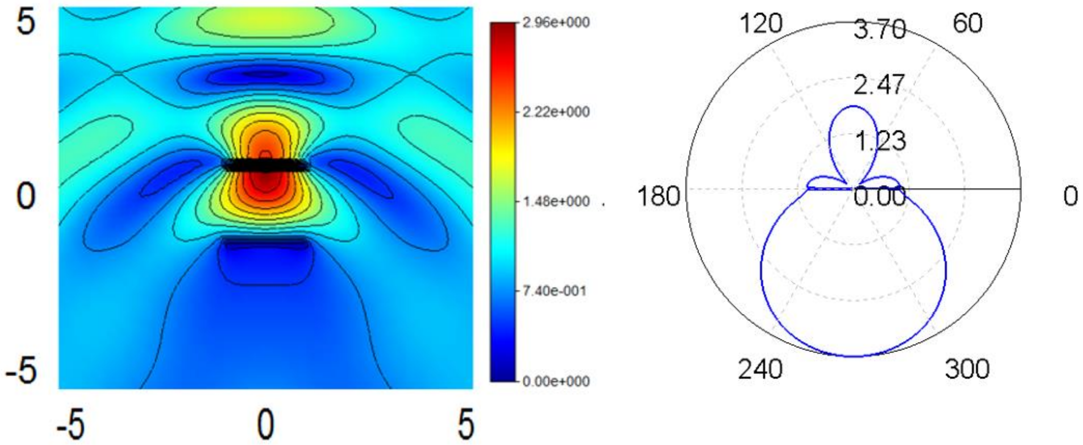

Figure 3.37 : Total near electric field and radiation pattern (RP) for $a_1 = 1, a_2 = 1, l = 1, \alpha_1 = 1, \alpha_2 = 0.01$ at the first resonance $k = 1.2$.

In Figure 3.38, the near and the far electric fields for the second resonance are illustrated (for $a_1 = 1, a_2 = 1, l = 1, \alpha_1 = 1, \alpha_2 = 0.01$). As it is seen from the far-field pattern, most of the scattered field is radiated below with a small back lobe. The comment on Figures 3.37 and 3.38 may be as the following. The radiation pattern is the far-field pattern that corresponds to the scattered field. The scattered field is directed through one direction mainly with small back lobes [35].

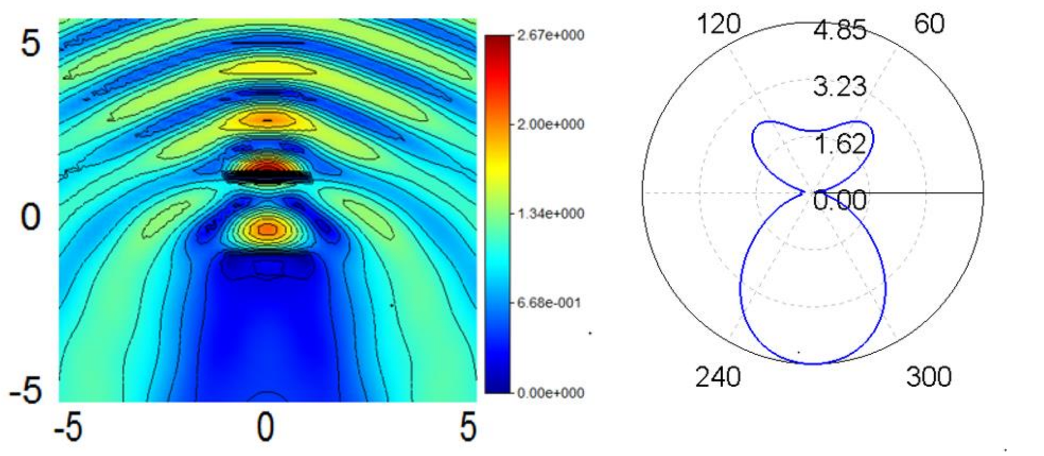

Figure 3.38 : Total near electric field and radiation pattern (RP at the second resonance $k = 2.6$.

Then, the fractional orders are flipped as $\alpha_1 = 0.01, \alpha_2 = 1$, respectively. In this case, the upper strip behaves as PEC and the lower strip is made up of PMC. Note that, the incidence angle is still the same. The corresponding TRCS and field distributions are given in Figures 3.39 and 3.40, respectively.

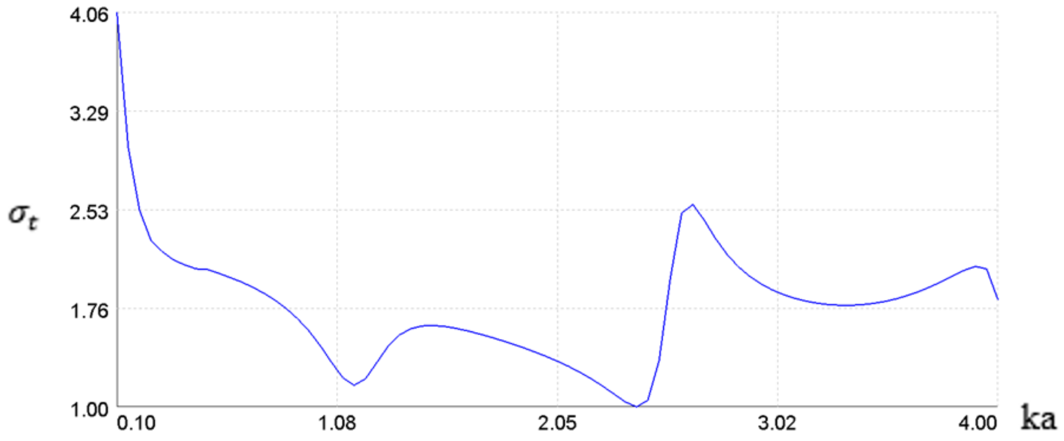

Figure 3.39 : Total radar cross-section for $a_1 = 1, a_2 = 1, l = 1, \alpha_1 = 0.01, \alpha_2 = 1$.

The results are very different compared to Figure 3.36. Here, only one sharp resonance exists in the ka range. A different result is expected because for this configuration, the upper strip is PEC and the field cannot penetrate through the strip. This case yields the lower field values between the strips. Furthermore, the lower strip satisfied the Neumann boundary condition. That is why the field between the strips has a lower amplitude distribution [35].

The resonance phenomena, in general, are related to the multiple reflections and diffraction of the electromagnetic wave between the strips. There exist the values of the frequencies for which the reflected and diffracted waves are in-phase and it increases the field value inside the strips from the superposition principle. This leads to having resonance peaks. The phase of the diffracted and reflected waves is different for different materials. Therefore, there is a difference between the TRCS graphs (Figure 3.36 and Figure 3.39). Figure 3.36 and Figure 3.39 illustrate quite different results because the incidence wave comes from above in both cases. If the angle of incidence is such that, it comes from below, the results would be the same but in a different order. In Figure 3.40, the near and far-field distributions of the electric field at the resonant wavenumber are obtained. Note that, the radiation pattern is directed mainly through the upper region (for $a_1 = 1, a_2 = 1, l = 1, \alpha_1 = 0.01, \alpha_2 = 1$) [35].

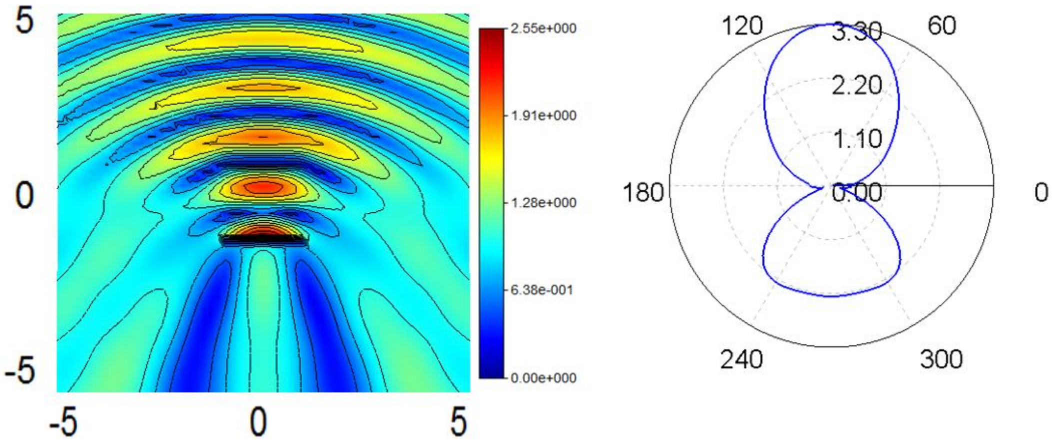

Figure 3.40 : Total near electric field and radiation pattern (RP) at the first resonance k = 2.64.

After analyzing and comparing the strips with PEC or PMC properties and their location dependency, the case with $\alpha_1 = 0.5, \alpha_2 = 1$ is studied. The corresponding TRCS is illustrated in Figure 3.41.

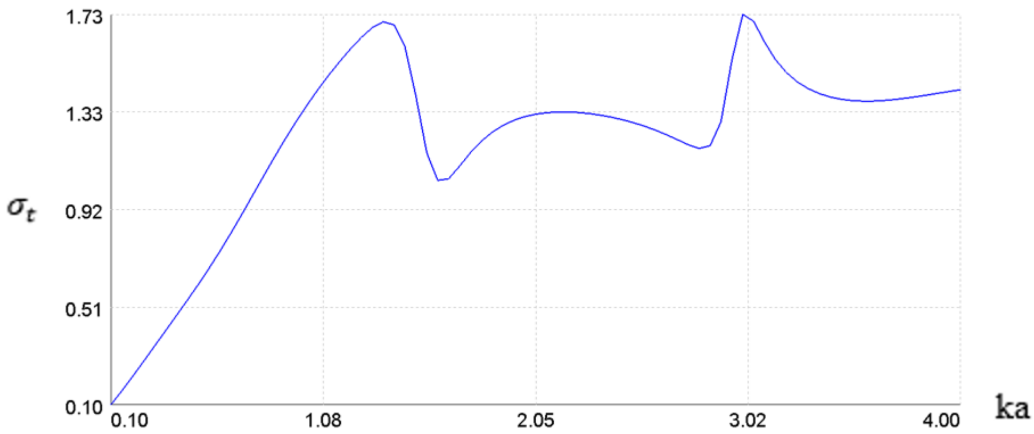

Figure 3.41 : Total radar cross section for $\mathrm{a}_1 = 1, \mathrm{a}_2 = 1, \mathrm{l} = 1, \alpha_1 = 0.5, \alpha_2 = 1$.

In Figure 3.41, there are two resonances in the range. At the first and the second resonances, the near and the far electric field distributions are given in Figure 3.42 and Figure 3.43, respectively (for $\mathrm{a}_1 = 1, \mathrm{a}_2 = 1, \mathrm{l} = 1, \alpha_1 = 0.5, \alpha_2 = 1$). Note that, for the PMC case, the Neumann Boundary condition is satisfied (lower strip) and for the upper strip, the boundary condition shows the intermediate case for the Dirichlet and the Neumann conditions [37].

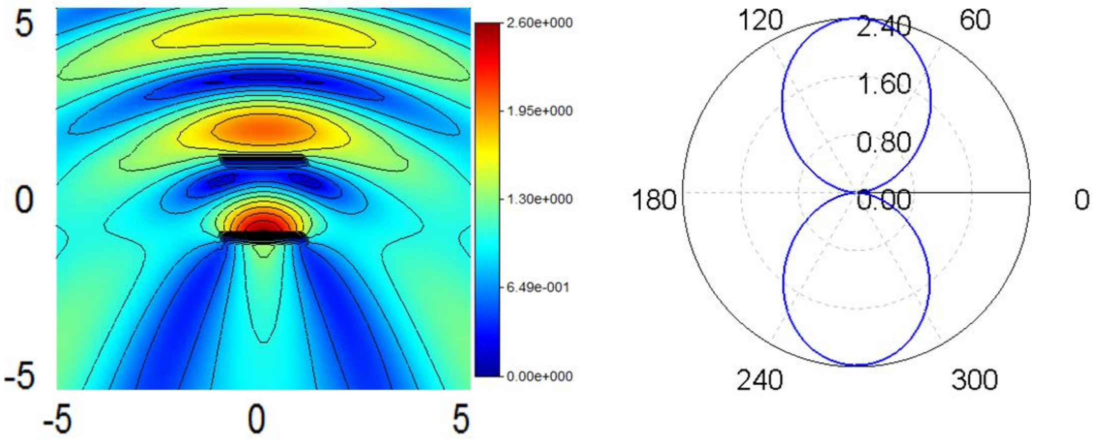

Figure 3.42 : Total near electric field and radiation pattern (RP) at the first resonance $\mathrm{k} = 1.35$.

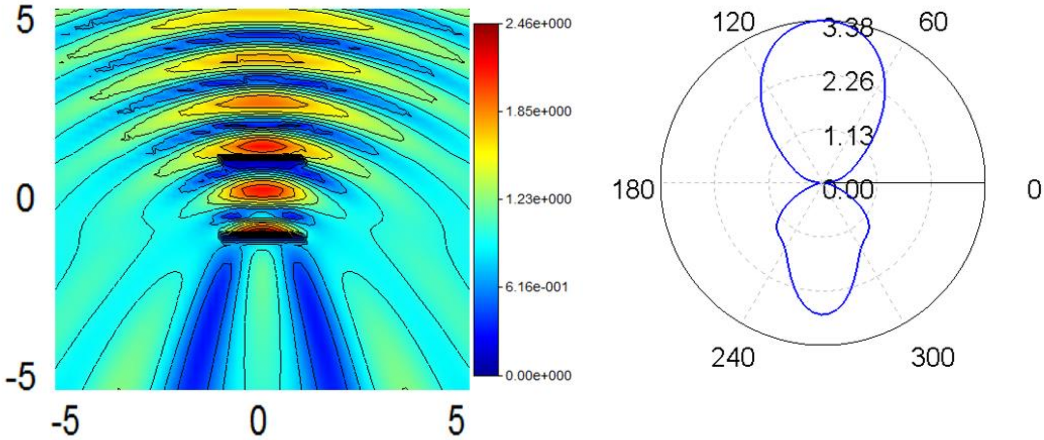

Figure 3.43 : Total near electric field and radiation pattern (RP) at the second resonance $\mathrm{k} = 3$.

Here, the fractional orders are $\alpha_1 = 1, \alpha_2 = 0.5$, respectively. The resultant TRCS is illustrated in Figure 3.44.

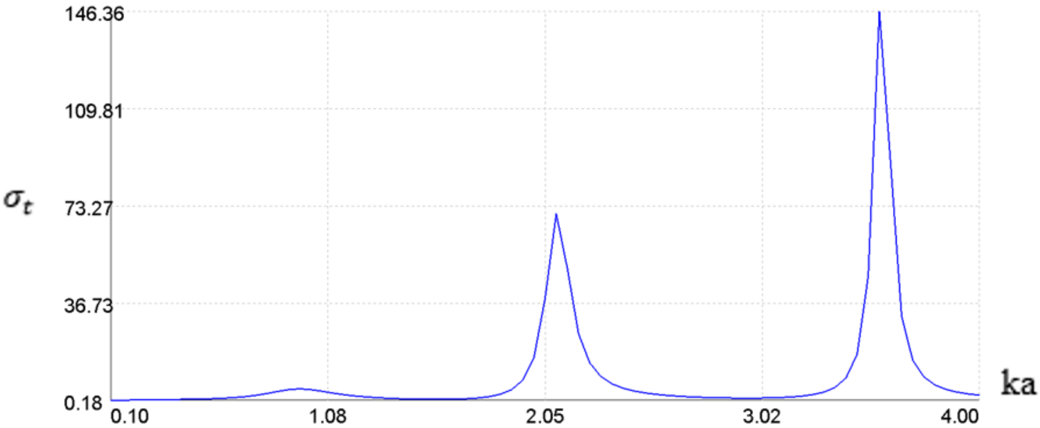

Figure 3.44 : Total radar cross section for $\mathrm{a}_1 = 1, \mathrm{a}_2 = 1, \mathrm{l} = 1, \alpha_1 = 1, \alpha_2 = 0.5$.

In Figure 3.44, there are two noticeable resonances in the interval. However, they are sharper and narrower compared to previous cases. The resonator with the sharp resonance characteristics may have an application in high-quality factor resonators for a narrow band apparatus [37]. Note that, also the TRCS value has a quite higher value compared to previous outcomes. Again, it can be used as a high-quality factor resonator for this wavenumber range. The corresponding near and far electric field distributions on the first resonance are given in Figure 3.45 (for $a_1 = 1, a_2 = 1, l = 1, \alpha_1 = 1, \alpha_2 = 0.5$).

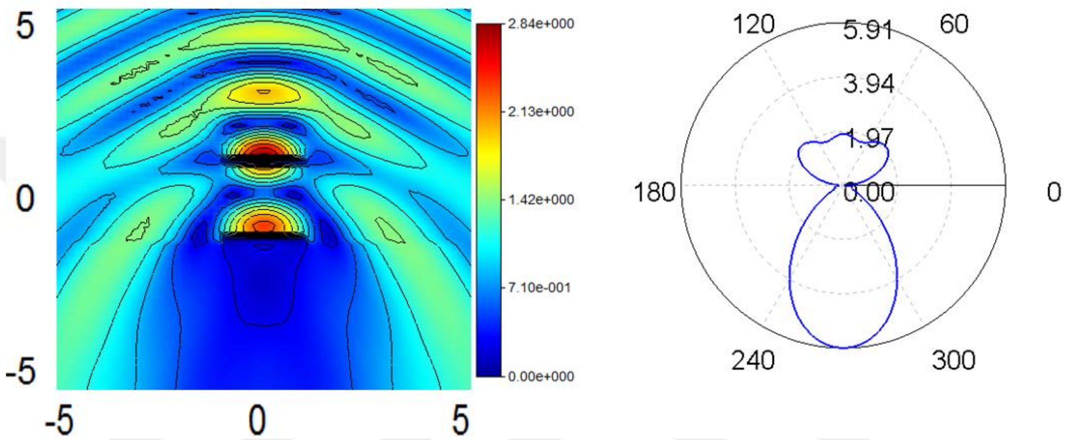

Figure 3.45 : Total near electric field and radiation pattern (RP) at the first resonance $k = 2.23$.

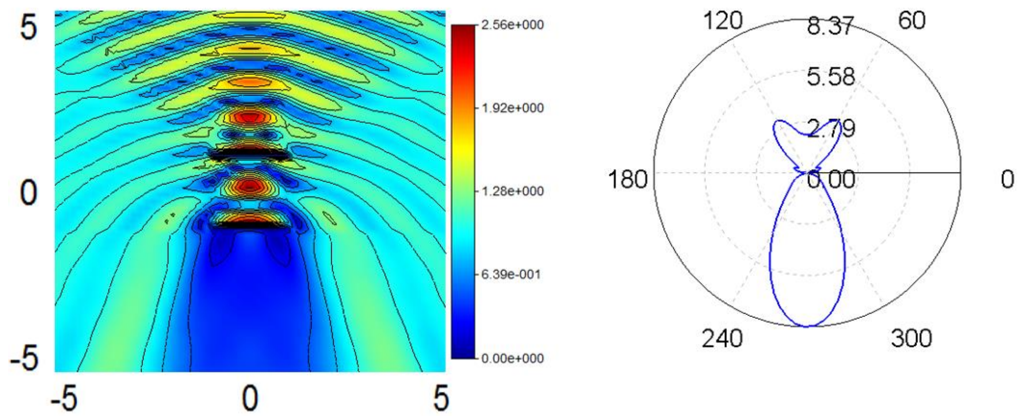

Figure 3.46 : Total near electric field and radiation pattern (RP) at the second resonance $k = 3.72$.

Now, it is better to investigate the second resonance for the same configuration above. The near and the far electric field distributions for the second case are illustrated in Figure 3.46 (for $a_1 = 1, a_2 = 1, l = 1, \alpha_1 = 1, \alpha_2 = 0.5$). The radiation patterns in

Figures 3.45 and 3.46 are similar to each other. As expected, scattering by the plane wave with a higher frequency is more directive as noticed in both figures.

The comparison between cases $\alpha_1 = 1, \alpha_2 = 0.01$ and $\alpha_1 = 1, \alpha_2 = 1$ is shown in Figure 3.47. The results are very different. In the first case, $\alpha_1 = 1, \alpha_2 = 0.01$ is compared with previous findings [18, 19]. The deviation is less than 2%.

The result for fractional orders $\alpha_1 = 1, \alpha_2 = 1$ corresponds to double strips with the PMC surface (surface satisfies the Neumann Boundary condition for the total tangential electric field) and the previous studies coincide with new results [35]. The deviation between previous findings [35] and our study is less than 2%. In Figure 3.47, the previous findings are given as blue circles whereas the dashed line is obtained with the fractional derivative method [35].

Figure 3.48 illustrates the comparison of two cases for the values of different boundary condition (fractional orders) $\alpha_1 = 0.01, \alpha_2 = 0.01$ and $\alpha_1 = 0.01, \alpha_2 = 1$. The results are quite different as expected. Note that, when Figure 3.47 and Figure 3.48 are compared, there is a noticeable difference between the two sequences of fractional boundary condition choices.

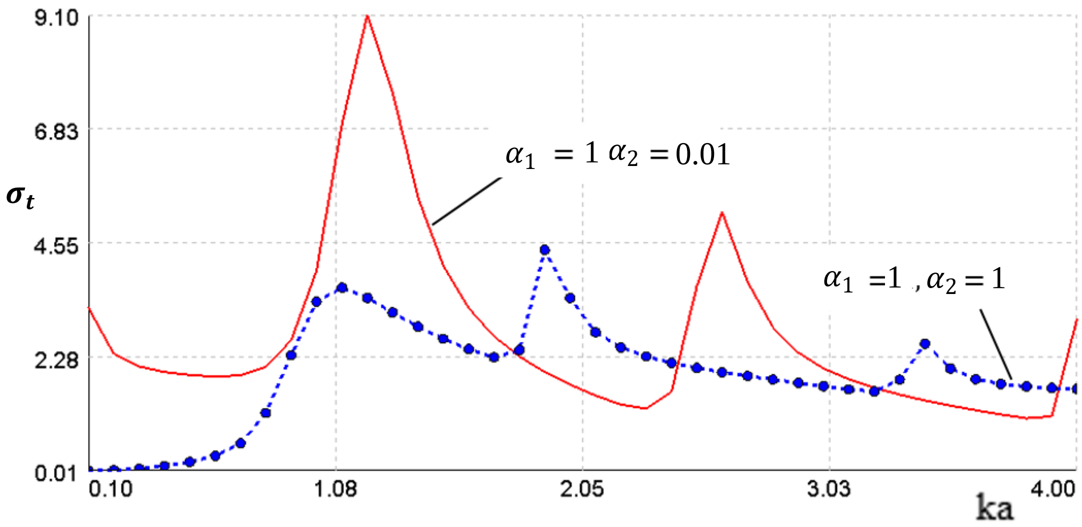

Figure 3.47 : Total radar cross section for $a_1 = 1, a_2 = 1, l = 1$ and comparison with previous findings [18, 19].

In other words, choices as $\alpha_1 = 1, \alpha_2 = 0.01$ in Figure 3.47 and $\alpha_1 = 0.01, \alpha_2 = 1$ in Figure 3.48 behaves distinctly. Note that the angle of incidence is the same (the normal incidence). In Figure 3.48, the sharp resonances are not noticed for this ka range. As the upper strip is a perfect electric conducting surface, the field cannot penetrate through the strip. This creates a shadow region below the strip with a perfectly electric conducting surface.

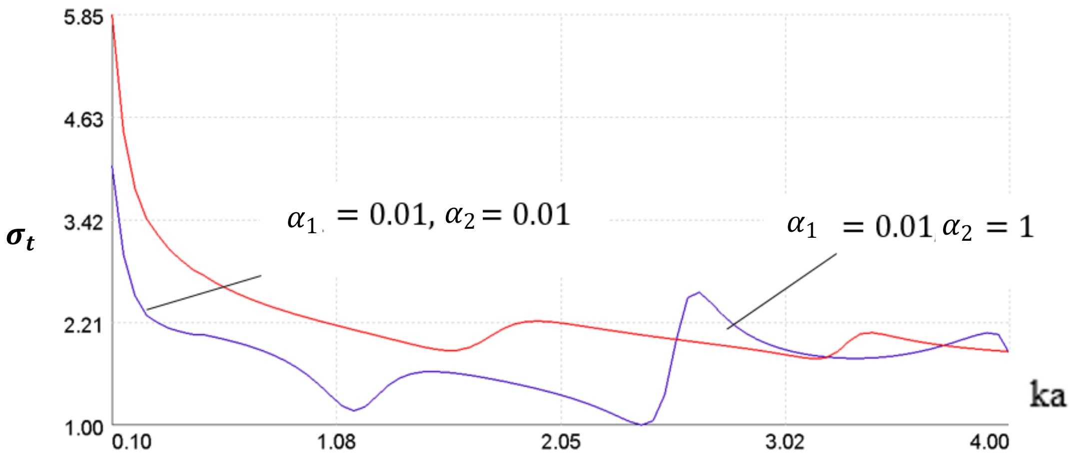

Figure 3.48 : Total radar cross section for $a_1 = 1, a_2 = 1, l = 1$.

In Figure 3.49, the analogy between the Method of Moments (MoM) and the fractional approach is obtained for the case that both strips are PEC (for $a_1 = 1, a_2 = 1, l = 0.5, \alpha_1 = 0.01, \alpha_2 = 0.01$ at $k = 3$.). This figure is done to compare the method with other well-known methods. As it is seen in these figures, the total electric field and normalized radiation patterns are very similar to each other. The error between the two results obtained by MoM and the fractional derivative method is less than 3%. In the radiation pattern, the blue line corresponds to the MoM solution whereas; the red line stands for the result employed by the fractional method.

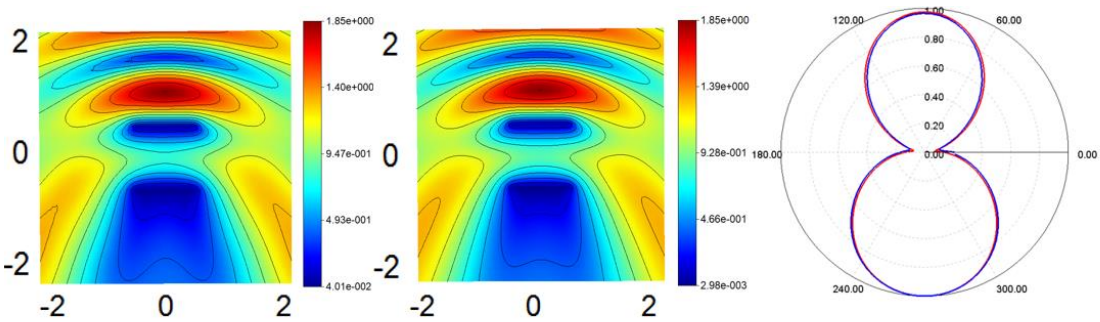

(a) (b) (c)

Figure 3.49 : Total near electric field with MoM (a), with Fractional approach (b) and radiation pattern (c)

In Figure 3.50, two important scenarios are shown. In the first one (a), the lower strip is larger than the upper strip compared to the electrical length ($a_1 = 0.5$, $a_2 = 2$, $k = 1, l = 1$, $\alpha_1 = 0.01$, $\alpha_2 = 1$). The field distribution is dominated by the characteristics of the lower strip corresponding to PMC material. It is an expected result since the width of the small strip and the distance between the two strips are comparable with the wavenumber. Therefore, the larger strip dominates the field characteristics. In the second one (b), the width of the two strips is chosen very similarly to each other to check the stability of the solution ($\mathrm{a}_1 = 1, \mathrm{a}_2 = 1.1, \mathrm{l} = 1,\ \mathrm{k} = 1.2, \alpha_1 = 1, \alpha_2 = 0.01$). The same parameters in Figure 3.37 are employed for that figure to compare. As can be seen from Figure 50(b), the field distributions are quite similar to Figure 3.37. The amplitudes are slightly different as expected because Figure 3.37 is obtained at resonance wavenumber [35].

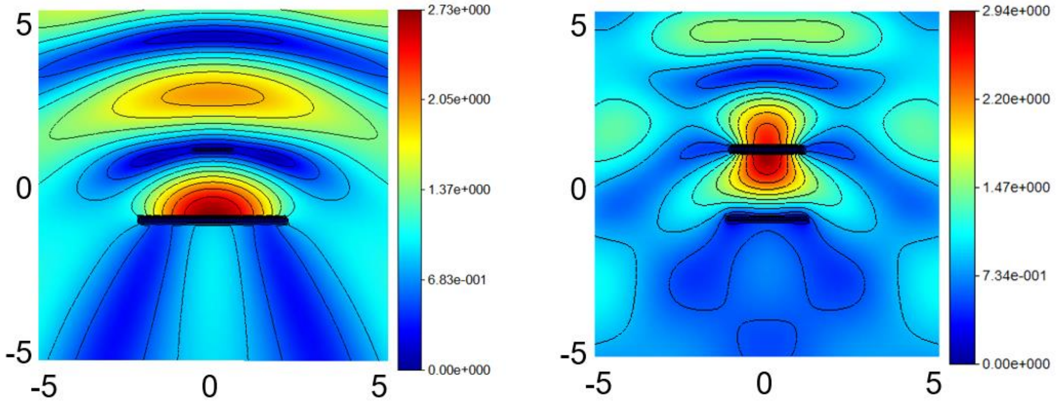

(a) (b)

Figure 3.50 : Total near electric field for the case (a), $\mathrm{a}_2 \gg \mathrm{a}_1$ and for the case (b), $\mathrm{a}_1 \approx \mathrm{a}_2$.

In Figure 3.51, the investigation is done on the width of the strips. The widths of strips are chosen very similarly to each other and the field distribution and the amplitude of the electric total electric field are approximately the same as expected because this is the non-resonance case. The parameters are given as follows. For Figure 3.51(a), the parameters are ($\mathrm{a}_1 = 2, \mathrm{a}_2 = 2, \mathrm{l} = 0.5,\ \mathrm{k} = 1, \alpha_1 = 1, \alpha_2 = 0.01$) and for Figure 3.51(b), parameters are ($\mathrm{a}_1 = 1.95, \mathrm{a}_2 = 2, \mathrm{l} = 0.5,\ \mathrm{k} = 1, \alpha_1 = 1, \alpha_2 = 0.01$).

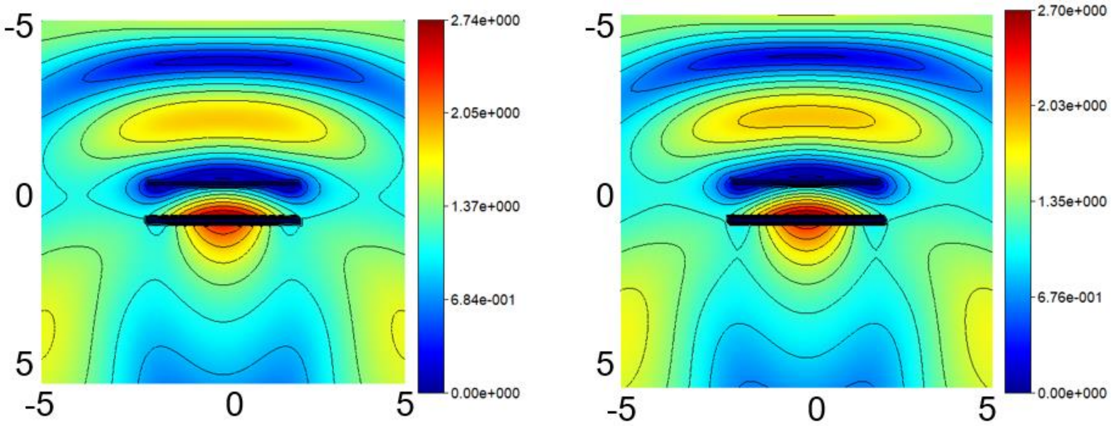

(a) (b)

Figure 3.51 : Total near electric field for the case (a), $a_2 = a_1$ and for the case (b), $a_1 \approx a_2$.

3.4 Single-strip with Fractional Boundary Conditions

In previous sections, the analytical and the numerical analysis have been studied for double strips. In this chapter, the investigation would be on the diffraction by one strip only for the fractional-order 0.5 case. Previously, diffraction by a strip by plane and cylindrical waves is investigated [6,33,38]. However, numerical and detailed analyses for the fractional-order 0.5 cases are not studied yet. In Figure 3.52, the geometry of the problem is given.

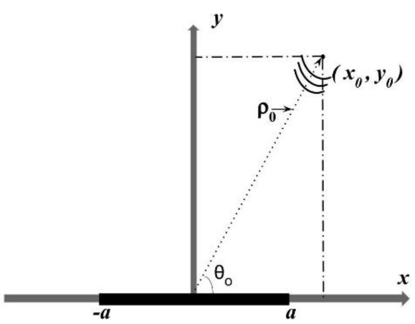

Figure 3.52 : The geometry of the problem.

The importance of the case when the fractional order is equal to 0.5 is that the analytical expression can be obtained for the plane wave case and also for the cylindrical wave as an incidence wave, closed-form of the induced current and the Fourier transform of the current can be found by some approximations [33,35,38]. Here, an investigation is done on the field, current distribution, and the bistatic radar cross-section. Note that, for the numerical analysis $B = -J_e \frac{\eta_0 k}{4\pi}$ used in (2.47) is assumed to be 1. In Figures 3.53 and 3.54, the amplitudes of scattered and total electric fields for the same configuration are obtained.

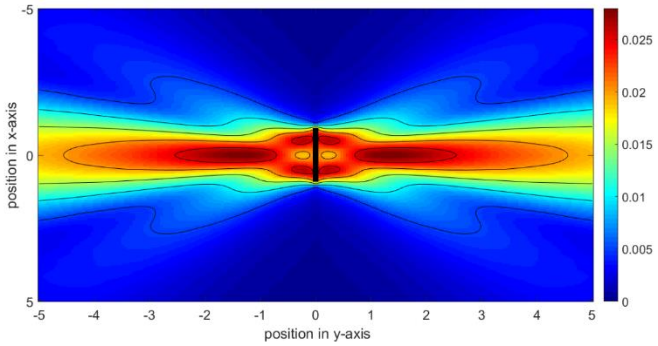

Figure 3.53 : The Amplitude of the Scattered Electric Field $\vec{E}_z^s$ for $a = 1$, $\epsilon = 2\pi$, $x_0 = 0$ and $y_0 = 2\pi$.

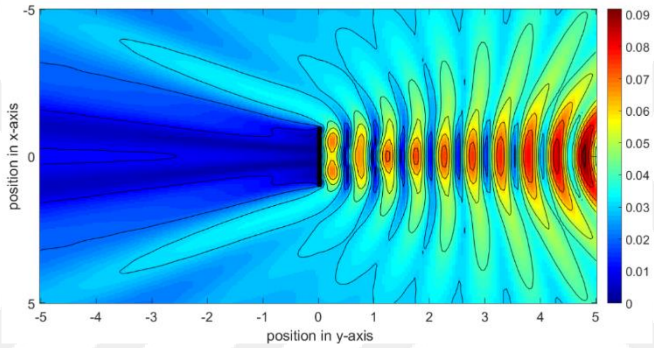

Figure 3.54 : The Amplitude of the Total Electric Field $\vec{E}_z^i$ for $a = 1$, $\epsilon = 2\pi$, $x_0 = 0$ and $y_0 = 2\pi$.

In Figures 3.55 and 3.56, the amplitudes of scattered and total electric fields for the same configuration are obtained. Note that, this is the oblique incidence $\left(\theta_0 = \frac{\pi}{4}\right)$.

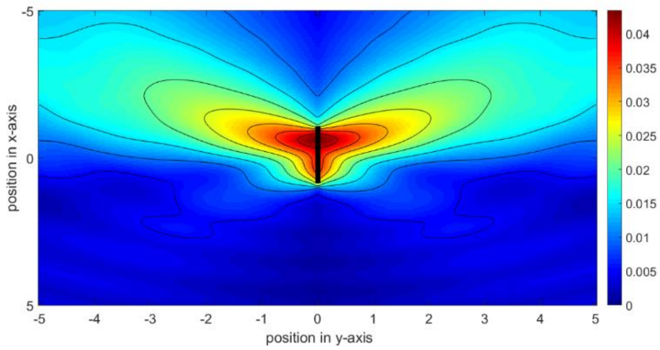

Figure 3.55 : The Amplitude of the Scattered Electric Field $\vec{E}_z^s$ for $a = 1$, $\epsilon = \pi$, $x_0 = 2\pi$ and $y_0 = 2\pi$.

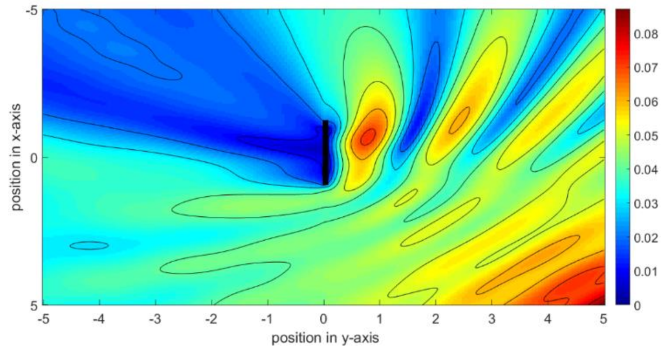

Figure 3.56 : The Amplitude of the Total Electric Field $\vec{E}_z^i$ for $a = 1$, $\epsilon = \pi$, $x_0 = 2\pi$ and $y_0 = 2\pi$.

In Figures 3.57 and 3.58, the amplitudes of the total electric fields are given for different parameters.

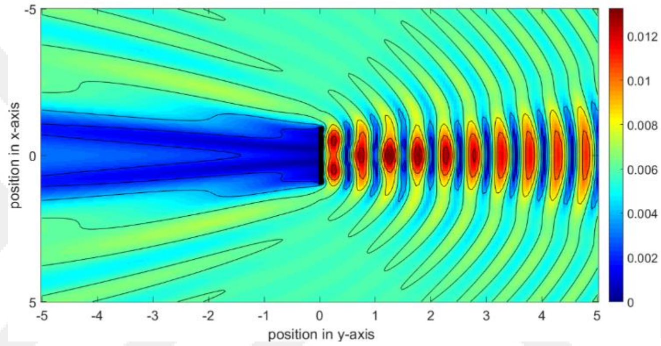

Figure 3.57 : The Amplitude of the Total Electric Field $\vec{E}_z^i$ for $a = 1$, $\epsilon = 2\pi$, $x_0 = 0$ and $y_0 = 6$.

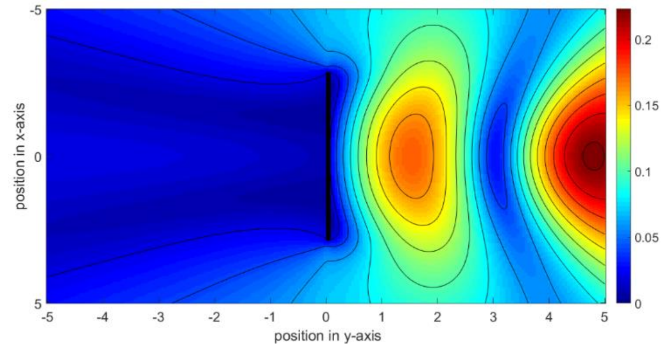

Figure 3.58 : The Amplitude of the Total Electric Field $\vec{E}_z^i$ for $a = 3$, $\epsilon = 2\pi$, $x_0 = 0$ and $y_0 = 2\pi$.

In Figures 3.59 and 3.60, Bi-static RCS with different frequency parameters $\epsilon = ka$ values is given. The main motivation for investigation on bi-static radar cross-section is to analyze the scattering properties of the surface and radiation characteristics depending on the angle. For bi-static radar cross-section studies, the source is located at one specific angle and the scattered field is found with this given angle for the incidence wave. The position of the source line and the angle with respect to the x-axis are presented. On the figures, Curve 1 stands for $\theta_0 = 90^0$, $x_0 = 0$, $y_0 = \epsilon$, Curve 2 corresponds to $\theta_0 = 90^0$, $x_0 = 0$, $y_0 = 20\epsilon$, Curve 3 is responsible for $\theta_0 = 45^0$, $x_0 = 3\epsilon$, $y_0 = 3\epsilon$ and finally Curve 4 stands for $\theta_0 = 60^0$, $x_0 = 3\epsilon$, $y_0 = 3\sqrt{3}\epsilon$ [6,33,38]. As it can be seen in the figures, for some specific angles, the amplitude of the scattered field is very low compared to other angle directions.

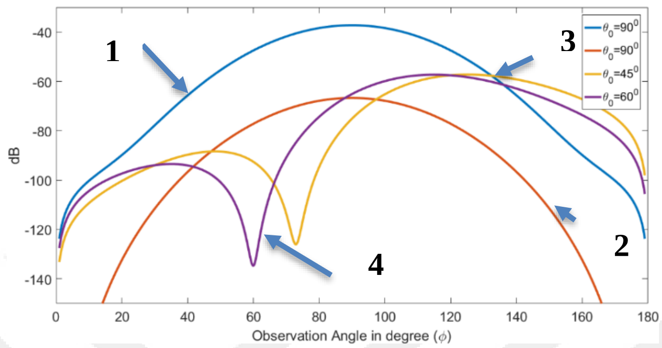

Figure 3.59 : Bi-static Radar Cross Section for $\epsilon = \pi$.

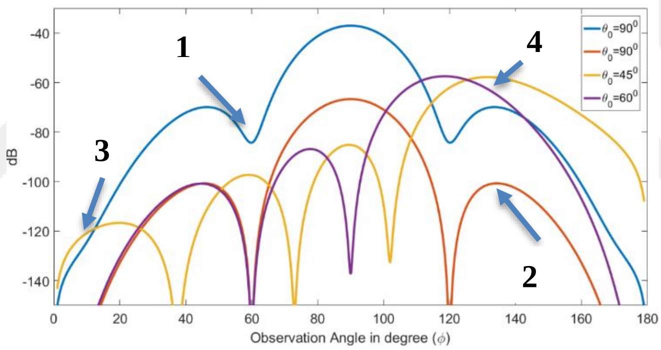

Figure 3.60 : Bi-static Radar Cross Section for $\epsilon = 2\pi$.

For the fractional-order $\alpha = 0.5$, the weighting function is given in the theoretical section is diminished. Therefore, it is a very special case worth investigating. The normalized fractional current density induced on the strip are given for the different ϵ parameter in Figures 3.61, 3.62, and 3.63. The source position is given as ρ_0. Curves 1, 2, and 3 on the figures stand for different incidence angle $\theta_0 = 90^0$, $\theta_0 = 45^0$, $\theta_0 = 60^0$, respectively. As it is seen, for the normal incidence case, the current distribution is symmetric. On the other hand, for the oblique incidence cases, they are asymmetric as expected because the incidence source is closer to the right side of the strip [6,33,38].

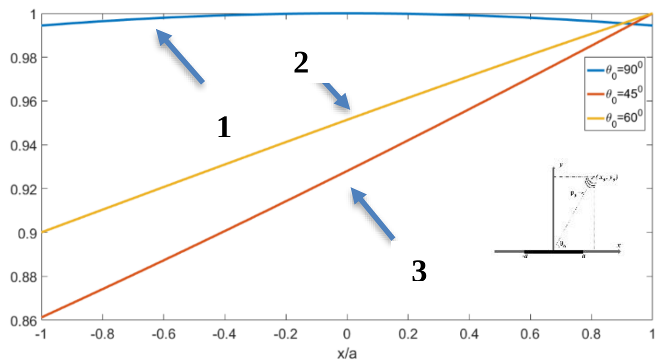

Figure 3.61 : The normalized Fractional Current Density $|\tilde{f}^{1-\alpha}(\xi)|$ for $\epsilon = \pi$ and $\rho_0 = 3$.

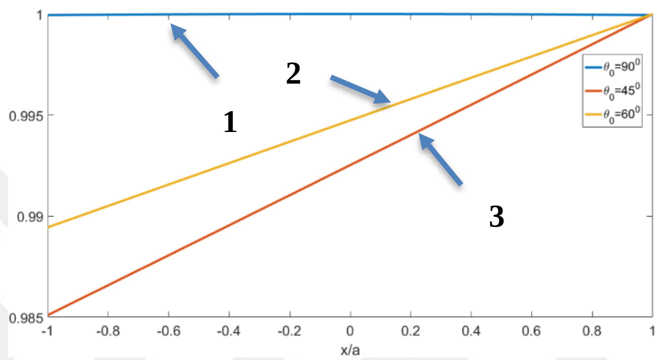

Figure 3.62 : The normalized Fractional Current Density $|\tilde{f}^{1-\alpha}(\xi)|$ for $\epsilon = \pi$ and $\rho_0 = 30$.

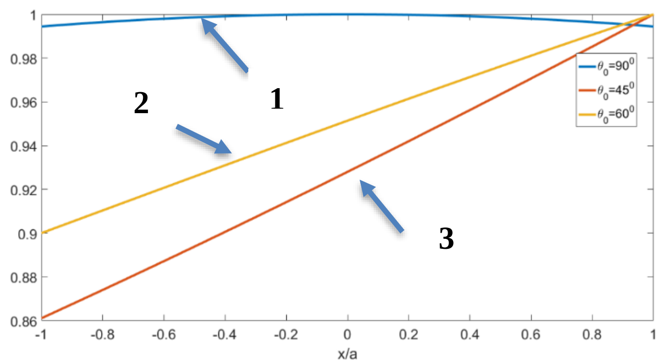

Figure 3.63 : The normalized Fractional Current Density $|\tilde{f}^{1-\alpha}(\xi)|$ for $\epsilon = 3\pi$ and $\rho_0 = 3$.

The comparison for the current density on perfectly conducting one strip is obtained in Figure 3.64. Note that in Figure 64, there is a comparison obtained by Physical Optics (PO), Method of Moments (MOM), and fractional derivative approach. All methods are almost coincident except the edges. The reason why there is a deviation for PO is that physical optics current density ($\vec{J}_s^{PO}$) is found using $\vec{J}_s^{PO} \cong 2\hat{e}_n \times \vec{H}^i$.

Here, $\vec{H}^i$ is the incidence magnetic field, $\hat{e}_n$ is the normal vector of the surface, and $(\times)$ is the cross product [51,52].

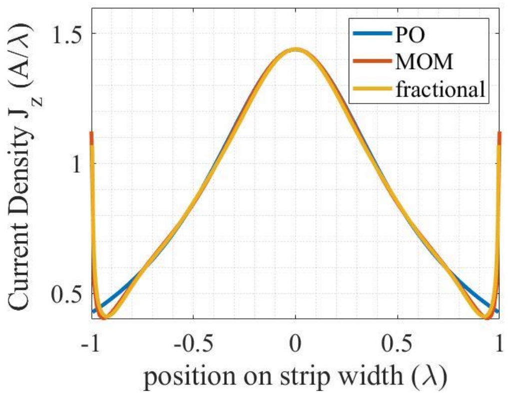

Figure 3.64 : Comparison of induced currents by one conducting strip induced for $x_0 = 0, y_0 = 0.5, k = 2\pi$, $a = 1$ and $\lambda = 1$.

4. CONCLUSION

Three different electromagnetic scattering problems have been analyzed with the hybrid method and compared with previous findings and the method of moments. Here, the investigations are done mainly on the diffraction by double strips with variable widths and boundary conditions. Besides, for a single strip, specifically, the fractional-order 0.5 case is analyzed. The fractional boundary condition (or integral boundary condition) that corresponds to an intermediate boundary condition between Dirichlet and Neumann boundary conditions is used to describe the scattering properties of different geometries. By determining the fractional-order, scattering properties of different materials are examined in the thesis. The new proposed boundary conditions describe a new material property (between Perfect Electric Conductor (PEC) and Perfect Magnetic Conductor (PMC)). The fractional boundary condition is the generalization of the Dirichlet and Neumann boundary conditions. In this case, the fractional derivative of the tangential component of the total electric field in the direction of the surface normal is zero on the surface of the scatterer. When the fractional-order becomes zero, this corresponds to Dirichlet Boundary Condition whereas, while the fractional-order is equal to one, this means the boundary condition is equal to Neumann Boundary Condition. In the middle, the boundary condition corresponds to different materials between perfectly electric conducting and perfectly magnetic conducting surfaces.

The problems are two-dimensional and for the solution of Helmholtz equations, the related Green's function is the Hankel function. To obtain the total field in the vicinity of the scatterer or far-fields, the scattered field is expressed in terms of an integral where the integrand is the Fourier transform of the current density on the strip multiplied by the Fourier transform of the Green's function. After that, the fractional boundary condition is employed in order to obtain an integral equation. Then, the Fourier transform of the current density on the strip needs to be determined. To achieve this goal, the integral equation is required to solve. For this, the current density is expressed at the summation of orthogonal polynomials. In our case, this orthogonal polynomial is chosen as Gegenbauer polynomial because the Gegenbauer polynomials are defined in a finite region since the problems solved in the thesis are strip geometries which are finite in the $x - y$ plane. To take into account the edge condition of the current density and fast converging of the polynomials to the actual value of the current density on the strip, the weighting is also inserted in the Gegenbauer polynomial expression. Then, orthogonality is employed to uniquely determine the unknown coefficients in the expression of the current density. After inversion of the system of linear algebraic equations, the coefficients are found. Finally, the current density, Fourier transform of the current density are obtained. This leads to finding electric field distribution for any desired accuracy. For the fractional-order 0.5 case, these expressions are achieved directly through analytical manipulations under some approximations (high-frequency regime). For the single strip problem, the current distribution and the bistatic radar cross-section investigations are done and analytical results are obtained when the source is put far-field and the field values are obtained for far-field. The results are similar to the same problem with the electromagnetic plane wave as a source. For a perfect electrical conducting single strip, the induced surface current due to the line source is also modeled by Physical Optics and Moments Method and compared with the method proposed in this thesis. The findings revealed that the Moments Method and the method used in the thesis give better results than Physical Optics. In the theoretical derivation, special functions, orthogonality properties of special functions, fractional derivative definition and fractional derivative of exponentials, Fourier analysis, boundary, radiation, and edge conditions in electromagnetics, the theory of the function with a complex variable and the steepest descent method are used not only for analyzing the integral equations but also, many of them are used to have the physical aspect of the electromagnetic scattering.

In the thesis, numerical simulations for the electromagnetic diffraction problem is reliable and fast converging. The results are compared with previous findings and the Method of Moment. The advantages of the fractional derivative approach can be summarized in the following sentence regarding the numerical analysis. Once, the theoretical part is completed for any given fractional-order, the numerical part is always the same. The only change is the fractional order. Therefore, one integral equation or one set of the coupled integral equation are solved for any fractional order. In other words, the fractional derivative approach is the generalization of the boundary condition and simplifies the computation load. One kind of current density can express the problem whereas, for the other methods, two different current densities are required to solve the same problem [8]. This hybrid method is very reliable and accurate for the $0 < ka < 15$ where a is the half-width of the strip and k is the wavenumber [8]. Even though in the summation expression of the fractional current density, $ka + 5$ terms are enough to obtain highly accurate results. For greater ka ($ka > 15$), to have a highly accurate result, terms in the summation expression of the fractional current density needs to be increased. For greater ka, the method gives approximate results. In the numerical analysis for problems, in general, the electric field distribution is presented. For double strip problems, the main focus is to investigate the total radar cross-section which allows one to analyze the resonance of the structure with given parameters. The resonance for the fractional-order 0.5 case is a very important outcome of these investigations. For some cases, the resonance values for this order is higher than the PEC and PMC surfaces. This is an important result that, such theoretical surfaces in the future can be employed in resonator or antenna structure for better performance. For the PEC double strips, resonance frequencies have an approximate analytical expression in the case of large strip widths compared to the distance between the strip and wavelength. The results coincide with the analytical formulation for the wide strips. Apart from this, several cases of different fractional orders are investigated. Also, the comparison between double strips with the same fractional-order and double strips with the different fractional orders is obtained. The choice of the fractional orders for each strip is very crucial for the radiation characteristics of the scattered field. The results demonstrate that the direction of the radiation pattern is highly correlated with the choice of fractional order. This kind of structure may be used in the antenna synthesis, waveguides, and resonators problem. Another important outcome of the study is that the field characteristics behave similarly to the field characteristic in the case of having PEC surface instead of PMC surface in the region of interest when the fractional order is closer to 0 (between 0-0.5) whereas, in the case of having the fractional-order between 0.5-1, the field characteristics is closer to the case when the surfaces PMC. In other words, the fractional-order 0.25 case demonstrates a similar outcome to the fractional-order 0 case, rather than the fractional-order 1 case.

For the future, the diffraction by arbitrarily located double strips with different boundary conditions and widths would be investigated.

REFERENCES

[1] **Rothwell, E. J. and Cloud, M. J.,** 2018: *Electromagnetics*, CRC Press.

[2] **Engheta, N.** (1996).Use of fractional integration to propose some ``fractional'' solutions for the scalar helmholtz equation, *Progress In Electromagnetics Research*, *12* 107–132.

[3] **Engheta, N.** (1998). Fractional curl operator in electromagnetics, *Microwave and Optical Technology Letters*, *17* (2), 86–91.

[4] **Engheta, N.** (1999). Phase and amplitude of fractional-order intermediate wave, *Microwave and optical technology letters*, *21* (5), 338–343.

[5] **Tabatadze, V., Karaçuha, K., and Veliyev, E. I.** (2019). The fractional derivative approach for diffraction problems: Plane wave diffraction by two strips with fractional boundary conditions, *Progress In Electromagnetics Research C*, *95* (August), 251–264.

[6] **Veliev, E. I., Karacuha, K., and Karaguha, E.**, 2018. Scattering of a cylindrical wave from an impedance strip by using the method of fractional derivatives, *Proceedings of 2018 XXIIIrd International Seminar/Workshop on Direct and Inverse Problems of Electromagnetic and Acoustic Wave Theory (DIPED)*, Tbilisi, Georgia.

[7] **Ivakhnychenko, M. V and Veliev, E. I.,** 2004. Fractional curl operator in radiation problems. *Proceedings of 10th International Conference on Mathematical Methods in Electromagnetic Theory*, Ukraine.

[8] **Ivakhnychenko, M. V, Veliev, E. I., and Ahmedov, T. M.** (2008). Scattering properties of the strip with fractional boundary conditions and comparison with the impedance strip, *Progress In Electromagnetics Research*, *2* 189–205.

[9] **Sadiku, M. N. O.,** 2018: *Numerical techniques in electromagnetics with MATLAB*. CRC press.

[10] **Gibson, W. C.**, 2014: *The method of moments in electromagnetics*. CRC press.

[11] **Anastassiu, H. T.** (2003). A review of electromagnetic scattering analysis for inlets, cavities, and open ducts, *IEEE Antennas and Propagation Magazine*, *45* (6), 27–40.

[12] **Copson, E. T.** (1946). An integral-equation method of solving plane diffraction problems, *Proceedings of the Royal Society of London. Series A. Mathematical and Physical Sciences*, *186* (1004), 100–118.

[13] **Senior, T. B. A.** (1952). Diffraction by a semi-infinite metallic sheet, *Proceedings of the Royal Society of London. Series A. Mathematical and Physical Sciences*, *213* (1115), 436–458.

[14] **Senior, T.** (1979). Backscattering from resistive strips, *IEEE Transactions on Antennas and Propagation*, *27* (6), 808–813.

[15] **Miles, J. W.** (1949). On Certain Integral Equations in Diffraction Theory, *Journal of Mathematics and Physics*, *28* (1–4), 223–226.

[16] **Maliuzhinets, G. D.**, 1958. Excitation, reflection and emission of surface waves from a wedge with given face impedances, *Proceedings of Sov. Phys. Dokl. Engl. Transl.*, Russia.

[17] **Meixner, J.** (1972). The behavior of electromagnetic fields at edges, *IEEE Transactions on antennas and propagation*, *20* (4), 442–446.

[18] **Pathak, P., Burnside, W. D., and Marhefka, R.** (1980). A uniform GTD analysis of the diffraction of electromagnetic waves by a smooth convex surface, *IEEE Transactions on antennas and propagation*, *28* (5), 631–642.

[19] **Herman, M. I. and Volakis, J. L.** (1987). High-frequency scattering by a resistive strip and extensions to conductive and impedance strips, *Radio Science*, *22* (3), 335–349.

[20] **Idemen, M. and Felsen, L.** (1981). Diffraction of a whispering gallery mode by the edge of a thin concave cylindrically curved surface, *IEEE Transactions on Antennas and Propagation*, *29* (4), 571–579

[21] **Kobayashi, K.** (1993). The Wiener-Hopf technique and its applications to diffraction problems involving two dimensional obstacles with finite cross section, *Lecture Notes*, *145* 1992–1999.

[20] **Lawrie, J. B. and Abrahams, I. D.** (2007). A brief historical perspective of the Wiener–Hopf technique, *Journal of Engineering Mathematics*, *59* (4), 351–358.

[22] **Idemen, M.** (2000). Confluent edge conditions for the electromagnetic wave at the edge of a wedge bounded by material sheets, *Wave Motion*, *32* (1), 37–55.

[23] **Avşar, E. and İkiz, T.** (2016). An approximate solution for the plane wave diffraction by an impedance strip: H-polarization case, *Tehnički glasnik, 10* (3–4), 79–97.

[24] **Avşar, E.**, 2016. *An approximate solution for the plane wave diffraction by an impedance strip: H-polarization case* (Ph.D. Thesis). Çukurova University, Turkey.

[25] **Ikiz, T. and Avşar, E. A.** (2017). An Approximate Solution for the Scattering of High-Frequency Plane Electromagnetic Waves from a Perfectly Conducting Strip, *Majlesi Journal of Telecommunication Devices*, *6* (2), 53-57.

[26] **Ikiz, T., Koshikawa, S., Kobayashi, K., Veliev, E. I., and Serbest, A. H.** (2001). Solution of the Plane Wave Diffraction Problem By an Impedance Strip Using a Numerical-Analytical Method: E-Polarized Case, *Journal of Electromagnetic Waves and Applications*, *15* (3), 315–340.

[27] **Veliev, E. I.,** 1993. Numerical-analytical approach for the solution to the wave scattering by polygonal cylinders and flat strip structures, in *Analytical*

and Numerical Methods in Electromagnetic Wave Theory, **10** , 471-514, Eds. Hashimoto, M., İdemen M. and Tretyakov O.A., Science House, Japan.

[28] **Veliev, E. I., Veremey, V. V, and Shestopalov, V. P.,** 1989. Electromagnetic wave diffraction on polygonal cylinders-new approach. *Proc. of 1989 URSI Int. Symp. on Electromagnetic Theory*, Stockholm, Sweden.

[29] **Butler, C.** (1985). General solutions of the narrow strip (and slot) integral equations, *IEEE transactions on antennas and propagation*, *33* (10), 1085–1090.

[30] **Veliev, E. I., Ivakhnychenko, M. V, and Ahmedov, T. M.** (2008). Fractional boundary conditions in plane waves diffraction on a strip, *Progress in electromagnetics research*, *79* 443–462.

[31] **Veliev, E., Ahmedov, T., and Ivakhnychenko, M.** (2011). Fractional operators approach and fractional boundary conditions, *Electromagnetic Waves*, 117.

[32] **Veliev, E. I. and Engheta, N.**, 2003. Generalization of Green's theorem with fractional differintegration. *Proceedings of 2003 IEEE AP-S International Symposium & USNC/URSI National Radio Science Meeting*, USA.

[33] **Veliyev, E. I., Karaçuha, K., Karaçuha, E., and Dur, O.** (2018). The use of the fractional derivatives approach to solve the problem of diffraction of a cylindrical wave on an impedance strip, *Progress In Electromagnetics Research*, *77* 19–25.

[34] **Veliyev, E. I., Tabatadze, V., Karaçuha, K., and Karaçuha, E.** (2020). The diffraction by the half-plane with the fractional boundary condition, *Progress In Electromagnetics Research*, *88* 101–110.

[35] **Tabatadze, V., Karaçuha, K., and Veliyev, E. I.** (2020). The solution of the plane wave diffraction problem by two strips with different fractional boundary conditions, *Journal of Electromagnetic Waves and Applications*, *34* (7), 881–893.

[36] **Tabatadze, V., Karaçuha, K., Veliyev, E. I., and Karaçuha, E.** (2020). The Diffraction by Two Half-Planes and Wedge with the Fractional Boundary Condition, *Progress In Electromagnetics Research*, *91* 1–10.

[37] **Karaçuha, K., Veliyev, E. I., Tabatadze, V., and Karaçuha, E.**, 2019. Application of the method of fractional derivatives to the solution of the problem of plane wave diffraction by two axisymmetric strips of different sizes. *Proceedings of 2019 URSI International Symposium on Electromagnetic Theory (EMTS)*, San Diego, USA, August.

[38] **Karaçuha, K., Veliyev, E. I., Tabatadze, V., and Karaçuha, E.** (2019). Analysis of Current Distributions and Radar Cross Sections of Line Source Scattering from Impedance Strip by Fractional Derivative Method, *Advanced Electromagnetics*, *8* (2), 108–113.

[39] **Tarasov, V. E.** (2019). On history of mathematical economics: Application of fractional calculus, *Mathematics*, *7* (6), 509.

[40] **Machado, J. T., Kiryakova, V., and Mainardi, F.** (2011). Recent history of fractional calculus, *Communications in nonlinear science and numerical simulation*, *16* (3), 1140–1153.

[41] **Önal, N. Ö., Karaçuha, K., Erdinç, G. H., Karaçuha, B. B., and Karaçuha, E.** (2019). A mathematical approach with fractional calculus for the modelling of children's physical development, *Computational and mathematical methods in medicine*, *2019*.

[42] **Machado, J. A. T. and Mata, M. E.** (2015). Pseudo phase plane and fractional calculus modeling of western global economic downturn, *Communications in Nonlinear Science and Numerical Simulation*, *22* (1–3), 396–406.

[43] **Gómez, F., Bernal, J., Rosales, J., and Cordova, T.** (2012). Modeling and simulation of equivalent circuits in description of biological systems-a fractional calculus approach, *Journal of Electrical Bioimpedance*, *3* (1), 2–11.

[44] **Samko, S. G., Kilbas, A. A., and Marichev, O. I.**, 1993: Fractional integrals and derivatives: Theory and applications. Gordan and Breach.

[45] **Oldham, K. and Spanier, J.**,1974: *The fractional calculus theory and applications of differentiation and integration to arbitrary order*. Elsevier.

[46] **Nagasaka, T. and Kobayashi, K.**, 2019. Wiener-Hopf Analysis of the Diffraction by a Strip with Fractional Boundary Conditions. *Proceedings of 2019 Photonics & Electromagnetics Research Symposium-Fall (PIERS-Fall)*, Xiamen, China, December.

[47] **Brown, J. W. and Churchill, R. V.,** 2009: *Complex variables and applications*. McGraw-Hill Higher Education. Boston, US.

[48] **Harrington, R. F.**, 1993: *Field computation by moment methods*.Wiley-IEEE Press.

[49] **Hönl, H., Maue, A. W., and Westpfahl, K.,** 1987, Theorie der beugung, in *Kristalloptik· Beugung/Crystal Optics· Diffraction*, 218–573.

[50] **Prudnikov, A. P., Brychkov, I. A., and Marichev, O. I.**, 1986: *Integrals and series: special functions*, (Vol. 2). CRC Press.

[51] **Balanis, C. A.,** 2016: Antenna theory: analysis and design. John Wiley & Sons, US.

[52] **Balanis, C. A.,** 2012: Advanced engineering electromagnetics. John Wiley & Sons, US.

[53] **Ishimaru, A.,** 2017: *Electromagnetic wave propagation, radiation, and scattering: from fundamentals to applications*. John Wiley & Sons, US.

[54] **Karacuha, K., Tabatadze, V., and Veliev, E. I.** (2020). Plane wave diffraction by strip with an integral boundary condition, *Turkish Journal of Electrical Engineering & Computer Sciences*, 28 (3), 1776–1790.

APPENDICIES

APPENDIX A: Edge Condition for the Current Density

The first time, the edge condition is studied by Senior and Meixner in the 20th century [14,17]. Their studies focus on the perfectly conducting half-plane and wedges at the first step. Then, the same structures are investigated with finite conductivity. The current behavior at the edge of the half-planes is the concern of this appendix. Here, some predefined solutions for the perfectly conducting wedges are taken and go through it. The solution for the diffraction by the wedge problem can be easily found in any electromagnetic graduate-level coursebooks [1]. In Figure A.1, the geometry of the problem is given. Note that, the electric current density (J_s) in this problem is taken as $\vec{J}_s = \hat{e}_z \tilde{I}\frac{\delta(\phi-\phi_0)}{\rho_0}$ where δ is the Dirac-delta function and $\tilde{I}$ is a constant. The general procedure is to divide the space ($\rho > \rho_0$ and $\rho < \rho_0$) into two regions and solve the boundary value problem. Each space has source-free. This yields to express the total field as the summation of non-uniform cylindrical waves. Then, the boundary condition for the total field on the surface of the wedge is applied. After that, the boundary condition coming from Green's Theorem for the $\rho = \rho_0$ is applied. Finally, the unknown coefficients are obtained. The detailed information can be found in [1]. Here, the motivation is to show the edge condition for the half-plane for different current densities flowing on the perfect electric conducting surfaces or perfect magnetic currents depending on the boundary conditions.

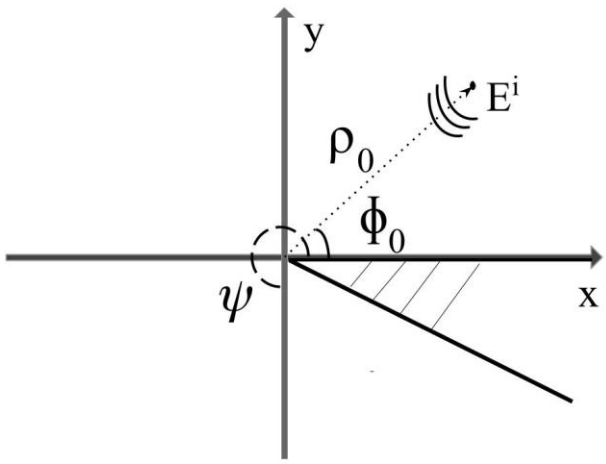

Figure A.1 : The geometry of the problem.

After the boundary condition satisfaction, the total electric field for this problem is found as (A.1) [1]

$$E_z(\rho,\phi,\omega) = \begin{cases} -\sum_{n=0}^{\infty} \tilde{I}\frac{\eta_0}{2\psi}\pi k\tilde{\epsilon}_n J_{\nu_n}(k\rho)H_{\nu_n}^{(1)}(k\rho_0)\sin\nu_n\phi\sin\nu_n\phi_0, & \rho < \rho_0 \\ -\sum_{n=0}^{\infty} \tilde{I}\frac{\eta_0}{2\psi}\pi k\tilde{\epsilon}_n J_{\nu_n}(k\rho_0)H_{\nu_n}^{(1)}(k\rho)\sin\nu_n\phi\sin\nu_n\phi_0, & \rho > \rho_0 \end{cases} \quad \text{(A.1)}$$

where ρ and ϕ is the radial and angular direction for cylindrical coordinates, respectively, k is the wavenumber, η_0 is the free-space impedance, $\nu_n = n\pi/\psi$, $J_{\nu_n}(k\rho)$ is the Bessel function, $H_{\nu_n}^{(1)}(k\rho_0)$ is the Hankel function of the first kind, and $\tilde{\epsilon}_n$ is Neumann's number

$$\tilde{\epsilon}_n = \begin{cases} 1, & n = 0 \\ 2, & n > 0 \end{cases} \tag{A.2}$$

Here the incidence wave has only z-independency and the incidence wave is the line source excitation. The reason why the incidence wave is chosen as the line source is that the line source at the far-field can be approaching the plane wave. Thus, a more general solution we can have by solving the line source diffraction by the wedge. In our problem, the field has TM polarization. Since the Total electric field is tangential to the surface of the scatterer, the form of the field needs to satisfy the boundary condition at $\phi = 0$ and $\phi = \psi$. Then, the total electric field can be expressed as (A.3) in the vicinity of the wedge. This is a very suitable assumption because both incidence wave and the scattered field are cylindrical waves for $\rho < \rho_0$.

$$E_z = \sum_{n=0}^{\infty} A_n \sin \nu_n \phi \, J_{\nu_n}(k_0 \rho) \tag{A.3}$$

where $\nu_n = n\pi/\psi$.

We are interested in how the current behaves while approaching $\rho \to 0$ on the surface of the wedge. From the boundary condition, the total current on the surface can be found as

$$\vec{J}_s(\rho, \omega) = \hat{\mathrm{e}}_\phi \times \left[\hat{\mathrm{e}}_\phi H_\phi + \hat{\mathrm{e}}_\rho H_\rho\right]_{\phi=0} = -\hat{\mathrm{e}}_z H_\rho(\rho, 0, \omega) \tag{A.5}$$

Here, $\hat{\mathrm{e}}_\phi$ and $\hat{\mathrm{e}}_\rho$ are the unit vectors in the angular and radial directions in the cylindrical coordinate system, respectively. Also, H is the magnetic field. For $\rho \to 0$, a small argument approximation for the Bessel function is taken into account by the following property [1].

$$J_\nu(z) \approx \frac{1}{\Gamma(\nu + 1)} \left(\frac{z}{2}\right)^\nu, \quad |z| \ll 1$$

Then,

$$\vec{J}_s(\rho, \omega) = -\hat{\mathrm{e}}_z \frac{1}{Z_{TM} k_0} \sum_{n=0}^{\infty} A_n \, \nu_n \frac{1}{\Gamma(\nu_n + 1)} \left(\frac{k_0}{2}\right)^{\nu_n} \rho^{\nu_n - 1}$$

where, Z_{TM} is the wave impedance for transverse magnetic polarization.
For $\rho \to 0$, a small argument approximation for the Bessel function is taken into account. Then,

$$\vec{J}_s(\rho, \omega) \sim \rho^{\frac{\pi}{\psi} - 1} \quad (\rho \to 0)$$

For the half-plane ($\psi = 2\pi$)

$$\vec{J}_s(\rho, \omega) \sim \frac{1}{\sqrt{\rho}}, \rho \to 0$$

As it can be seen, for the perfectly electric conducting surfaces, square root singularity dominates for the edges. With the same approach, for the perfectly magnetic conducting case, the singularity is given below.
For $\rho \to 0$

$$\vec{M}_s(\rho, \omega) \sim \sqrt{\rho}$$

$\vec{M}_s$ is the magnetic current the density.

APPENDIX B: Fourier Transform of the Current Density

Here, the derivation of the fractional current density's Fourier transform will be given. Since the current density only exists on the surface of the strips, the fractional current density has only non-zero values on the strips. The Fourier transform of the fractional current density is given in (B.1) [50].

$$F(\beta) = \int_{-1}^{1} \tilde{f}(\zeta) e^{-i\xi\beta\zeta} d\zeta \tag{B.1}$$

The fractional current density is denoted as

$$\tilde{f}^{1-\alpha}(\zeta) = (1-\zeta^2)^{\alpha-\frac{1}{2}} \sum_{n=0}^{\infty} f_n^\alpha \frac{C_n^\alpha(\zeta)}{\alpha} \tag{B.2}$$

Where $C_n^\alpha(\zeta)$ is the Gegenbauer polynomials. Here, f_n^α is the unknown constant-coefficient and the edge condition for the surface is satisfied by $(1-\zeta^2)^{\alpha-\frac{1}{2}}$ weighting. For different fractional-order $\alpha,$ the asymptotic behaviors of the current density at the edges of the strips changes.

After expressing the fractional current density, (B.1) is divided into two parts for further manipulations

$$F(\beta) = \int_{-1}^{0} \tilde{f}(\zeta) e^{-i\xi\beta\zeta} d\zeta + \int_{0}^{1} \tilde{f}(\zeta) e^{-i\xi\beta\zeta} d\zeta \tag{B.3}$$

In the right part of the integral by replacing the ζ with $-\zeta$, the limits can change and the integration could be combined as (B.4).

$$F(\beta) = \int_{0}^{1} \tilde{f}(-\zeta) e^{i\xi\beta\zeta} d\zeta + \int_{0}^{1} \tilde{f}(\zeta) e^{-i\xi\beta\zeta} d\zeta \tag{B.4}$$

From [24,50], the following property is employed

$$C_n^\alpha(-\zeta) = (-1)^n C_n^\alpha(\zeta) \tag{B.5}$$

Then, $\tilde{f}(-\zeta)$ becomes as

$$\tilde{f}^{1-\alpha}(-\zeta) = (1-\zeta^2)^{\alpha-\frac{1}{2}} \sum_{n=0}^{\infty} f_n^\alpha \frac{(-1)^n C_n^\alpha(\zeta)}{\alpha} \tag{B.6}$$

After putting (B.2) and (B.6) into (B.4) and separating the equations into even and odd parts, the following expressions are obtained. Note that $F(\beta) = F_{even}(\beta) + F_{odd}(\beta)$.

$$F_{even}(\beta) = \int_{0}^{1} (1-\zeta^2)^{\alpha-\frac{1}{2}} \sum_{p=0}^{\infty} f_{2p}^\alpha \frac{C_{2p}^\alpha(\zeta)}{\alpha} \left\{e^{i\xi\beta\zeta} + e^{-i\xi\beta\zeta}\right\} d\zeta \tag{B.7}$$

Here, $n = 2p$ and $F_{even}(\beta)$ is the even part of the Fourier transform of the fractional current density.

$$F_{odd}(\beta) = \int_0^1 (1-\zeta^2)^{\alpha-\frac{1}{2}} \sum_{p=0}^{\infty} f_{2p+1}^{\alpha} \frac{C_{2p+1}^{\alpha}(\zeta)}{\alpha} \left\{e^{i\xi\beta\zeta} - e^{-i\xi\beta\zeta}\right\} d\zeta \tag{B.8}$$

Here, $n = 2p + 1$ and $F_{even}(\beta)$ is the odd part of the Fourier transform of the fractional current density.

(B.7) and (B.8) can be written in a more convenient form as (B.9) and (B.10), respectively.

$$F_{even}(\beta) = 2\int_0^1 (1-\zeta^2)^{\alpha-\frac{1}{2}} \sum_{p=0}^{\infty} f_{2p}^{\alpha} \frac{C_{2p}^{\alpha}(\zeta)}{\alpha} \cos(\xi\beta\zeta) d\zeta \tag{B.9}$$

$$F_{odd}(\beta) = -2i\int_0^1 (1-\zeta^2)^{\alpha-\frac{1}{2}} \sum_{p=0}^{\infty} f_{2p+1}^{\alpha} \frac{C_{2p+1}^{\alpha}(\zeta)}{\alpha} \sin(\xi\beta\zeta)\, d\zeta \tag{B.10}$$

To proceed easily, the constants and the summations in (B.9) and (B.10) are taken outside of the integrand and the integral denoted as K_n.

$$K_{n=2p} = \int_0^1 C_{2p}^{\alpha}(\zeta)(1-\zeta^2)^{\alpha-\frac{1}{2}} \cos(\xi\beta\zeta) d\zeta \tag{B.11}$$

$$K_{n=2p+1} = \int_0^1 C_{2p+1}^{\alpha}(\zeta)(1-\zeta^2)^{\alpha-\frac{1}{2}} \sin(\xi\beta\zeta) d\zeta \tag{B.12}$$

From [24,50], K_{2p} and K_{2p+1} have the analytical solution as

$$\int_0^a (a^2-x^2)^{\lambda-\frac{1}{2}} \begin{Bmatrix} \sin bx \;\; C_{2n+1}^{\lambda}\left(\frac{x}{a}\right) dx \\ \cos bx \;\; C_{2n+1}^{\lambda}\left(\frac{x}{a}\right) dx \end{Bmatrix} = \frac{(-1)^n \pi}{(2n+\delta)!} \left(\frac{a}{2b}\right)^{\lambda} \Gamma\begin{bmatrix} 2\lambda + 2n + \delta \\ \lambda \end{bmatrix} J_{2n+\lambda+\delta}(ab) \tag{B.13}$$

where $\delta = \begin{Bmatrix} 1 \\ 0 \end{Bmatrix}$.

After using (13) and arranging the Gamma function in the expression, the Fourier transform of the fractional current density function is found as (B.14).

$$F(\beta) = \frac{2\pi}{\Gamma(\alpha+1)} \sum_{n=0}^{\infty} (-i)^n f_n^{\alpha} \frac{\Gamma(n+2\alpha)}{\Gamma(n+1)} \frac{J_{n+\alpha}(\xi\beta)}{(2\xi\beta)^{\alpha}} \tag{B.14}$$

APPENDIX C: Formulation of the Steepest Descent Method

In this appendix, the steepest descent method is given. The final result is presented directly. The procedure can be bound from [51]. Note that, the notation and the formulation are taken from this reference book. This method is utilized for taking some integrals with some approximation under some conditions.

For large values of β, the value of the following integral can be found approximately.

$$I(\beta) = \int_C F(z)e^{\beta f(z)}dz \tag{C.1}$$

where $f(z)$ is an analytical function and the path of integration C is on the complex plane [51]. $I(\beta)$ can be found as follows if there exists one saddle point.

$$I(\beta) \cong \sqrt{\frac{2\pi}{-\beta f''(z_s)}}F(z_s)e^{\beta f(z_s)} \tag{C.2}$$

where $z_s = x_s + iy_s$ and $\left.\frac{df}{dz}\right|_{z=z_s} = f'(z = z_s) = 0$.

CURRICULUM VITAE

Name Surname: Kamil KARAÇUHA

Place and Date of Birth:

Address:

E-Mail:

B.Sc.: 2017, Middle East Technical University, Engineering Faculty, Electrical and Electronics Engineering

B.Sc.: 2018, Middle East Technical University, Faculty of Arts and Science, Physics

Professional Experience and Rewards:

Research Assistant at Istanbul Technical University (2018-...)

List of Publications and Patents:

PUBLICATIONS/PRESENTATIONS ON THE THESIS

- **Karaçuha, K.**, Veliyev, E. I., Tabatadze, V., and Karaçuha, E. (2019). Analysis of Current Distributions and Radar Cross Sections of Line Source Scattering from Impedance Strip by Fractional Derivative Method, *Advanced Electromagnetics*, *8* (2), 108–113.
- **Karacuha, K.**, Tabatadze, V., and Veliev, E. I. (2020). Plane wave diffraction by strip with an integral boundary condition, *Turkish Journal of Electrical Engineering & Computer Sciences*, *28* (3), 1776–1790.
- Tabatadze, V., **Karaçuha, K.**, and Veliyev, E. I. (2019). The fractional derivative approach for diffraction problems: Plane wave diffraction by two strips with fractional boundary conditions, *Progress In Electromagnetics Research C*, *95* (August), 251–264.
- Tabatadze, V., **Karaçuha, K.**, and Veliyev, E. I. (2020). The solution of the plane wave diffraction problem by two strips with different fractional boundary conditions, *Journal of Electromagnetic Waves and Applications*, *34* (7), 881–893.